The Dissertation Committee for Saba Asif Baig
certifies that this is the approved version of the following dissertation:

Energy Transmission across 2d Holographic Interface Conformal Field Theories.

Committee:

Andreas Karch, Supervisor

David Ben-Zvi

Elena Caceres

Jacques Distler

Energy Transmission across 2d Holographic Interface Conformal Field Theories.

by

Saba Asif Baig

Dissertation

Presented to the Faculty of the Graduate School of

The University of Texas at Austin

in Partial Fulfillment

of the Requirements

for the Degree of

Doctor of Philosophy

The University of Texas at Austin

August 2025

Dedication

To my parents, you are all my reasons.

Acknowledgments

I would like to take this moment to thank all those who supported me during my graduate studies.

I'd like to begin by thanking my advisor, Andreas Karch, who took me on as a student shortly before my qualifier and has been an invaluable support ever since. Your guidance and patience helped me grow as a scientist and a scholar, and your enthusiasm and encouragement motivated me to avail numerous opportunities. Thank you for being generous with your time and knowledge, and for your unwavering positivity even when things didn't work as planned. I have learnt a lot from you.

I'd also like to thank many members of the '9th floor' who were a prt of this journey. I want to appreciate my other collaborators in this research, namely Sanjit Shashi and Mianqi Wang, who were always generous with their time and ideas, as well as my other collaborators in the group, Jacques Distler, Amir Raz and Hao-Yu Sun. I'd also like to acknowledge my committee members David Ben-Zvi, Elena Caceres, and Jacques Distler, who with their journal clubs provided a valuable space to learn and discuss new ideas. I also want to thank Antonia Chimonidou and Ram Sudha who helped me navigate being an instructor, which helped me appreciate teaching.

None of this would be possible without the support, encouragement and love of my family. I want to thank my parents, Samina and Asif, my siblings, Maria, Jamal, Haris and Fatima, my grandparents especially my dearest Dado, and all my family members! I'm grateful to my parents who always nurtured my curiosity and encouraged my ambition, in the process instilling a joy for science, math and reading. To my siblings, thank you for being my biggest cheerleaders. They always had faith in me and my abilities, and were supportive in successes and failures alike. You are my sunshine in human form!

Lastly, but definitely not least, I'm deeply grateful to all my friends. To my

friends from the Physics department, Stacie, Rodrigo, Nicolas, Carlos and Merna, thank you for always being helpful and generous with your friendship. To Sundas, Charulata, Fiza and Emaan, thank you for helping make Austin feel like home. To some of my old friends, Aman, Abeera, Rabbiya, Humdah and Sonia, thank you for always cheering me on and giving me wake-up calls from across the ocean!

Abstract

Energy Transmission across 2d Holographic Interface Conformal Field Theories.

Saba Asif Baig, PhD
The University of Texas at Austin, 2025

SUPERVISOR: Andreas Karch

This dissertation uses conformal interfaces as a tool to better understand two-dimensional irrational conformal field theories. The central focus is on extracting physical data encoded in conformally invariant interfaces in both weakly and strongly interacting limits, by using field-theoretic and holographic methods (AdS/CFT correspondence) respectively. It consists of 4 chapters. The first chapter introduces the reader to the gravitational wave scattering problem used to probe the interface and relevant underlying ideas in 2d CFTs, the holographic principle, energy transmission coefficient, and entanglement entropy. Chapter 2 is based on work with Andreas Karch on a holographic toy model involving a double-brane interface geometry, showing that energy transmission and boundary entropy can be independently varied[1]. Chapter 3 is based on work with Sanjit Shashi on a symmetric orbifold interface conformal field theory dual to a non-supersymmetric Janus solution and finds that the transmission coefficient functionally differs between weak and strong coupling, unlike what was known for boundary entropy[2]. Chapter 4 is based on work with Andreas Karch and Mianqi Wang on investigating the supersymmetric Janus solution to find exact agreement in transmission coefficients between weak and strong limits, showing that supersymmetry protects transport data, like in the case of boundary entropy[3].

Table of Contents

List of Figures

Chapter 1: Introduction

This dissertation was completed as a Ph.D. student in the Weinberg Theory Group at the University of Texas at Austin and uses codimension-1 interfaces as a tool to better understand 2d conformal field theories (CFTs). The main idea is to investigate the physical data encoded in a conformally invariant interface that separates two CFTs with different central charges or parameters, which could be useful in characterizing interface conformal field theories (ICFTs). ICFTs can be mapped to the more widely recognized boundary conformal field theories (BCFTs) by applying the folding trick, and imposing the same symmetry constraints. However, certain physical quantities are more intuitive in the ICFT picture and can be computed relatively easily without explicitly solving for a particular boundary state. In the 2d ICFTs in this thesis, we investigate two such physical quantities: a transmission coefficient which measures the proportion of energy flux transmitted across an interface, and the additional entanglement entropy of an interval due to the presence of the interface.

Many CFTs can be marginally deformed without breaking conformal invariance. This means that we are describing an interacting quantum field theory (QFT) with non-trivial dynamics, but where the coupling constant that controls this interaction does not depend on the energy scale, so the theory is still conformal. Physical observables in CFTs can be calculated in terms of the correlation functions of local operators. When the deformation (or interaction) is weak, a perturbative computation using Feynman diagrams is a valid prescription for such physical observables, but in the strongly deformed limit, the perturbative expansion fails as higher-loop diagrams contribute significantly. This brings us to holography, which offers tools to analyze the behaviour of strongly-coupled CFTs in an alternate theory of gravity.

In the large N and strongly deformed limit, according to the Anti-de Sitter/Conformal Field Theory (AdS/CFT) correspondence [5], CFTs living on the

'boundary' of an AdS spacetime have an equivalent classical gravity description in the higher-dimensional 'bulk' spacetime. N is the effective number of interacting degrees of freedom and can correspond to large central charge[1]. Similarly, BCFTs (and ICFTs) can also have dual gravity descriptions[6, 7]. These are given by those solutions to Einstein's equations that obey the symmetry constraints imposed on the boundary/interface. In a simple toy-model ICFT, these solutions turn out to be AdS spacetimes with different curvature radii separated by fixed tension thin-branes[6, 4].

We can scatter gravitational waves across these ICFTs and calculate the energy proportion transmitted across the interface, in both bottom-up and top-down models. In 2d, this depends on one 'parameter'/piece of CFT data: the 2-point function of the left and right stress tensors, often labeled in the literature as c_{LR}. The energy transmission coefficient can be calculated in both the weakly and strongly interacting limits of the CFTs. In the weak limit, we use field theory techniques to calculate it for a non-interacting ICFT. In the strong limit, we make use of the AdS/CFT correspondence and compute transmission in the semi-classical supergravity solution.

The other interesting quantity is additional entanglement entropy due to the presence of this interface, which can be identified with the boundary entropy in the BCFT. In 2d, this quantity also depends on one parameter/piece of data: $\log g$ where g is a measure of the ground state degeneracy. In this thesis, we calculate the additional entanglement entropy in a bottom-up toy model, and use results produced in [8, 9] for the genuine top-down constructions where the CFTs and their holographic duals are well-known.

In principle, c_{LR} and $\log g$ are two different pieces of information. In Chapter 2 which is based on the previously published work "Double brane holographic model dual to 2d ICFTs" by Saba Asif Baig and Andreas Karch [1], we look at a bottom-up toy model. Since the generic field theory dual is not known (and may not exist), we

[1]E.g., N can be number of copies in an orbifold or number of branes, size of the gauge group, etc. Depending on the theory, central charge scales with it as $c \sim N, N^2$, etc.

calculate the energy transmission coefficient and the additional entanglement entropy in the dual gravitational bulk only. In the single-brane case [4, 10], there was a $1-1$ correspondence between the transmission coefficient and the boundary entropy. Our toy model consists of the fusion of two single-brane interfaces and this fusion does not yield another single-brane interface but rather a new object. For this 'double-brane' model, the transmission coefficient and boundary entanglement entropy can be independently dialed. Therefore, for generic holographic toy models with Randall Sundrum branes, both these pieces of physical data can be independent of one another.

In top-down constructions, where the AdS/CFT duals from string theory are well-known, we can compute the transmission coefficient in both the weakly and strongly coupled limits. We consider two top-down constructions: a sigma model 2d ICFT with a dual non-supersymmetric Janus solution, and its supersymmetric formulation. The interest in calculating the transmission coefficient in these stems from the fact that the boundary entropy for these Janus models, produced in [8, 9], turns out to be fairly well-protected as you go from the weak to the strong limit. While in the Janus solution, this difference is numerically small, in supersymmetric Janus, the boundary entropy in the weak and strong limits match exactly. This raises the question of whether a transport property (transmission coefficient) behaves similarly to an entropic property (additional entanglement entropy) when supersymmetry is imposed in ICFTs.

In Chapter 3, which is based on previously published work "Transport across interfaces in symmetric orbifolds" by Saba Asif Baig and Sanjit Shashi [2], we look at conformal interfaces in the symmetric orbifold of a non-linear sigma model (NLSM), which is a theory of $\mathcal{N}=4$ free compact scalars on a $\mathrm{Sym}^N(T^4)$ target space. It is dual to the Janus solution: a non-supersymmetric dilatonic deformation of $\mathrm{AdS}_3\times S^3\times\mathbb{T}^4$. It turns out that the transmission coefficient has different functional forms in the weak and strongly coupled limits. The functional forms in both regimes depend on the dilatonic deformation parameter and the energy transmission is always greater in the strongly coupled limit. However, the strongly and weakly interacting limits

match at the extreme values of the dilatonic deformation, that is, when you turn off the deformation altogether, or when you deform it maximally to $\mathrm{AdS}_2 \times R \times S^3 \times \mathbb{T}^4$.

In Chapter 4, which is based on the previously published work "Transmission Coefficient of Super-Janus Solution" by Saba Asif Baig, Andreas Karch and Mianqi Wang [3], we look at a theory of $\mathcal{N} = (4, 4)$ free compact scalars and their free fermionic super partners dual to the supersymmetric realization of the Janus solution, where appropriate boundary conditions at the interface restore half of the supersymmetry to the usual Janus solution. Here, it turns out the transmission coefficient is the exact same in both the strongly and weakly coupled limits. Supersymmetry protects energy transmission as effectively as it protects boundary entropy. We also observe that in supersymmetric Janus, two pieces of CFT data, c_{LR} (which the transmission coefficient depends on), and c_{eff} (which the additional entanglement entropy for a region entirely to one side of the interface depends on) are related and not independent.

This thesis begins with an overview of conformal field theories and their symmetries, the AdS/CFT correspondence, the scattering problem that calculates the proportion of energy transmitted across an interface, and the additional entanglement entropy due to the interface. The work of Chapters $2 - 4$ reproduce the work found in [1, 2, 3] with the appendices compiled at the end.

1.1 Conformal Field Theories

1.1.1 Interactions in Quantum Field Theories

Quantum field theories (QFTs) have a wide range of applications, from describing electromagnetic, weak and strong nuclear forces in the standard model to describing second order phase transitions in statistical mechanics. For a weakly interacting QFT, we can treat the interaction as a perturbation on top of the initial dynamics of the underlying field content, and the first few Feynman diagrams will then make the dominant contribution to path integrals which can be used to evaluate

observables. If the system is strongly interacting, this expansion can't be truncated as higher-order terms (diagrams) contribute more and more.

Strongly coupled systems do appear extensively in physics, from condensed matter to particle physics. The strength of the interaction is denoted by the coupling constant λ and can depend on the energy of the system. For example, in quantum chromodynamics (QCD) λ weakens at high energies, so low-energy rest mass calculations are difficult to perform due to the strong coupling. One useful analytic method for dealing with this is to use strong-weak duality. The gauge/gravity duality refers to equivalent descriptions of the same physics in terms of either a strongly coupled QFT or a weakly coupled gravitational theory. The scope of this duality is somewhat restricted as it does not directly describe known physical systems. However, theories can still capture essential features of real-world theories or offer approximations, such as $\mathcal{N} = 4$ supersymmetric Yang–Mills (SYM) in 4d can be considered a supersymmetric version of QCD.

1.1.2 Symmetry considerations in 2d Conformal Field Theory

Some interesting QFTs are often approximately scale-invariant. Examples include QCD at high energies, near second-order phase transitions or quantum critical points in condensed matter. Translations and Lorentz transformations, spacetime inversions and scaling symmetries all together form the conformal group. A QFT with these symmetries is called a conformal field theory (CFT).

Local conformal symmetry in 2d is special because the symmetry algebra is infinite-dimensional. In 2d, conformal transformations are locally analytic (holomorphic) functions and there can be an infinite number of such holomorphic mappings of the complex plane into itself: $z \to f(z)$, $\bar{z} \to \bar{f}(\bar{z})$. Consequently, 2d CFTs have an infinite number of conserved quantities and the symmetry group is infinite-dimensional. The generators of these local conformal transformations are the modes

$L_n = -z^{n+1}\frac{d}{dz},\ n \in \mathbb{Z}$. These satisfy the Virasoro algebra with a central extension:

$$[L_m, L_n] = (m-n)L_{m+n} + \frac{c}{12}(m^3 - m)\delta_{m+n,0} \tag{1.1}$$

where L_n are the symmetry generators and c is the central charge that arises from quantum effects.

Some of the important physical observables in CFTs are the correlation functions of local operators. In 2d, infinitely enhanced conformal symmetry highly constrains the form of correlation functions. The 2-point function of primary operators is completely fixed (up to normalization). Most physical observables in 2d CFTs are either correlation functions of local operators or can be derived from them. These include operator dimensions (extracted from 2-point functions), operator product expansion (OPE) coefficients (appear in 3-point functions) that determine the interactions of the theory, conformal blocks (arise from decomposing 4-point functions via the OPE), and central charge (appears in the stress tensor OPE) that measures degrees of freedom.

A universal local operator, present in any field theory, is the symmetric stress tensor $T_{\alpha,\beta}$. In 2d CFTs, the holomorphic and anti-holomorphic stress tensors, $T(z)$ and $\bar{T}(\bar{z})$, play a central role in defining the conformal structure, operator algebra, and symmetries of the theory. The OPE of the holomorphic stress tensor with itself defines the central charge $(c/2)$ of the 2d CFT:

$$T(z)T(w) \sim \frac{c/2}{(z-w)^4} + \frac{2T(w)}{(z-w)^2} + \frac{\partial T(w)}{z-w} + \cdots \tag{1.2}$$

The 2d conformal theory has an anomaly. Classically, the trace of the stress tensor vanishes, but in the quantized theory its vacuum expectation value (VEV) is proportional to the central charge c of the CFT.

1.1.3 Marginal Deformations of Conformal Field Theory

Exactly marginal deformations to the CFTs are of interest as they allow the interface and CFTs to remain conformal but with possibly different correlation func-

tions and thereby physical observables. Whether a marginal deformation is exactly marginal depends on the structure of the theory, its symmetries and anomalies. In dimensions greater than 2, conformal symmetry is finite-dimensional, so marginal operators ($\Delta_{\text{classical}} = d$) might receive quantum corrections. However, in 2d, the infinite-dimensional Virasoro algebra tightly controls not just the correlation functions and OPEs, but also the allowed deformations. The space of potentially marginal operators is smaller and more rigidly structured.

Conformal primary operators are classified by their Virasoro weights $(h, \bar{h})$. In 2d, for an operator to be exactly marginal, it must be a Virasoro primary with $(h, \bar{h}) = (1, 1)$, and be local with respect to other operators in the theory. Chapter 3 has details on the restricted exactly marginal deformations when we compute the transmission coefficient in the noninteracting limit[2] of the symmetric orbifold ICFTs. Below is a short overview of deformations and the anomalous dimensions of their coupling constants that determine whether there is an renormalization group (RG) flow.

The action of a d-dimensional CFT can be deformed by adding any local operator $O(x)$ where the deformation strength is controlled by a coupling constant λ:

$$S_{CFT} \to S_{CFT} + \lambda \int d^d x \; O(x) \tag{1.3}$$

The scaling dimension Δ of the operator $O(x)$[3] tells us how it behaves under a rescaling of spacetime coordinates:

$$\begin{aligned} x^\nu &\to \mu x^\nu \\ O(x) &\to \mu^{-\Delta} O(\mu x) \\ \lambda \int d^d x \; O(x) &\to \lambda \mu^{d-\Delta} \int d^d x \; O(\mu x) \end{aligned}$$

[2]The seed theory is non-interacting with copies of itself. The CFTs on the right and the left can still exchange energy via the interface.

[3]Physical units of an operator $[O] = \text{m}^\Delta$ where Δ is classical.

For the deformation of the action to be dimensionless, the coupling constant must have mass dimension $[\lambda] = m^{d-\Delta}$. To keep the form of the action invariant, the pre-factor is absorbed into a redefined coupling constant $\lambda(\mu)$. Hence, the scaling dimension Δ of an operator $O(x)$ determines its importance at different energy scales:

- $\Delta < d$: Relevant operator (λ has positive mass dimension and grows in IR)
- $\Delta = d$: Marginal operator (λ is dimensionless and scale-invariant)
- $\Delta > d$: Irrelevant operator (λ has negative mass dimension and shrinks in IR)

Due to interactions, the scaling dimension can have quantum corrections. The total scaling dimension is given by: $\Delta_{\text{quantum}} = \Delta_{\text{classical}} + \gamma(\lambda)$. Exactly marginal deformations occur when there is no anomalous dimension $\gamma(\lambda)$, so $\Delta_{\text{quantum}} = d$. This is a non-trivial quantum condition. It means λ is constant and does not affect the scaling behavior of the theory at low energies. Such operators preserve conformal invariance to all orders in perturbation theory or non-perturbatively. λ labels a family of CFTs, and these operators shift you along the conformal manifold (such as the moduli space of the compact boson CFT). The low-energy behavior remains conformal but with possibly different correlation functions.

There are deformations that are marginal but not exact, so the anomalous dimension makes the operator marginally relevant or marginally irrelevant. Even if λ runs slowly under RG flow, it will change the low-energy physics, even though the operator is marginal at the classical level. The RG flow that governs how physics looks at different energy scales μ is encapsulated by a beta function $\beta(\lambda) = \mu\frac{d\lambda}{d\mu}$. CFTs occur precisely at fixed points where all beta functions vanish:

$$\beta(\lambda_i^*) = 0 \quad \forall i$$

. Whether an operator stays marginal is often decidable from symmetry arguments alone without computing the beta function explicitly.

1.2 Holographic Principle

1.2.1 Applying CFT to string theory

A string moves through D-dimensional spacetime, sweeping out a 2d surface called the worldsheet[4] with co-ordinates σ and τ (that label spacetime on the string). This 2d worldsheet's embedding in D-dimensional spacetime can be described using target space coordinates $X^\mu(\sigma, \tau)$ which are essentially D free scalar fields defined on the worldsheet. The dynamics of the string are governed by the Polyakov action:

$$S = -\frac{1}{4\pi\alpha'} \int d^2\sigma \, \sqrt{-h} \, h^{ab} \, \partial_a X^\mu \partial_b X^\nu \eta_{\mu\nu}$$

Where h_{ab} is the worldsheet metric and $\eta_{\mu\nu}$ is the spacetime metric. This action is invariant under diffeomorphisms of the worldsheet co-ordinates and local rescalings of the 2d worldsheet metric. Together, that is conformal invariance in 2 dimensions, so string theory described from a worldsheet perspective is a 2d CFT.

When we quantize the string, we look for solutions to the equations of motion of the scalar fields X^μ. These Fourier mode solutions are the vibrational string modes, and they correspond to states in the Hilbert space of the 2d CFT. Different string excitations like gravitons (massless spin-2 mode), photons (massless spin-1 mode), dilatons (scalar mode), etc are identified with specific states or vertex operators in the 2d CFT.

1.2.2 Gauge/gravity duality

Gauge/gravity duality is an equivalence between two different descriptions of the same physics. On one side are QFTs (or gauge theories such as Yang-Mills) that describe interacting particles moving in flat d-dimensional spacetime, and on the other side are (d+1)-dimensional[5] theories that include gravity (such as Einstein's general relativity or string theory descriptions). The (d+1)-dimensional gravitational theory

[4] A $(1+1)$d analog of the worldline of a point particle.

[5] d dimensions of the particle theory and one additional infinite dimension.

has a dynamical curved spacetime and the duality asserts that bulk dynamics are encoded in a d-dimensional QFT. Operators in the QFT correspond to fields in the gravitational theory, and there is a one-to-one map between the two: a dictionary relating the field-theory and gravity languages.

In a gauge theory with rank N and coupling g, the dual gravitational description becomes reliable when both $N \gg 1$ and the 't Hooft coupling $\lambda = g^2 N \gg 1$. In this regime, the AdS curvature radius scales as $L \sim \ell_s (g^2 N)^{1/4}$ where ℓ_s is the fundamental string length. When $\lambda \gg 1$, L is much larger than ℓ_s, so the spacetime is weakly curved and classical general relativity provides a valid approximation. Note that string theories are described by general relativity only at low energies; at high energies, they will contain a large set of string excitations. Conversely, when $\lambda \ll 1$, the curvature radius becomes smaller than the string scale, and stringy effects dominate, invalidating the classical gravity description.

Thus, a strongly-coupled large N gauge theory corresponds to a weakly curved gravitational dual where physics in the bulk can be studied using Einstein's equations. This is also what makes the duality harder to prove because it's difficult to do reliable computations in a strongly coupled field theory to match them to gravitational ones.

An irrational CFT has an infinite number of primary fields, even under the maximally extended chiral algebra. In the large N and strongly coupled limit, the CFT typically becomes irrational, with an infinite spectrum and an irrational central - rich enough to match the degrees of freedom of a bulk theory in AdS. In contrast, rational CFTs are too constrained to support a dual gravitational description.

Symmetric orbifold theories, which we discuss ahead, constitute a large and important class of irrational CFTs. Although each seed theory $\mathcal{M}$ may be rational, the orbifold introduces twist sectors and the resulting theory has infinitely many primaries. Also, when the seed theory is compactified on a torus, say an NLSM with target space T^4, unless the radius is tuned to rational points, the theory is not rational. Even at rational points, the addition of free fermions generally makes the

combined theory irrational.

1.2.3 AdS/CFT correspondence

The most precise correspondence is the anti–de Sitter/conformal field theory (Ads/CFT) correspondence that maps CFT to string theory formulated in AdS space. One of the most famous examples is the duality between 4d $\mathcal{N} = 4$ supersymmetric Yang Mills (SYM) with gauge group SU(N) and Type IIB string theory on $\mathrm{AdS}_5 \times S^5$.

Under AdS/CFT correspondence, fluctuations of fields in the bulk spacetime correspond to distinct local operators in the CFT at the boundary. Small fluctuations of the metric tensor around a background geometry give rise to the graviton in the bulk: a massless spin-2 excitation of string theory. The boundary value of the graviton sources the energy-momentum tensor $T^{\mu\nu}$ in the CFT.

Our goal is to study the scattering of gravitational waves carrying energy in the holographic ICFT. On the CFT side, this is encoded in correlation functions of the energy–momentum tensor. In the dual gravitational description, an insertion of $T_{\mu\nu}(x)$ corresponds to a graviton emitted from point x on the AdS boundary. These gravitons propagate into the bulk and interact according to general relativity. Thus, computing correlation functions of $\langle T_{\alpha,\beta}(x) T_{\mu,\nu}(y)\rangle$ reduces to a gravitational scattering problem in curved spacetime. Note that in 2d CFT, the correlation function separates into holomorphic $\langle T(z)T(w)\rangle$ and anti-holomorphic $\langle \bar{T}(\bar{z})\bar{T}(\bar{w})\rangle$ parts. The stress tensor is not an exactly marginal operator, but rather generates conformal transformations and is a conserved current with spin 2.

Similarly, scalar fields in the bulk correspond to scalar operators on the CFT. Dilaton (arising in the NS-NS sector) and axion (arising in the RR sector of type IIB string theory) are examples of fundamental scalar and pseudoscalar fields in the bulk that are dual to marginal scalar and marginal pseudoscalar operators in the boundary. Dilaton controls the string coupling $g_s = e^{\Phi}$, and if the dilaton in the bulk asymptotes to different values on each side of the boundary, it leads to a position-

dependent marginal coupling, which is essentially an ICFT. Moduli fields that arise from compactification of the metric and form fields on internal manifolds can control the size of the internal manifolds on the boundary.

1.2.4 Anti-de Sitter spacetime

Anti-de Sitter (AdS) geometry arises in string theory as the near-horizon limit of D3-branes in type IIB supergravity [11]. The string coupling ℓ_s and the number of branes N set the curvature scale: $L \sim \ell_s \, (g^2 N)^{1/4}$. In the low-energy decoupling-gravity limit, the geometry asymptotes to $AdS_5 \times S^5$.

Anti-de Sitter spacetime AdS_{d+1} is a maximally symmetric Lorentzian manifold with constant negative curvature. It solves the vacuum Einstein equations with a negative cosmological constant $\Lambda = -\frac{1}{L^2}$:

$$R_{\mu\nu} - \frac{1}{2} R \, g_{\mu\nu} + \Lambda g_{\mu\nu} = 0 \tag{1.4}$$

The isometry group of AdS_{d+1} is $\mathrm{SO}(2, d)$, coinciding with the conformal group in d dimensions. Lower dimensional cases provide analytically tractable models, particularly in AdS_3, where the algebra splits $\mathrm{SO}(2,2) \cong \mathfrak{sl}(2,\mathbb{R}) \oplus \mathfrak{sl}(2,\mathbb{R})$. This means we can think of AdS_3 gravity as having left and right-moving sectors, mirroring 2d CFT's left and right-moving Virasoro algebras.

The AdS_3 metric in Poincaré coordinates is

$$ds^2 = \frac{L^2}{z^2}(-dt^2 + dx^2 + dz^2), \tag{1.5}$$

where $z > 0$ and the conformal boundary lies at $z \to 0$. Note that this coordinate patch covers only a portion of the full spacetime.

In global coordinates that cover the entire manifold, the metric is:

$$ds^2 = L^2(-\cosh^2 \rho \, d\tau^2 + d\rho^2 + \sinh^2 \rho \, d\phi^2) \tag{1.6}$$

with $\tau \in \mathbb{R}$, $\rho \in [0, \infty)$, and $\phi \sim \phi + 2\pi$.

When the QFT is not scale invariant, the dual spacetime has varying curvature. For asymptotically AdS geometries that have non-constant curvature radius, the metric can be written in 'warped' product form:

$$ds^2 = e^{2A(y)}\eta_{\mu\nu}dx^\mu dx^\nu + dy^2 \tag{1.7}$$

with warp factor $A(y)$ encoding curvature along the radial direction. This form will appear in Chapters 3 and 4, where in the latter a higher dimensional spacetime metric is reduced to asymptotically AdS_3 metric of this form.

1.3 Transmission Coefficient in the boundary theory

1.3.1 Interface Conformal Field Theory (ICFT)

A 2d ICFT consists of two 2d conformal field theories, CFT_L and CFT_R, joined at a pointlike (0+1)-dimensional interface that preserves conformal invariance. CFT_L and CFT_R can have different central charges, c_L and c_R, or parameters (volume of the target space, etc). Since splitting into holomorphic and anti-holomorphic components is a local property, each side has left and right moving Virasoro generators. We can scatter energy at the boundary. However, a conformal interface conserves energy. When the excitations hit the interface, to preserve conformal invariance, they must satisfy the following gluing condition[12, 13]:

$$T_L(z = i\tau) - T_L(\bar{z} = -i\tau) = T_R(z = i\tau) - T_R(\bar{z} = -i\tau), \quad \tau \in \mathbb{R} \tag{1.8}$$

Consider the scattering *gedankenexperiment* in the ICFT [14] where they send a wave packet towards the interface and define transport coefficients in terms of ratios of average energy fluxes. These energy fluxes can be calculated as the expectation values of the ANEC operators computed in states created by acting with a local operator on a compact region in the far past:

$$\begin{aligned} \mathcal{T}_L &= \lim_{D\to\infty} \frac{\langle \mathcal{O}_L, D|\mathcal{E}_R|\mathcal{O}_L, D\rangle_I}{\langle \mathcal{O}_L, D|\mathcal{E}_L|\mathcal{O}_L, D\rangle} \\ \mathcal{R}_L &= \lim_{D\to\infty} \frac{\langle \mathcal{O}_L, D|\bar{\mathcal{E}}_L|\mathcal{O}_L, D\rangle_I - \langle \mathcal{O}_L, D|\bar{\mathcal{E}}_L|\mathcal{O}_L, D\rangle}{\langle \mathcal{O}_L, D|\mathcal{E}_L|\mathcal{O}_L, D\rangle} \end{aligned} \tag{1.9}$$

Using operator algebra in 2d, the energy flux ratios simplify from a 3-point function to being determined by the coefficients of 2-point functions between spin-2 quasi-primary holomorphic currents on the left and on the right of the interface. These would usually be state-dependent. However, if the only such current in the theory is the stress tensor, then the transmission coefficient is *universal*, regardless of the in-state. Transmission is a function of one piece of CFT data $c_{\rm LR}$ ($c_{\rm L}, c_{\rm R}$ are fixed):

$$\begin{aligned}
\langle T_L T_L\rangle_I &= \langle \bar{T}\bar{T}_L\rangle_I \propto \frac{c_L}{2} \\
\langle T_R T_R\rangle_I &= \langle \bar{T}_R\bar{T}_R\rangle_I \propto \frac{c_R}{2} \\
\langle T_L \bar{T}_L\rangle_I &\propto \frac{c_L - c_{LR}}{2} \\
\langle T_R \bar{T}_R\rangle_I &\propto \frac{c_R - c_{LR}}{2} \\
\langle T_L T_R\rangle_I &= \langle \bar{T}_R\bar{T}_L\rangle_I \propto \frac{c_{LR}}{2}
\end{aligned} \tag{1.10}$$

In a generic CFT, the transport coefficients are state-dependent obviously. However, if the scattering state has been prepared by the stress tensor, then even for a generic CFT, we have the same outcome and the transport coefficient just depends on one parameter $c_{\rm LR}$. From the two point functions above, the transmission coefficient can be constructed as follows:

$$\mathcal{T} = \frac{\langle T^L T^R + \bar{T}^L\bar{T}^R\rangle_{L|R}}{\langle (T^L + \bar{T}^R)(\bar{T}^L + T^R)\rangle_{L|R}} \tag{1.11}$$

Another approach is to measures the overlap of two states[14]. The incoming state describes incoming energy brought in from far, and the outgoing state describes the energy scattered far from the beam (in the future), so like a transmitted or reflected beam. The easiest way to perform this is by creating the in and out states by the appropriate holomorphic and anti-holomorphic stress tensor insertions. The overlap of the in and out states would define an S matrix. The entries in the matrix consist of the same 2-point functions defined above.

From the ICFT methods discussed above, it appears that the transmission coefficient can be expressed in term of the 2-point function of quasi spin-2 operators.

If you choose those to be the stress tensor, or if the stress tensor is the only spin-2 operator in the theory, the transmission coefficient is universal and described by one parameter.

1.3.2 Boundary Conformal Field Theory (BCFT)

The ICFT above can be mapped to BCFT by the folding trick. This gives a conformal field theory $CFT_L \otimes \overline{CFT_R}$ with a boundary. A generic CFT boundary state $|B\rangle$ must satisfy the Cardy gluing condition[12]:

$$\left(L_n - \overline{L}_{-n}\right)|B\rangle = 0, \quad \forall n \in \mathbb{Z}, \tag{1.12}$$

A 2d BCFT possesses a reduced but still infinite-dimensional Virasoro symmetry, so the energy momentum tensor still splits into a holomorphic and anti-holomorphic part. Thus, for a 2d BCFT, the energy momentum tensors T_L and $\overline{T_R}$ are separately conserved in the bulk, and their sum $T_{tot} = T_L + \overline{T_R}$ is conserved on the boundary. Any exchange of energy (fluctuations in the energy momentum tensor) between the two CFTs is measured by a relative spin-2 current $T_{rel} = c_R T_L - c_L \overline{T_R}$. In 2d, this is controlled by a single real transmission/reflection coefficient: $\mathcal{T} + \mathcal{R} = 1$ [4].

In the folded BCFT picture where we have boundary state $|B\rangle$, an energy transmission measure[15] can be defined as a 2×2 "transport matrix"[15]:

$$R_{IJ}(|B\rangle) = \frac{\langle\Omega|\, L_2^{[I]} \overline{L}_2^{[J]}\, |B\rangle}{\langle\Omega|\, B\rangle}, \quad I, J = \mathrm{L}, \mathrm{R}, \tag{1.13}$$

where $|\Omega\rangle = |\Omega_{\mathrm{L}}\rangle \otimes |\Omega_{\mathrm{R}}\rangle$ is the vacuum of the generic folded theory.

The transmission coefficient given in terms of the transport matrix's entries:

$$\mathcal{T}(|B\rangle) = \frac{2}{c_{\mathrm{L}} + c_{\mathrm{R}}} \left[R_{\mathrm{LR}}(|B\rangle) + R_{\mathrm{RL}}(|B\rangle)\right] \equiv \frac{2c_{\mathrm{LR}}(|B\rangle)}{c_{\mathrm{L}} + c_{\mathrm{R}}}. \tag{1.14}$$

The purely BCFT prescription for transmission coefficient relies on solving the boundary state, which may be an easy or difficult task depending on the actual conformal field theory. For the case of the free boson, this is manageable. For the

case of the symmetric orbifold theory away from the orbifold point where you'd have twist operators, this is hard to solve analytically.

One option can be to start with the ICFT picture where there are fields on both sides of the interface. Based on the (non-interacting) action, we can solve for the equations of motion for both the fields. This will provide (Neumann)boundary conditions/constraints on the fields which can be arranged in the form of an S matrix. Now, folding the ICFT to form a BCFT picture, the Virasoro gluing condition for the boundary is:

$$\left(L^i_m - S_{ij}L^j_{-m}\right)|b\rangle = 0 \tag{1.15}$$

where $m > 0$, $i, j = \mathrm{L}, \mathrm{R}$ and $S_{i,j}$ is the boundary constraints matrix.

$$\begin{aligned}|b\rangle &= \mathcal{N}\prod_{n=1}^{\infty}\exp\left(\frac{1}{n}a^i_{-n}\bar{a}^j_{-n}S_{ij}\right)|0\rangle \\ &= \mathcal{N}\left(1 + a^i_{-1}\bar{a}^j_{-1}S_{ij} + \frac{1}{2}(a^i_{-1}\bar{a}^j_{-1}S_{ij})^2 + a^i_{-2}\bar{a}^j_{-2}S_{ij} + \cdots\right)|0\rangle\end{aligned}$$

where $\mathcal{N}$ is a normalization constant, a^i_n and $\bar{a}^i_n$ are the modes of the fields ϕ^i, such that $[a^i_m, a^j_n] = m\delta_{m+n,0}\delta^{ij}$.

This expression can be used to write the transport matrix in terms of the S matrix, which can then be evaluated and used to find the transport coefficient.

1.4 Transmission Coefficient in semi-classical gravity

1.4.1 Holographic dual to a Boundary Conformal Field Theory

The holographic dual of a BCFT is constructed by Takayanagi [7] by extending the AdS spacetime N with a codimension-1 hypersurface Q, such that $\partial N = M \cup Q$. M is the conformal boundary with the BCFT and Q is a dynamical "end-of-the-world" brane that joins ∂M on the boundary. In this AdS/BCFT dual, Dirichlet boundary conditions are imposed on M, while a Neumann boundary condition is imposed on Q, making its embedding in the bulk dynamical. This configuration resembles the

Randall–Sundrum[16] braneworld setup, with a finite tension brane that modifies the bulk geometry and supports localized gravity.

The gravitational action in this setup is given by

$$I = \frac{1}{16\pi G_N}\int_N \sqrt{-g}\,(R - 2\Lambda) + \frac{1}{8\pi G_N}\int_Q \sqrt{-h}\,(K - T) \tag{1.16}$$

where h_{ab} is the induced metric on the brane Q, K is the trace of its extrinsic curvature, and T is the brane tension. Imposing the variational principle leads to the Neumann-type boundary condition:

$$K_{ab} - h_{ab}K = T\,h_{ab} \tag{1.17}$$

where K_{ab} is the extrinsic curvature tensor. This equation describes the brane's embedding in terms of its tension.

1.4.2 Holographic dual for ICFT picture

In the more general holographic interface setups, we have two AdS spacetimes (with different AdS radii if the CFTs have different central charge) joined across a hypersurface of finite fixed tension. The appropriate boundary conditions are the Israel junction conditions[4]:

$$h_{ab}^{(L)} = h_{ab}^{(R)} \tag{1.18}$$

$$[K_{ab}] - h_{ab}[K] = -8\pi G_N\,T\,h_{ab}, \tag{1.19}$$

where $[K_{ab}] = K_{ab}^{(L)} - K_{ab}^{(R)}$ and $[K] = K^{(L)} - K^{(R)}$ denote the jumps in extrinsic curvature tensor and its trace respectively across the interface. The first condition imposes continuity of the metric on the induced brane, and the second accounts for the discontinuity in the extrinsic curvature due to the localized brane tension.

For strongly-coupled CFTs, the gravitational dual may not have constant curvature, or it may have scalar fields that smoothly interpolate through the bulk between different asymptotic values at the boundary. Idealized thin-brane models with

localized stress-energy are not sufficient to provide an interpolation in the bulk. Chapter 2 of this thesis extended that work to a configuration of 2 stacked thin branes, which then formed the basis for Bachas and collaborators to further generalize the framework to thick branes[17], modeling smooth domain walls with finite thickness.

Consider Einstein gravity coupled to a scalar field. The action is given by:

$$I_{\rm gr} = \frac{1}{2}\int d^{n+1}x\,\sqrt{-g}\,[R - \partial_\mu\phi\,\partial^\mu\phi - 2V(\phi)]$$

The gravitational solution to this action is Janus: asymptotically AdS_{d+1} with the warping factor deforming smoothly, corresponding to changing curvature radius in the bulk. The scalar dilaton also interpolates smoothly between different asymptotic values. The idea of a piecewise bulk from Chapter 2 suggests that this geometry can be discretized. Non-constant smooth curvature of the bulk can be seen as a series of AdS_{d+1} slices of different radii ℓ_j, separated by thin (AdS_d) branes: like a "pizza" of AdS_{n+1} slices[17]. The radius ℓ_j of the j^{th} AdS_{d+1} slice will jump to radius ℓ_{j+1} of the $(j+1)^{th}$ AdS_{d+1} slice, sourced by a thin AdS_d brane with radius a_j and tension σ_j. In this thin-brane array model, the Israel junction conditions becomes:

$$\sigma_j a_j = \sqrt{\left(\frac{a_j}{\ell_j}\right)^2 - 1} - \sqrt{\left(\frac{a_j}{\ell_{j+1}}\right)^2 - 1}, \tag{16}$$

for $\ell_{j+1} > \ell_j$. The continuum limit of these boundary conditions satisfy the Einstein and scalar equations of the smooth Janus solution. For warped geometries, the matter energy-momentum tensor can be written in terms of a tension density as:

$$T^{\rm matter}_{\mu\nu} = -\Lambda\ g_{\mu\nu} - \frac{d\sigma}{dy}\Pi_{\mu\nu} \tag{1.20}$$

For the Janus solution, it takes the form:

$$T^{\phi}_{\mu\nu} = (\frac{1}{2}\partial^\rho\phi\partial_\rho\phi - V)g_{\mu\nu} - \partial^\rho\phi\partial_\rho\phi\Pi_{\mu\nu} \tag{1.21}$$

Comparing the two relates the tension density to the dilaton: $d\sigma = (\phi')^2 dy$. The varying dilaton's backreaction results in a tension density, which can be integrated to

give an effective tension for the Janus background. Using the effective tension in the double-brane analog instead of the summed tensions[4], yields a γ-exact holographic transmission coefficient. Chapters 3 and 4 build on these results to apply to brane-induced continuously warping geometries.

1.4.3 Fefferman–Graham formalism

Scattering gravitational waves at the boundary corresponds to fluctuations in the CFT stress-tensor. As discussed in the section on Holographic Principle, these are dual to the graviton in the bulk which arises from fluctuations in the metric tensor.

The Fefferman-Graham formalism [18], provides a systematic method to express asymptotically AdS spacetimes near the conformal boundary. It uses a special coordinates called Fefferman-Graham (FG) coordinates that include a foliation by hypersurfaces of constant radial coordinate ρ. The conformal boundary is located at $\rho \to 0$. In these coordinates, the bulk metric takes the form

$$ds^2 = \frac{\ell^2}{4\rho^2} d\rho^2 + \frac{1}{\rho} g_{ij}(x,\rho)\, dx^i dx^j \tag{1.22}$$

where ℓ is the AdS_{d+1} radius, and $g_{ij}(x,\rho)$ is a metric on slices of constant ρ expanded near the boundary as:

$$g(x,\rho) = g^{(0)}(x) + \rho\, g^{(2)}(x) + \cdots + \rho^{d/2}\big(g^{(d)}(x) + \log\rho\, h^{(d)}(x)\big) + \cdots . \tag{1.23}$$

The term $g^{(d)}(x)$ is not fixed by localized data and instead relates to the expectation value of the dual stress tensor. The logarithmic term $h^{(d)}(x)$ appears only when d is even and captures the conformal anomaly.

For $d \geq 3$, the expectation value of the renormalized stress tensor is given as:

$$\langle T_{ij} \rangle = \frac{d\ell^{d-1}}{16\pi G_N}\, g_{ij}^{(d)} + X_{ij}[g^{(0)}] \tag{1.24}$$

where G_N is the Newton constant in $(d+1)$ dimensions, and $X_{ij}[g^{(0)}]$ accounts for trace anomalies when d is even. The term $g_{ij}^{(d)}$ captures the non-local state-dependent information and is the leading non-trivial contribution to $\langle T_{ij} \rangle$.

An important exception occurs in $d = 2$, corresponding to asymptotic AdS_3, where the expansion truncates and the entire bulk metric is determined algebraically by the boundary data and the Brown-Henneaux conditions. In this case, the stress tensor is fully determined by $g_{ij}^{(2)}$.

1.4.4 Transmission coefficient in semi-classical gravity

Scatter the incoming monochromatic waves from one side (left), proportional to some coefficient I_L. The transmission coefficient $\mathcal{T}_L$ is defined as proportional to the transmitted gravitational wave on the right side, and the reflection coefficient $\mathcal{R}_L$ is proportional to the reflected wave on the left side[4]. These fluctuations source the metric. Writing the metric in Fefferman-Graham co-ordinates, the expectation value of the stress tensor can be expressed as vacuum expectation value (vev) of the incoming flux ϵ. Previously, Einstein's linearized equations were solved to give Israel Junction conditions in the various cases discussed above. Imposing the junction conditions to linear order in ϵ gives us a system of equation to solve for $\mathcal{T}_L$.

The prescription is extended in Chapter 2 to a double brane holographic model where we stack two interfaces. For interfaces which are holographically described by continuous $(d+1)$-dimensional bulk geometries that can be foliated into AdS_d slices, we essentially reduce them to asymptotically AdS_3 geomertries where there is an "effective" tension for the thick-brane prescription to apply. In applying these, we have to be cautious in case there are other fields sourced by the fluctuation, such as dilatons, axions, etc. In that case, their equations of motion should also be satisfied.

1.5 Boundary Entanglement Entropy

Entanglement entropy quantifies the quantum correlations between a spatial subregion and its complement in a given quantum state. For a quantum system with density matrix ρ and region A, the reduced density matrix ρ_A is obtained by tracing out degrees of freedom in the complement A^c: $\rho_A = \mathrm{Tr}\ A^c$. The entanglement entropy

is given by the von Neumann entropy $S_A = -\mathrm{Tr}(\rho_A \log \rho_A)$.

Entanglement entropy in BCFTs was pioneered by Calabrese and Cardy[19], who used the replica trick, a technique that expresses S_A in terms of the limit $n \to 1$ of $\mathrm{Tr}(\rho_A^n)$. This maps the problem to computing partition functions on n-sheeted Riemann surfaces branched over the entangling region A, incorporating boundary effects through twist operator insertions. In the BCFT setup, the theory is defined on a half-plane or an interval with boundary conditions specified along the spatial boundary. For an interval $A = [0, \ell]$ adjacent to the boundary at $x = 0$, this procedure yields the universal answer[20]:

$$S_A = \frac{c}{6} \log \left(\frac{\ell}{\epsilon} \right) + \log g \tag{1.25}$$

where c is the central charge, ϵ is the UV cutoff, and $\log g$ is the boundary entropy. The $\log g$ term captures the boundary degrees of freedom and appears as a universal constant additive correction to the entanglement entropy, distinct from the leading bulk logarithmic scaling. Crucially, it obeys the g-theorem: under RG flow, it decreases monotonically from the UV to the IR fixed points $g_{\mathrm{UV}} > g_{\mathrm{IR}}$, showing the loss of boundary degrees of freedom while the bulk remains conformal.

Thus, boundary entanglement entropy fits naturally into the AdS/BCFT holography setup discussed above[7]. The bulk spacetime N with conformal boundary M has an end-of-the-world brane Q, such that $\partial N = M \cup Q$, and Q ends on ∂M, the boundary of the BCFT. The holographic entanglement entropy for a boundary region $A \subset M$ can be computed using the Ryu–Takayanagi prescription[21], which states

$$S_A = \frac{\mathrm{Area}(\gamma_A)}{4G_N} \tag{1.26}$$

where γ_A is the codimension-2 minimal surface in the bulk anchored on the boundary of A on M and possibly ending on the brane Q, and G_N is Newton's constant in the bulk. The holographic calculation reproduces the universal $\log g$ term. The geometry and tension of Q affect the minimal surface area γ_A. This correspondence between the boundary entropy $\log g$ and a geometric quantity (minimal area in the bulk) provides a powerful tool for studying boundary RG flows.

Chapter 2: Double brane holographic model dual to 2d ICFTs[1]

Abstract

A minimal single brane holographic model can be used as a dual to 2d conformal interfaces (ICFTs) to calculate the transmission coefficient $\mathcal{T}$ of energy transported across the defect as well as boundary entropy $\log g$, the additional entanglement entropy for some sub-region that encloses the defect. Both $\mathcal{T}$ and $\log g$ are uniquely determined by the tension characterizing the brane. In contrast, in field theory defects, typically the transmission coefficient can be dialed from 0 to 1 independently for each allowed value of $\log g$. To address this discrepancy, we look at a double-brane (3-region bulk) holographic model. Merger of two single brane interfaces creates genuinely new interfaces which indeed allow a range of accessible transmission coefficients for a fixed value of $\log g$. In particular, the $\mathcal{T} = 0$ limit of two completely decoupled BCFTs can be achieved.

2.1 Introduction

Conformal interfaces refer to the local gluing of two scale-invariant conformal field theories, CFT_L and CFT_R. Such interfaces are well studied in condensed matter physics, in describing junctions [22], defects in Ising Models [23], etc, as well as in the string theory literature [10]. This work considers 1+1 dimensional CFTs where the interface is a point-like defect, and bottom-up AdS/CFT correspondence gives the

[1]Published in JHEP with Andreas Karch

dual holographic model as an AdS_3 geometry with a codimension-one brane representing the defect, anchored at the boundary [24, 25, 26]. CFT_L and CFT_R have central charges c_L and c_R respectively, and their corresponding holographic duals $AdS_{3,L}$ and $AdS_{3,R}$ have radii l_L and l_R. The Brown-Henneaux formula $c_{L,R} = 3l_{L,R}/2G$ [27] relates the two where G is the 3 dimensional Newton's constant.

Recent studies use this holographic model to evaluate two properties for 2d ICFTs: a transmission coefficient of energy transported across the defect [4], and entanglement entropy for some sub-region of length a, that encloses the defect [8, 28]. Our work probes this defect further by looking at the behaviour of these properties under the fusion of two point-like defects, in the limit that they lie on top of one another. This gives a wedge-shaped bulk with AdS_3 radius l_C for the 'centre' region between the two defects. Our double brane holographic model gives closed form expressions for $\mathcal{T}$ and $\log g$ that clearly show the merger of two single brane defects can not be described by another single brane defect. There is no closed algebra to describe the fusing behaviour for these general single brane 2d ICFTs, unlike what is present in critical defects in 2d Ising Models [29, 30] and other well understood CFTs [31]. The allowed interfaces in an ICFT must form a closed algebra under fusion. Therefore, multi-brane defects can either be considered as genuinely new objects in the system or as a non-trivial quantum superposition of existing defects. We'll argue that the former is this case and so fusion only has a chance of closing in this extended space of allowed interfaces. Presumably, the underlying reason for this failure of fusion to close on the single brane defects is the large N limit that is required in any holographic theory. One would expect that quantum effects allow a multi-brane interface with N branes, where N is a large integer related to the central charge, to become equivalent to a single brane interface, very much like in the Ising model where a fusion of two branes with $g = \sqrt{2}$ does not yield a new brane with $g = 2$ but instead a superposition of two separate $g = 1$ theories. [29, 30]. Such a purely quantum effect clearly will not be visible in our large N classical limit holographic setting. The fact that multi-brane interfaces can be used to enlarge the space of

allowed holographic interfaces has also been recently used in [32] in the context of the co-bordism conjecture.[33]. Unlike in our case with a small intermediate region, they consider triple CFT interfaces.

We show that multi-brane interfaces permit the bottom-up holographic defect to sustain more tension and therefore allow increasingly more reflection while maintaining AdS_3 geometry. With 2 branes, the transmission coefficient can be dialed to 0 by setting l_C to 0, regardless of the values of $l_{L,R}$. Increasing the number of defects fused together also enables imposing reflecting boundary conditions ($\mathcal{T} \to 0$) for the same AdS radius describing all regions.

The paper is organized as follows. In section 2, we describe the scattering states in the double brane holographic model, compute the transmission coefficient and comment on its useful limits. In section 3, we use the constraints from the double brane model to evaluate the additional entanglement entropy $\log g$ and present the results for a specific $\mathbb{Z}_2$ parity symmetry. In the last section, we conclude and discuss possible future work. Appendix A contains the details of the linear order differential system solved to obtain the transmission coefficient result and in appendix B, we present expressions for $\log g$ in the general double brane model.

2.2 Transmission coefficient for the double brane model

2.2.1 Review: Single brane toy model

In order to use established properties of B(oundary)CFTs, the ICFT can be mapped to a BCFT of the product theory $\mathrm{CFT}_L \otimes \overline{\mathrm{CFT}_R}$ by folding spacetime along the interface. The BCFT conserves energy momentum tensors T_L and $\overline{\mathrm{T}_R}$ separately in the bulk, and their sum on the boundary. It also conserves a relative spin-2 current $\mathrm{T}_{rel} = c_R \mathrm{T}_L - c_L \overline{\mathrm{T}_R}$ that measures the relative exchange of energy across the interface between the two CFTs. In 2d, this exchange of energy can be expressed using a single real transmission or reflection coefficient [15], which is computed using a toy holographic model.

The toy model is given by two AdS_3 slices separated by a string of tension σ [6, 24, 26, 10]. The AdS_3 slices have radius l_L and l_R. The string's worldsheet geometry is AdS_2, corresponding to the ground state of the ICFT for the following tension range [24]:

$$\left|\frac{1}{l_L} - \frac{1}{l_R}\right| \leq 8\pi G\sigma \leq \frac{1}{l_L} + \frac{1}{l_R} \tag{2.1}$$

The lower tension bound corresponds to the Coleman De Lucia bound [34]. Below this, the space with the higher AdS_3 radius ('false vacuum') is unstable to the nucleation of bubbles (which permit 'decays' between vacua). However, since for decays in AdS tunnelling is not always allowed (the false vacuum can be stable) or when allowed, the endpoint cannot be the true vacuum, this can't always be understood in terms of vacuum decay. Instead it is more useful to interpret it as holographic RG flows between conformal fixed points [35]. The upper tension bound corresponds to the Randall-Sundrum fine tuned tension beyond which the string worldsheet geometry becomes de-Sitter [16].

2.2.2 Fusion of interfaces: 3-region holographic model

Consider two distinct interfaces (CFTs prescribed for three regions) and then shrink the intermediate region's size to 0 so the interfaces lie on top of one another. In this limit, the 1+1 dimensional ICFT can be represented by this new 3-region 'double brane' holographic model, as shown in Figure 2.1. The main idea is to check if this double brane model belongs in the same class as the single brane models. If fused interfaces belong to a different class, then this technique may help complete the classification of holographic defects and check if they compose under an algebra.

In a single defect holographic setting, the tension σ uniquely determines $\mathcal{T}$ and g. In contrast, as emphasized in the introduction, in field theories all values of the transmission coefficient $\mathcal{T}$ are realizable for a given g [29]. $\log g$ is the additional entanglement entropy due to the presence of a defect within the given sub-system (of length a) [20, 36, 8]. For a symmetric interval, the entanglement entropy takes a

form [8, 26] that agrees with the standard BCFT result [36] for a BCFT with central charge $c_L + c_R$:

$$EE = \frac{c_L + c_R}{6} \log\left(\frac{a}{\epsilon}\right) + \log g \tag{2.2}$$

We find that indeed fused interfaces are genuinely different from single brane defects, with an infinite number of classes possible, where the g values increase unbounded and the transmission coefficient is given by the sum of the allowed tensions. This classification of defects is in contrast with the Ising model where g values can be used to classify between Ising models with Neumann and Dirichlet boundary conditions, and fusion of defects follows the Verlinde algebra.

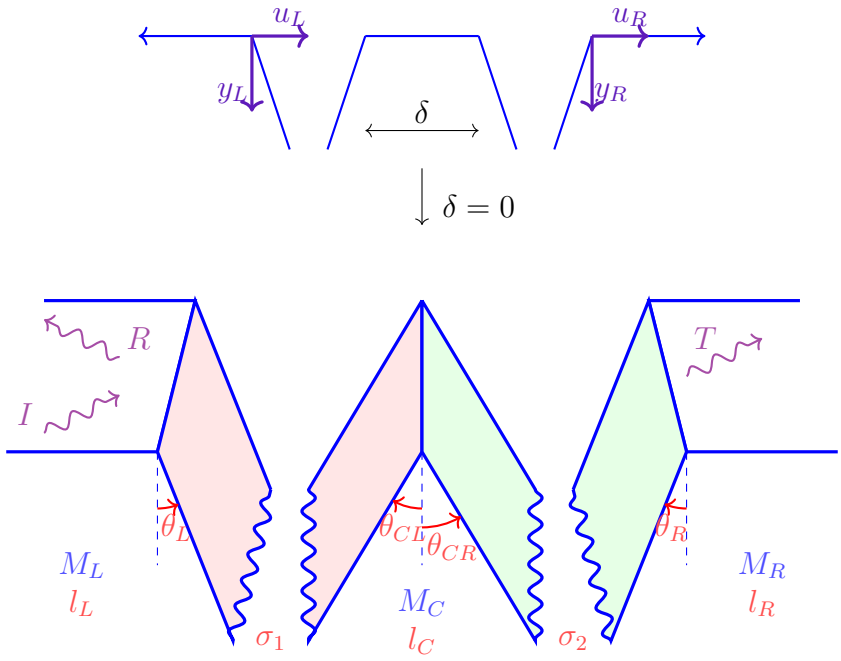

Figure 2.1: The 3 region holographic model representing the fusion of two defects. I is the gravitational wave scattered from the left, and R and T are the reflected and transmitted waves on the left and right of the interface respectively.

2.2.3 Holographic scattering states

We use a 3-region holographic model for the ICFT, consisting of three locally AdS_3 manifolds M_L, M_C and M_R with radii l_L, l_C and l_R respectively. The asymptotic boundaries of M_L and M_R are the left and right half-planes of the CFT glued along the interface. The asymptotic boundary of M_C is a single line that gives the worldline of the same interface. The interface extends in the bulk as two pairs of branes and a central region M_C: the branes from M_L and the left side of M_C are identified with each other as the worldsheet of one tensile string and the branes from M_R and the right side of M_C are identified with one another and as the worldsheet of a second tensile string. This identification implies that the M_C wedge always has a 'non-negative length.' While solving (2.27) which arises from these matching conditions, we obtain conditional solutions that give valid tension bounds. For an M_C wedge found entirely on either side of the interface line, a 'non-negative length' requirement gives a lower bound on σ_2 which depends on σ_1 (or vice versa) and, while it can be written in closed form, it does not appear illuminating. Therefore, going forward, we will only present scenarios where the wedge extends on both sides of the interface line and we can write down independent bounds for σ_1 and σ_2.

For the case where $l_{L,R} > l_C$, the tension bounds are given as [4, 37]:

$$\frac{1}{l_C} - \frac{1}{l_L} \leq 8\pi G\sigma_1 \leq \frac{1}{l_L} + \frac{1}{l_C} \qquad \frac{1}{l_C} - \frac{1}{l_R} \leq 8\pi G\sigma_2 \leq \frac{1}{l_C} + \frac{1}{l_R} \tag{2.3}$$

As it turns out, for $l_{L,R} > l_C$ the only wedge possible extends on both sides of the interface line. But for other scenarios where one or both of l_L and l_R are smaller than l_C, the wedge may extend on both sides, or just one. In those scenarios, while imposing a central wedge that occurs on both sides of the interface permits σ_1 and σ_2 to be independently dialed in the solutions, it does constrain the lower bound to a higher value than the Coleman De Lucia bound in (2.3).

For $l_{L,R} < l_C$, while maintaining a central wedge on both sides of the interface

line, the tension bounds are:

$$\sqrt{\frac{1}{l_L^2}-\frac{1}{l_C^2}} \leq 8\pi G\sigma_1 \leq \frac{1}{l_L}+\frac{1}{l_C}, \qquad \sqrt{\frac{1}{l_R^2}-\frac{1}{l_C^2}} \leq 8\pi G\sigma_2 \leq \frac{1}{l_C}+\frac{1}{l_R} \tag{2.4}$$

This new lower bound on tension also appears in [37] as a critical tension in a finite temperature AdS/CFT model[2].

For $l_L > l_C > l_R$, while maintaining a central wedge on both sides of the interface line, the tension bounds span:

$$\frac{1}{l_C}-\frac{1}{l_L} \leq 8\pi G\sigma_1 \leq \frac{1}{l_C}+\frac{1}{l_L}, \qquad \sqrt{\frac{1}{l_R^2}-\frac{1}{l_C^2}} \leq 8\pi G\sigma_2 \leq \frac{1}{l_C}+\frac{1}{l_R} \tag{2.5}$$

Similarly, for $l_L < l_C < l_R$, while maintaining a central wedge on both sides of the interface line, the tension bounds span:

$$\sqrt{\frac{1}{l_L^2}-\frac{1}{l_C^2}} \leq 8\pi G\sigma_1 \leq \frac{1}{l_L}+\frac{1}{l_C}, \qquad \frac{1}{l_C}-\frac{1}{l_R} \leq 8\pi G\sigma_2 \leq \frac{1}{l_C}+\frac{1}{l_R} \tag{2.6}$$

As we will see in Section 2.4, the lower tension bounds correspond to upper bounds on the transmission coefficient which is the same as the one following the achronal average-null-energy condition (AANEC). Therefore, this nuanced behaviour of the tension bounds and the position of the central wedge is noteworthy even though it isn't a feature directly observable from the boundary CFTs.

Our model has several parameters. In addition to the asymptotic curvature radii l_L and l_R, which specify the central charges of the two CFTs connected by the interface, we have to specify several model parameters characterizing the interface itself: the central curvature radius l_C and the string tensions σ_1 and σ_2. For the purposes of presenting our results, it is convenient to cut models down to a slightly smaller parameter space. One way to do this in a consistent manner is to restrict to systems which respect a $\mathbb{Z}_2$ parity symmetry across the interface. Obviously, this

[2]Below this value, the hot solution disappears for some part of the parameter space.

parity symmetric scenario is only possible if $l_L = l_R$, as well as $\sigma_1 = \sigma_2$. While more general forms of the results can be obtained, we will use the restricted parameter space when we are presenting our results in Figures 2.3, 2.4, 2.5 and 2.6. The expressions for the general case are relegated to the appendix. For convenience we'll use τ_1 and τ_2 for the respective tensions with $\tau_1 = 8\pi G\sigma_1$ and $\tau_2 = 8\pi G\sigma_2$.

While in our drawing in Figure 2.1 it appears that we are describing 4 branes, the right most brane of the left wedge is really the same brane as the left brane of the central wedge. These are one and the same object across which the various spacetime wedges get glued together. The same is true for the second apparent pair of branes. This identification between the branes translates to an identification of the metrics on the branes. In addition, we can use the Israel Junction conditions [38] to assign the jump in the extrinsic curvature tensor across a brane to the tension of the corresponding string. Together these matching conditions are given by:

$$\gamma_{L,\alpha\beta} = \gamma_{CL,\alpha\beta} \tag{2.7a}$$

$$\gamma_{CR,\alpha\beta} = \gamma_{R,\alpha\beta} \tag{2.7b}$$

$$K_{L,\alpha\beta} - K_{CL,\alpha\beta} - tr(K_L - K_{CL})\gamma_{L,\alpha\beta} = \tau_1\gamma_{L,\alpha\beta} \tag{2.7c}$$

$$K_{CR,\alpha\beta} - K_{R,\alpha\beta} - tr(K_{CR} - K_R)\gamma_{R,\alpha\beta} = \tau_2\gamma_{R,\alpha\beta} \tag{2.7d}$$

where $\gamma_{L,CL,CR,R}$ and $K_{L,CL,CR,R\alpha\beta}$ are the induced metric and extrinsic curvature tensor on the branes suspended by $M_{L,C,R}$ respectively.

In pure AdS_3, Einstein's equations can be solved completely and the full solution for the metric in Fefferman-Graham co-ordinates can be written as [39]:

$$ds^2 = \frac{l^2 dy^2}{y^2} + \left[\frac{l^2}{y^2}g^{(0)}_{\alpha\beta} + g^{(2)}_{\alpha\beta} + \frac{y^2}{4l^2}g^{(4)}_{\alpha\beta}\right] dw^\alpha dw^\beta \tag{2.8}$$

with $g^{(4)} = g^{(2)}(g^{(0)})^{-1}g^{(2)}$. For a flat boundary metric, we can furthermore identify $g^{(2)}_{\alpha\beta} = 4Gl < T_{\alpha\beta} >$ with $< T_{\alpha\beta} >$ being the vacuum expectation value of the canonically-normalized, traceless conserved energy-momentum tensor in some state of the dual CFT.

Therefore the ICFT vacuum metric in Fefferman-Graham co-ordinates for the three regions is given by [24]:

$$\begin{aligned} ds_L^2 &= \frac{l_L^2}{y_L^2}\left[dy_L^2 + du_L^2 - dt_L^2\right] \qquad u_L \leq y_L \tan\theta_L \\ ds_R^2 &= \frac{l_R^2}{y_R^2}\left[dy_R^2 + du_R^2 - dt_R^2\right] \qquad u_R \geq y_R \tan\theta_R \\ ds_C^2 &= \frac{l_C^2}{y_C^2}\left[dy_C^2 + du_C^2 - dt_C^2\right] \qquad y_C \tan\theta_{CL} \leq u_C \leq y_C \tan\theta_{CR} \end{aligned} \tag{2.9}$$

where $0 < y_{L,R,C} < \infty$ and the branes subtend at angles where the inequalities saturate.

In general, all the angles $\theta_{L,R,CL,CR}$ can be positive or negative as long as they satisfy $(\theta_{CL} - \theta_{CR}) > 0$ which imposes that some non-zero central region exists. For the M_C wedge extending on both sides of the interface, $\theta_{CL} < 0$ and $\theta_{CR} > 0$ while θ_L and θ_R can be positive or negative, subject to the AdS radii and tension bounds.

Like the setup in [14, 4], we consider right-moving monochromatic gravitational wave excitations coming from the left side on the surface. We solve the matching equations in (2.7) up to linear order in ϵ, the magnitude of the incoming flux, following the technique in [4]. This allows us to drop the $g^{(4)}$ term from the full metric solution and the correction to the AdS_3 Poincare metric just has arbitrary left and right moving waves $g^{(2)}_{++}(w^+)$ and $g^{(2)}_{--}(w^-)$. Here we can identify $w^\pm$ as $u \pm t$.

The incoming surface monochromatic wave from the left undergoes reflections and transmissions at both branes, leading to a reflected and transmitted wave on the surface of M_L and M_R respectively, with a left and right moving wave in M_C. Incoming excitation corresponds to $\langle T_{--}\rangle$ and all subsequent reflections/transmissions are expressed in terms of this, the reflection/transmission coefficient from the corresponding boundary and the corresponding left/right moving exponential. The corrections

to the AdS_3 Poincare metrics in the three regions are given as:

$$\begin{aligned}
[ds_L^2]^{(2)} &= 4Gl_L\epsilon\left[e^{iw(t_L-u_L)}d(t_L-u_L)^2+\mathcal{R}_{L1}e^{iw(t_L+u_L)}d(t_L+u_L)^2\right]+c.c.\\
[ds_C^2]^{(2)} &= 4Gl_C\epsilon\left[\mathcal{T}_{L1}e^{iw(t_C-u_C)}d(t_C-u_C)^2+\mathcal{R}_{L2}e^{iw(t_C+u_C)}d(t_C+u_C)^2\right]+c.c.\\
[ds_R^2]^{(2)} &= 4Gl_R\epsilon\left[\mathcal{T}_{L2}e^{iw(t_R-u_R)}d(t_R-u_R)^2\right]+c.c.
\end{aligned} \tag{2.10}$$

where $|\langle T_{--}\rangle| = \epsilon$ is the magnitude of the incoming flux and $\mathcal{R}_{L1}, \mathcal{T}_{L1}, \mathcal{R}_{L2}$ and $\mathcal{T}_{L2}$ are the a priori complex relative amplitudes of the reflected and transmitted waves from the first and second brane respectively. The subscript L indicates the incident wave originated on the left hand side.

In order to glue the metrics on the branes, it will first be easier to rotate from the Poincare co-ordinates to those parallel(z) and perpendicular(x) to each brane. This rotation is given by:

$$\begin{pmatrix} u_L \\ y_L \end{pmatrix} = \begin{pmatrix} \cos\theta_L & \sin\theta_L \\ -\sin\theta_L & \cos\theta_L \end{pmatrix} \begin{pmatrix} x_L \\ z_L \end{pmatrix} \tag{2.11}$$

$(x_R, z_R), (x_{CL}, z_{CL}), (x_{CR}, z_{CR})$ transform similarly using their respective angles θ_R, θ_{CL} and θ_{CR}.

Gluing one pair of branes together requires matching co-ordinates on the world-sheet that gives the AdS_2 vacuum metric. Additionally, due to time translation invariance, the co-ordinates can be defined for a fixed frequency w. Such co-ordinates can be expressed as:

$$\begin{aligned}
t_L &= t_1+\tilde{\epsilon}e^{iwt_1}\lambda_L[z_1], & z_L &= z_1+\tilde{\epsilon}e^{iwt_1}\zeta_L[z_1], & x_L &= \tilde{\epsilon}e^{iwt_1}\delta_L[z_1].\\
t_R &= t_2+\tilde{\epsilon}e^{iwt_2}\lambda_L[z_2], & z_R &= z_2+\tilde{\epsilon}e^{iwt_2}\zeta_R[z_2], & x_R &= \tilde{\epsilon}e^{iwt_2}\delta_R[z_2].\\
t_{CL} &= t_1+\tilde{\epsilon}e^{iwt_1}\lambda_{CL}[z_1], & z_{CL} &= z_1+\tilde{\epsilon}e^{iwt_1}\zeta_{CL}[z_1], & x_{CL} &= \tilde{\epsilon}e^{iwt_1}\delta_{CL}[z_1].\\
t_{CR} &= t_2+\tilde{\epsilon}e^{iwt_2}\lambda_{CR}[z_2], & z_{CR} &= z_2+\tilde{\epsilon}e^{iwt_2}\zeta_{CR}[z_2], & x_{CR} &= \tilde{\epsilon}e^{iwt_2}\delta_{CR}[z_2].
\end{aligned} \tag{2.12}$$

where (t_1, z_1) and (t_2, z_2) are the Poincare cooridnates on the AdS_2 metrics for the first and second brane respectively. $\tilde{\epsilon} = \frac{4G\epsilon}{l_{S1,S2}}$ is used for convenience.

Applying the matching conditions to the ICFT vacuum (0 order in ϵ) for the induced metric shows that the worldsheet metric is AdS_2 with radius l_{S1} and l_{S2} for the left and right tensile strings respectively and gives the first two equalities in (2.13). The jump in the extrinsic curvature condition gives the last equality:

$$\begin{aligned} l_{S1} &= \frac{l_L}{\cos\theta_L} = \frac{l_{CL}}{\cos\theta_{CL}} = \frac{\tan\theta_L - \tan\theta_{CL}}{\tau_1} \\ l_{S2} &= \frac{l_{CR}}{\cos\theta_{CR}} = \frac{l_R}{\cos\theta_R} = \frac{\tan\theta_{CR} - \tan\theta_R}{\tau_2} \end{aligned} \tag{2.13}$$

Applying matching conditions of order 1 in ϵ leads to a set of linearized differential equations instead of simplified constraints as above. The differential equations and their solutions are presented in Appendix A. Below, we will only highlight that instead of the 12 unknown functions we've used to describe the co-ordinates, what actually appears in the differential equations are re-parametrizations of the above functions, some of which represent physical sources that can fluctuate the interface in different ways.

There are 12 unknown functions and 12 matching equations (symmetric metric and tensors). However, the extrinsic curvature tensor's elements are not all independent as they obey a momentum constraint. Thus, Israel junction condition gives 1 equation instead of 3. That leaves a total of 8 constraints and 12 functions. Due to a re-parametrization, only the following functions actually appear:

$$\begin{aligned} \lambda_1 &= \lambda_L - \lambda_{CL}, \qquad \zeta_1 = \zeta_L - \zeta_{CL}, \\ \lambda_2 &= \lambda_{CR} - \lambda_R, \qquad \zeta_2 = \zeta_{CR} - \zeta_R. \end{aligned} \tag{2.14}$$

Thus, there are 8 constraints and 8 functions. Furthermore, the matching equations are expressed neatly using the following definitions:

$$\begin{aligned} D_1 &= \delta_L - \delta_{CL}, \qquad \Delta_1 = \tan\theta_L\delta_L - \tan\theta_{CL}\delta_{CL} - \zeta_1, \\ D_2 &= \delta_{CR} - \delta_R, \qquad \Delta_2 = \tan\theta_{CR}\delta_{CR} - \tan\theta_R\delta_R - \zeta_2. \end{aligned} \tag{2.15}$$

The $z_1 = 0$ and $z_2 = 0$ limits of these functions correspond to sources in the dual ICFT - fluctuating the interface. $D_1(0)$ and $D_2(0)$ are sources for the interface displacement operator and $\lambda_1(0)$ and $\lambda_2(0)$ for an operator reparametrizing the interface.

Appendix A can show that only the re-parametrizations stated above appear as variables in the differential equations. You can solve for the homogeneous solution to the differential equations, that is where no gravitational waves are scattered at the boundary. The homogeneous solutions for λ_1, ζ_1 and λ_2, ζ_2 all comprise of linear combinations of solutions going in and out of the horizon (travelling along the branes). The coefficients for those modes are labelled a_{1-}, a_{1+} and a_{2-}, a_{2+}. The solution for D_1 and D_2 are constants.

However, for a non-fluctuating interface such as the one we have, we need to set the sources to zero. For example $D_1(0) = 0 \rightarrow \delta_L(0) = \delta_{CL}(0)$ so there is no relative displacement of the interface. For the homogeneous solutions, this sets the constants for D_1 and D_2 to 0. Imposing the other sources to 0 at the boundary ends up setting all the incoming and outgoing solutions on both the right and left branes to 0. Therefore, no solutions in the empty background can be supported by a purely non-fluctuating interface.

2.2.4 Results and comments

We can solve for the particular solution to the full differential equations, which is present in Appendix A. Considering the non-fluctuating interface, we set all the sources to go to 0 at the boundary.

$D_1(0) = 0$ and $D_2(0) = 0$ gives:

$$\mathcal{R}_{L1} + \mathcal{T}_{L2} = 1 \tag{2.16}$$

$\lambda_1(0) = 0$, $\zeta_1(0) = 0$, and $\lambda_2(0) = 0$, $\zeta_2(0) = 0$ give expressions for the modes going in and out of the horizon: $a_{1-}, a_{1+}, a_{2-}, a_{2+}$ (travelling along the branes in both directions, for both branes). These expressions can be found in Appendix A.

We now impose the physical condition that both the modes coming out of the horizon, a_{1+} and a_{2+}, should be removed as they are not physical [40, 41]. So $D_1(0) = 0$, $D_2(0) = 0$, $a_{1+} = 0$ and $a_{2+} = 0$ give expressions for the transmission/reflection

coefficients. The expressions are in terms of the angles, and can be found in Appendix A. Simplifying them using the relations from (2.13), we obtain:

$$\mathcal{T}_{L2} = \frac{2}{l_L}\left(\frac{1}{l_L} + \frac{1}{l_R} + \tau_1 + \tau_2\right)^{-1} \tag{2.17}$$

Note that the AdS radius of the central region plays an important role in constraining the bounds of the tensions but does not explicitly appear in the expression for transmission or reflection coefficient on either side of the physical CFT regions with non-zero length. In particular, to take the limit of $l_C \to 0$ the tensions $\tau_{1,2}$ have to go to infinity and the transmission vanishes. This allows a manifest bulk realization of the limit of two decoupled BCFTs: there is simply no space left in the middle wedge to connect the two BCFTs.

The transmission and reflection coefficient for the waves that would live within the central region is given by:

$$\begin{aligned} \mathcal{R}_{L2} &= \frac{l_C}{2}\left(\frac{1}{l_R} - \frac{1}{l_C} + \tau_2\right)\mathcal{T}_{L2} \\ \mathcal{T}_{L1} &= \frac{l_C}{2}\left(\frac{1}{l_R} + \frac{1}{l_C} + \tau_2\right)\mathcal{T}_{L2} \end{aligned} \tag{2.18}$$

To highlight the difference in how the transmission coefficient depends on the AdS radius, consider the transmission coefficient for the single tensile string case [4]:

$$\mathcal{T}_{L} = \frac{2}{l_L}\left(\frac{1}{l_L} + \frac{1}{l_R} + \tau_1\right)^{-1} \tag{2.19}$$

$\mathcal{T}_{L2}$ in (2.19) and (2.17) has the same form as a function of τ_1 and the net tension $(\tau_1 + \tau_2)$ respectively but it is important to keep in mind that the 3-region model has additional freedom in l_C. Figure 2.2 shows the different transmission coefficient curves for the 2-region model (2.19) for various combinations of l_L and l_R. Figure 2.3 shows the transmission coefficient (2.17) for the parity symmetric 3-region model ($l_L = l_R$ and $\tau_1 = \tau_2$) for different l_C values. For a given l_L and l_R, figure 2.2 gives a single transmission coefficient curve dialled by tension with a

fixed beginning and end point, while in figure 2.3, different l_C values correspond to segments[3] (transmission curves dialled by the tension) on an overall curve. For a given l_L and l_R, fixing the tension (the only parameter) in the 2-region model gives exactly one point on the transmission curve. The important difference in the parity symmetric 3-region model is that we can instead fix l_C and cover a finite range of transmission values by dialling the other parameter, tension. Here we fix l_C but alternatively we could choose to fix g instead.[4] Either way, a range of transmission coefficients are possible.

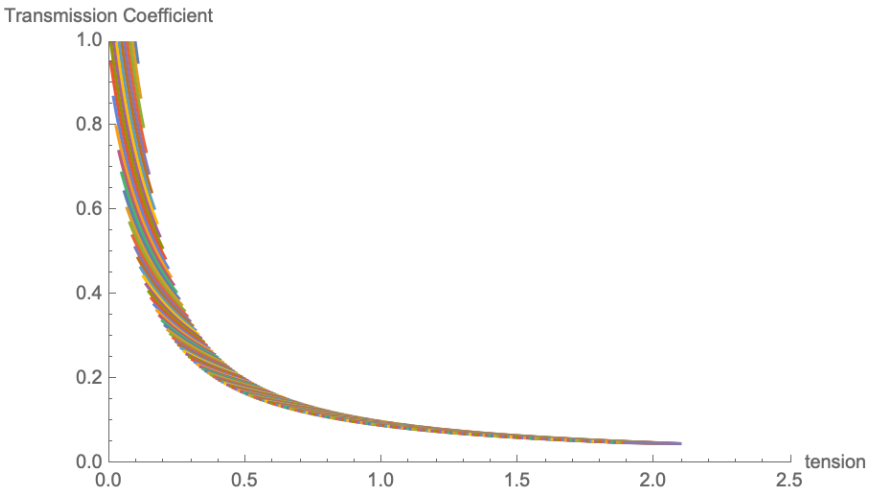

Figure 2.2: Transmission coefficient for the 2-region holographic model for different l_L and l_R where l_L/l_R ranges from 0.05 to 20.

Besides the difference in the way in which the transmission coefficient depends on the boundary's radius and the center's radius, the other difference is in the range of transmission coefficient values as one goes from the 2-region to the 3-region model. The lower and upper bounds for the transmission coefficient can be obtained by using

[3]Segments may overlap.

[4](In the interest of completeness, let us say in advance) For a fixed $l_{L,R}$ and log g, the single brane corresponds to one tension and therefore one point on the transmission curve, but for the double brane, it correlates to multiple possible (l_C values and so) tensions and therefore multiple points on the transmission coefficient curve.

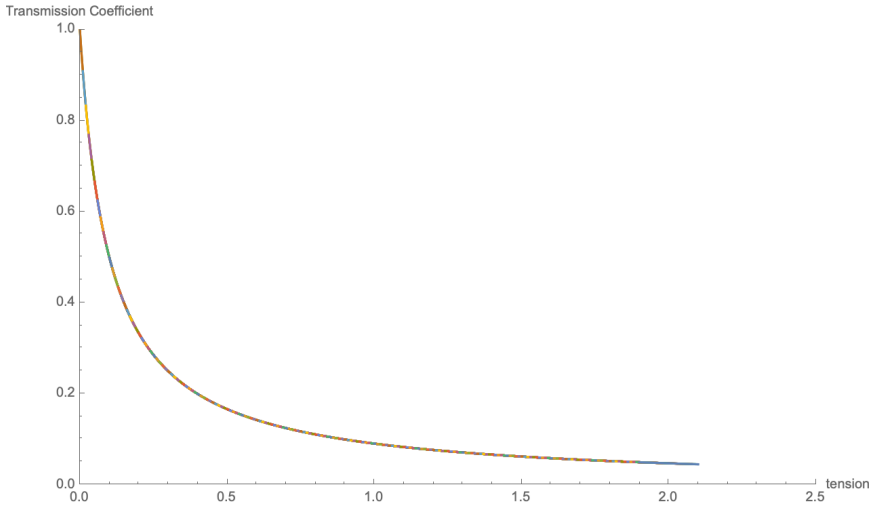

Figure 2.3: Transmission coefficient for the 3-region holographic model where we consider a symmetric fusion of defects $l_L = l_R$ and $\tau_1 = \tau_2$, where l_L/l_C ranges from 0.05 to 20.

the upper and lower limits of tensions respectively. $\mathcal{T}_{L2}$'s upper bound would differ depending on how the AdS radii vary.

$$\mathcal{T}_{L2_{min,all}} = \left(1 + \frac{l_L}{l_R} + \frac{l_L}{l_C}\right)^{-1}$$

$$\mathcal{T}_{L2_{max,A}} = \frac{l_C}{l_L}$$

$$\mathcal{T}_{L2_{max,B}} = \frac{2}{1 + \frac{l_L}{l_R} + \sqrt{1 - (\frac{l_L}{l_C})^2} + \sqrt{(\frac{l_L}{l_R})^2 - (\frac{l_L}{l_C})^2}}$$

$$\mathcal{T}_{L2_{max,C}} = \frac{2}{\frac{l_L}{l_R} + \frac{l_L}{l_C} + \sqrt{(\frac{l_L}{l_R})^2 - (\frac{l_L}{l_C})^2}}$$

$$\mathcal{T}_{L2_{max,D}} = \frac{2}{1 + \frac{l_L}{l_C} + \sqrt{1 - (\frac{l_L}{l_C})^2}} \tag{2.20}$$

where A, B, C and D respectively denote scenarios $l_{L,R} > l_C$, $l_{L,R} < l_C$, $l_L > l_C > l_R$ and $l_L < l_C < l_R$.

In the single brane case, the upper bound on the transmission coefficient[4] is the same as the one following from the achronal average-null-energy condition (AANEC) [14]. In the double brane model, we observe the maximum transmission coefficient values are all consistent with the AANEC bound, and for specific l_C values saturate it for scenarios A, C and D, but not for B (in general).

The AANEC bound is given by [14]:

$$\begin{aligned} \mathcal{T}_{L2} &\leq \frac{l_R}{l_L} \qquad l_R < l_L \\ \mathcal{T}_{L2} &\leq 1 \qquad\quad l_R > l_L \end{aligned} \tag{2.21}$$

When $l_{L,R} > l_C$ (A), (2.20) shows $\mathcal{T}_{L2_{max}}$ is consistent with (2.21) for all allowed values of l_C, and saturates the AANEC bound as $l_C = l_R$ for $l_R < l_L$ and $l_C = l_L$ for $l_R > l_L$.

In the regimes where l_C is intermediate (C and D), $\mathcal{T}_{L2_{max}}$ is continuous and saturates the AANEC bound in 2.21 for limits on l_C. For $l_L > l_C > l_R$ (C), 2.20 saturates the bound in the limit $l_C \to l_R$ from above. For $l_L < l_C < l_R$ (D), it saturates the bound in the limit $l_C \to l_L$ from above.

When $l_{L,R} < l_C$ (B), $\mathcal{T}_{L2_{max}}$ has no local maxima as a function of l_C, so the maximum value is reached at either l_C's maximum value of ∞, or at l_C's minimum value, given by maximum(l_L, l_R). From (2.20), as $l_C \to \infty, \mathcal{T}_{L2_{max}} = \frac{l_R}{l_R + l_L}$. While this is always consistent with 2.21, it only saturates the AANEC bound in the (trivial) limiting scenario: $l_R \to 0$ for $l_R < l_L$, and $l_L \to 0$ for $l_R > l_L$. As l_C approaches it's minimum allowed value:

$$\begin{aligned} &\text{For } l_R < l_L \qquad l_C \to l_L \qquad \mathcal{T}_{L2_{max}} = \frac{2}{1 + \frac{l_L}{l_R} + \sqrt{(\frac{l_L}{l_R})^2 - 1}} < \frac{l_R}{l_L} \\ &\text{For } l_R > l_L \qquad l_C \to l_R \qquad \mathcal{T}_{L2_{max}} = \frac{2}{1 + \frac{l_L}{l_R} + \sqrt{1 - (\frac{l_L}{l_R})^2}} < 1 \end{aligned} \tag{2.22}$$

This does not saturate the AANEC bound in general. It is consistent with 2.21 but only saturates for the specific case $l_R = l_L$ (or in the (trivial) limiting scenario mentioned above).

We look at the upper and lower bounds of the transmission coefficient for the specific case where the boundary radii are the same. The result is shown in Figure 2.4. We can see that the maximum difference between the upper and lower bound of

the transmission coefficient occurs for the limiting case where all three radii are the same. The values of $\mathcal{T}_{L2}$ for $l_L = l_R = l_C$ can be given by

$$\mathcal{T}_{L2_{min}} = \frac{1}{3}, \qquad \mathcal{T}_{L2_{max}} = 1. \tag{2.23}$$

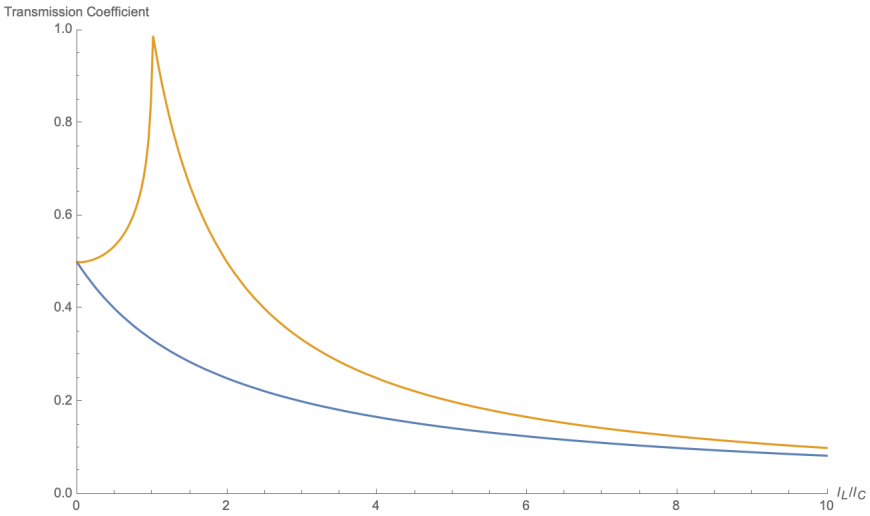

Figure 2.4: The upper and lower bound of the transmission coefficient for the 3-region holographic model with the same boundary radius. As $l_c \to 0$ both upper and lower bound go to 0.

This is in contrast with the 2-region model where the lower bound is 1/2 for the case where both the boundary radii are the same. This goes to show that for the same AdS radii, one can dial the transmission coefficient's minimum value down by adding central wedges that represent point-like defects lying on top of one another. As the number of wedges increases, the minimum transmission coefficient goes to 0.

2.3 Calculating entanglement entropy to find g

In holography, we know that entanglement entropy for a subsystem M, of length a, is given by the area of the minimum extremal RT surface in the d+1 dimensional bulk suspended by the boundary of the d-dimensional CFT subsystem

M: [21, 42]

$$S = \frac{Area_{min}}{4G_N^{d+1}}$$

where G_N^{d+1} is the d+1 dimensional Newton's constant.

For an AdS_3 background, this minimal area turns out to be simpler in global co-ordinates. Therefore, it will be advantageous to express the metric (2.9) and the constraints from the matching equations (2.13) in these.

2.3.1 Global co-ordinates

Relating the Poincare coordinates (t, u, y) to the global co-ordinates (t, x, r)[5]:

$$y_L = \frac{x_L}{\cosh\left(\frac{r_L}{l_L}\right)} \qquad u_L = x_L \tanh\left(\frac{r_L}{l_L}\right) \tag{2.24}$$

The AdS_3 metric in global co-ordinates is given by:

$$\begin{aligned} ds_L^2 &= l_L^2 \cosh^2\left(\frac{r_L}{l_L}\right) ds_2^2 + dr_L^2 \qquad -\infty < r_L < R_L \\ ds_C^2 &= l_C^2 \cosh^2\left(\frac{r_C}{l_C}\right) ds_2^2 + dr_C^2 \qquad R_{CL} < r_C < R_{CR} \\ ds_R^2 &= l_R^2 \cosh^2\left(\frac{r_R}{l_R}\right) ds_2^2 + dr_R^2 \qquad R_R < r_R < \infty \end{aligned} \tag{2.25}$$

where r_L,r_C, r_R are the hyperbolic angles and ds_2^2 is the metric for a constant r AdS_2 slice given by:

$$ds_2^2 = \frac{-dt_L^2 + dx_L^2}{x_L^2} = -\cosh^2\mu \; dt^2 + d\mu^2 \tag{2.26}$$

ds_2^2 can similarly be expressed in (t_C, x_C) and (t_R, x_R). For the same reasons stated in Section 2, note that R_L, R_{CL}, R_{CR} and R_R can in general be positive or negative as long as $(R_{CR} - R_{CL}) > 0$. An M_C wedge extending on both sides of the interface line translates to $R_{CL} < 0$ and $R_{CR} > 0$.

[5]x is a radial co-ordinate here, not the co-ordinate orthogonal to the branes as in Section 2.

The matching conditions (2.7) for the vacuum solution are given as:

$$\begin{aligned} l_L \cosh\left(\frac{R_L}{l_L}\right) &= l_C \cosh\left(\frac{R_{CL}}{l_C}\right) \qquad & l_C \cosh\left(\frac{R_{CR}}{l_C}\right) &= l_R \cosh\left(\frac{R_R}{l_R}\right) \\ \frac{Tanh\left(\frac{R_L}{l_L}\right)}{l_L} - \frac{Tanh\left(\frac{R_{CL}}{l_C}\right)}{l_C} &= \tau_1 \qquad & \frac{Tanh\left(\frac{R_{CR}}{l_C}\right)}{l_C} - \frac{Tanh\left(\frac{R_R}{l_R}\right)}{l_R} &= \tau_2 \end{aligned} \tag{2.27}$$

2.3.2 Review: Entanglement entropy for a 2-region ICFT

Entanglement entropy for a subsystem that encloses a defect has been worked out in [8, 28]. For a symmetric interval of total length a, that is where the defect is at the center of the interval, the entanglement entropy of this subsystem is given as:

$$S = \frac{(l_R + l_L) Log(\frac{a}{\epsilon})}{4G} + \log g_0 \tag{2.28}$$

where ϵ is the UV cut-off, and G is the 3 dimensional Newton's constant.

For the single brane model, the presence of the defect provides the additional contribution to the entanglement entropy given by:

$$\log g_0 = \frac{1}{4G}(R_L - R_R) \tag{2.29}$$

2.3.2.1 Entanglement entropy for a 3-region ICFT

The method from [28] is implemented for the 3-region holographic model to calculate the area of the minimal RT surface and the entanglement entropy form.

To write the entanglement entropy, we start with the minimal area functional - as this method is the same for all three regions, for this part of the calculation, we will drop the subscript L from the AdS radius and from the co-ordinates (t, r, x). This is given by the square root of the metric, for a constant time slice ($t = 0$) and parameterized by r so that x becomes $x(r)$:

$$\mathcal{A} = \sqrt{l^2 \cosh^2\left(\frac{r}{l}\right) \frac{x'^2}{x^2} + 1} \;\; dr \tag{2.30}$$

where x' is $\frac{\partial x}{\partial r}$.

The constraint on $x(r)$ is obtained by using the scale isometry of AdS_2, that is $x \to \lambda x$ is a symmetry of $\mathcal{A}$ that corresponds to a Noether charge. Noether's charge for some functional $\mathcal{L}$ with fields ψ_i is given below and when applied to (2.30) gives:

$$\begin{aligned} j^\mu &= -\mathcal{L}\delta x^\mu + \frac{\partial \mathcal{L}}{\partial(\partial_\mu \psi_i)}(\partial_\alpha \psi_i)\delta x^\alpha \\ c_s &= \frac{l^2 \cosh^2(\frac{r}{l})x'}{\sqrt{l^2\cosh^2(\frac{r}{l})x'^2 + x^2}} \end{aligned} \tag{2.31}$$

Solving for $\frac{x'}{x}$ and plugging into Eq (2.30), we get:

$$\mathcal{A} = \frac{l\cosh\left(\frac{r}{l}\right)}{\sqrt{l^2\cosh^2(\frac{r}{l}) - c_s^2}}dr \tag{2.32}$$

From (2.31), $c_s = 0$ corresponds to $x' = 0$ so $x(r) =$ constant. To fix this constant, we look independently at our regions. For $r = \infty$, $x = a_R$ (area curve hits the right boundary of the subsystem) and for $r = -\infty$, $x = a_L$ (area curve hits the left boundary of the subsystem). In order to have the minimal area surface continuous across the brane, $a_L = a_R = a/2$. Therefore, $c_s = 0$ corresponds to the symmetric case where the defect is in the center of the interval. Then, the minimal area is given by:

$$\mathcal{A} = \int dr = \int_{-\infty}^{R_L} dr + \int_{R_{CL}}^{R_{CR}} dr + \int_{R_R}^{\infty} dr \tag{2.33}$$

This area needs to be regulated by truncating the integral as it goes to large positive and negative r's (r_+ and -r_-). Using (2.24) and setting $y = \epsilon$ as the UV cut-off, and $x_L = x_R = a/2$:

$$\begin{aligned} \frac{e^{\frac{r_+}{l_R}}}{2} &= \frac{x_R}{y_R} & \qquad \frac{e^{\frac{r_-}{l_L}}}{2} &= \frac{x_L}{y_L} \\ r_+ &= \log\left(\frac{a}{\epsilon}\right)l_R & \qquad r_- &= \log\left(\frac{a}{\epsilon}\right)l_L \end{aligned} \tag{2.34}$$

Using (2.33) and (2.34) gives the entanglement entropy for a symmetric, defect enclosing, interval of length a:

$$S = \frac{(l_R + l_L)Log(\frac{a}{\epsilon})}{4G} + \log g_1 \tag{2.35}$$

$$\log g_1 = \frac{1}{4G}(R_L - R_{CL} + R_{CR} - R_R) \tag{2.36}$$

In general, log g is additive under the fusion of branes, evidenced by how (2.29) extends to (2.36). The constraints from the matching conditions (2.27) can be used to calculate these 4 unknowns at which the branes end and then using (2.36), express $\log g_1$. Since these expressions don't simplify out in general, we lay out their details in Appendix B.

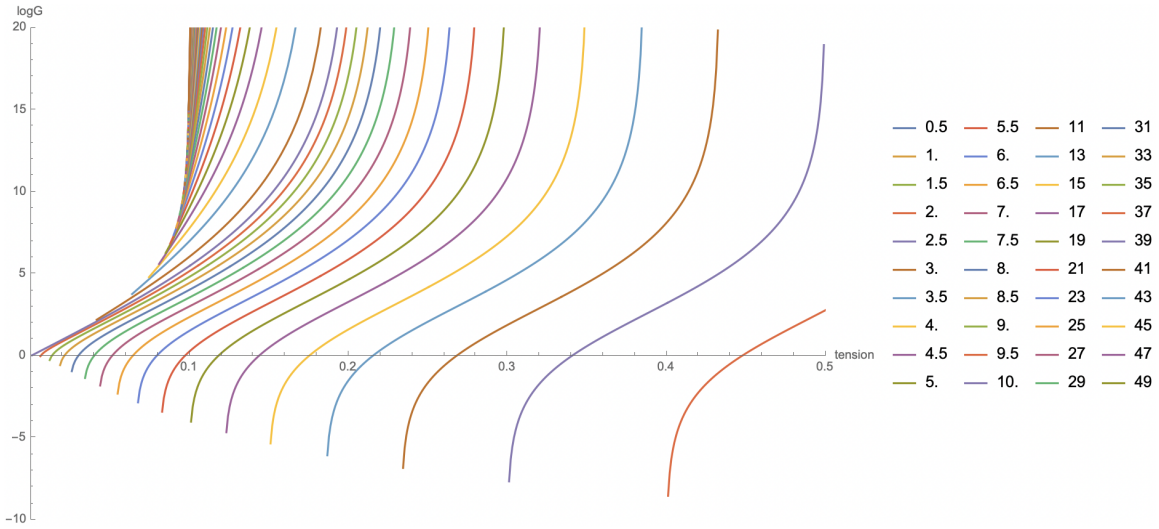

Figure 2.5: The additional entanglement entropy ($\log g$) for the 3-region holographic model, where we consider a symmetric fusion of defects with $l_L = l_R = 10$, $\tau_1 = \tau_2$. Legend shows l_C values. Moving left to right, the curves are given by decreasing l_C values.

2.3.3 Results and comments

It is more expository to instead plot $\log g_1$. For an easy to visualize 2d plot, we take $l_L = l_R$ and $\tau_1 = \tau_2$ representing a parity symmetric 'fusion' of defects. Figure 2.5 shows that the correction to entanglement entropy can be positive or negative and unbounded in general, for different values of tension. Most interestingly, it shows that for the same $\log g_1$ value, we can have many different 3-region models, given by different l_C. This is exactly the freedom we were looking for that was absent in the

single brane model. Additionally, we see that when the center's radius is greater than boundary's radius, there seems to be low tension region where $\log g_1$ has a maximal upper bound, depending on l_C. This can be explicitly seen in Figure 2.6.

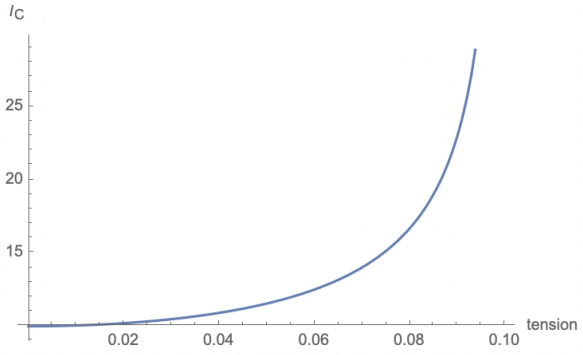

Figure 2.6: $\log g$ has a finite maximum value when $l_C > l_L (l_L = l_R = 10$ and $\tau_1 = \tau_2)$.

Using (B.3) in Appendix B, if one evaluates $\log g_1$ for $l_R = l_L = l_C$, and then converts from log to $\tanh^{-1}$ (using the mathematical identity), the increment in entropy is:

$$\begin{aligned} \Delta S &= \frac{l_L \log\left(\frac{(\tau_1 l_L+2)(\tau_2 l_L+2)}{(\tau_1 l_L-2)(\tau_2 l_L-2)}\right)}{4G} \\ &= \frac{c_L}{3}\left(\tanh^{-1}\left(\frac{l_L\tau_1}{2}\right)+\tanh^{-1}\left(\frac{l_L\tau_2}{2}\right)\right) \\ &= \log g_{0_1} + \log g_{0_2} = \log\left(g_{0_1} g_{0_2}\right) = \log g_1 \\ &= \frac{c_L}{3}\tanh^{-1}\frac{l_L\tau_3}{2} \end{aligned} \tag{2.37}$$

where $\log g_{0_1}$ and $\log g_{0_2}$ are contributions from a single brane defect with tension τ_1 and τ_2 respectively [8, 28].

Thus, the increment in entropy has a pleasingly simple form and agrees with field theory expectations: the $\log g$ values simply add.[6] As we introduce more freedom into the interface by looking at the fusion of multiple defects, the value of g increases

[6]In general, log g is additive under fusion of the branes, evidenced in how (2.29) extends to (2.36). However, it takes this simple form only when the AdS radii are the same.

unbounded, indicating an infinite class if you want to interpret g as classifying your defects.

This result has to be compared and contrasted with our analogous results for the transmission coefficient (2.17). There, we also found that the brane contributions add, but there it was the *tensions* that added. Due to the non-linear relation in terms of the $\tanh^{-1}$ function between $\log g$ and tension, this makes it very clear that merging two single brane defects gives us a genuinely new defect. We could, for example, try to fix the effective tension of a defect arising from the merger of two single brane interfaces with tensions τ_1 and τ_2 by requiring that the resulting $\log g$ should be that of a single brane with tension τ_3 as shown in the last line of (2.37). Re-expressing the $\tanh^{-1}$ in (2.37) as a log we find

$$\tau_3 = \frac{l_L(\tau_1 + \tau_2)}{1 + \frac{l_L^2 \tau_1 \tau_2}{4}} \tag{2.38}$$

If τ_3 were just the sum $\tau_1 + \tau_2$, this would be consistent with our result for the transmission coefficient (2.17). The extra non-linear term ruins the equivalence.

Note that this even applies in the special case $l_R = l_L = l_C$ where we do not make use of the freedom to connect our original CFT to any "auxilliary" CFT with a different central charge. We only look at interfaces from a given CFT to itself. Once again, looking at $\log g$ alone it appears that the system can be effectively described as a 2-region model with some tension τ_3. But the transmission coefficient for a 2-region model with tension τ_3 will not match the transmission coefficient expression obtained for the 3-region model.

2.4 Conclusion and extensions

In this work we have clearly demonstrated that in holographic bottom-up models for ICFTs based on RS branes, the fusion of two single brane interfaces does not yield back another single brane interface but instead should be thought of as a novel

object in the theory. This somewhat alleviates the tension between the properties of the holographic toy interfaces and generic ICFTs: the 1-to-1 link between transmission coefficient and boundary entropy that was found in the single brane case is broken and the two can be independently dialed, at least over a certain range.

We only briefly touched upon the case of multiple interfaces. Clearly it would be of interest to consider the merger of not just two but of multiple branes. Presumably the list of all multi-brane interfaces will give a complete set of allowed interfaces.

Beyond that, it would be of much interest to compare and contrast our findings to those in a genuine top-down holographic model. As of now, the transmission coefficient has only been determined for the bottom-up scenario. g has been calculated more widely. This will help determine whether the lack of fusion is indeed a generic feature inherent in the large N limit underlying holographic constructions as we speculated in the introduction, or whether it is just a peculiarity of the particular bottom-up realization in terms of RS branes.

Acknowledgments

We appreciate helpful conversations with Costas Bachas, Ilka Brunner, Dongsheng Ge, and Marcos Riojas. This work was supported, in part, by the U.S. Department of Energy under Grant DE-SC0022021 and by a grant from the Simons Foundation (Grant 651678, AK).

Chapter 3: Transport across interfaces in symmetric orbifolds[1]

Abstract

We examine how conformal boundaries encode energy transport coefficients—namely transmission and reflection probabilities—of corresponding conformal interfaces in symmetric orbifold theories. These constitute a large class of irrational theories and are closely related to holographic setups. Our central goal is to compare such coefficients at the orbifold point (a field theory calculation) against their values when the orbifold is highly deformed (a gravity calculation)—an approach akin to past AdS/CFT-guided comparisons of physical quantities at strong versus weak coupling. At the orbifold point, we find that the (weighted-average) transport coefficients are simply averages of coefficients in the underlying seed theory. We then focus on the symmetric orbifold of the $\mathbb{T}^4$ sigma model interface CFT dual to type IIB supergravity on the 3d Janus solution. We compare the holographic transmission coefficient, which was found by [17], to that of the orbifold point. We find that the profile of the transmission coefficient substantially increases with the coupling, in contrast to boundary entropy. We also present some related ideas about twisted-sector data encoded by boundary states.

101077

[1]Published in JHEP with Sanjit Shashi

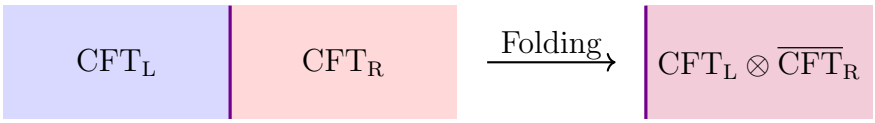

Figure 3.1: An ICFT consists of a "left" CFT and a "right" CFT glued together along a defect (left). This can be mapped to a BCFT (right) by folding along the defect.

3.1 Introduction

2-dimensional conformal field theories with boundaries have a long history in the literature [12, 19], with applications to both condensed matter theory [43, 44] and worldsheet string theory [45, 46, 47, 48]. However, given a generic (particularly, irrational) theory, the underlying classification principles of such boundaries consistent with conformal structure are unknown.

As a first pass to studying conformal boundaries, we can examine physical data "encoded" by the boundary. One example is the ground-state degeneracy g (called the g-function) of the boundary state [20]. This is a c-number that counts the "boundary degrees of freedom." It is also associated with a thermodynamic *boundary entropy* $S_\mathrm{b} = \log g$ [19].

Instead of a CFT with a boundary, we may consider two CFTs glued along a defect surface (in 2d, a line) preserving (reduced) conformal symmetry. This defect is an interface between the constituent systems [22], so the full theory is called an *interface CFT (ICFT)*. Like with boundaries, a general classification of conformal interfaces is unknown. However, an ICFT can be mapped to a boundary (B)CFT by folding along the interface (Figure 3.1), so these are related problems (cf. [23]). In particular, physical parameters characterizing interfaces are encoded by boundary states, with the g-function being an example [8].

Notably, interfaces make manifest additional physics encoded by the folded boundary states. One example is energy transport, which is characterized by *transport coefficients* associated with the interface [15, 49, 14]. The proportion of energy

transported across the interface is quantified by a transmission coefficient $\mathcal{T}$, while the proportion that is bounced back is described by a reflection coefficient $\mathcal{R}$. These transport coefficients are defined through expectation values of the stress tensor by [15] and sum to 1 by construction. Furthermore, unitarity can be used to bound them between 0 and 1 [49, 14].

An underlying motivation of this work is to advocate for transport coefficients as describing a facet of the physics of conformal defects apart from the g-function. This is a rather broad goal, so to narrow our focus we examine a particular class of CFT—*symmetric orbifold theories*. These are defined by taking N copies of some "seed" theory $\mathcal{M}$ and quotienting by the permutations constituting the symmetric group S_N. Motivated by the recent classification of boundaries and g-functions in symmetric orbifolds [50],[2] our main reasons for considering these theories lie in both their tractability (given information about the seed theory) and their connections to holographic CFT (cf. [52, 53]). The general review and analysis of symmetric orbifold CFT at the orbifold point constitutes Section 3.2.

Furthermore, some symmetric orbifold theories can be understood directly at strong coupling[3] via the AdS/CFT correspondence [5], thereby giving us access to a regime in which field-theoretic calculations are otherwise typically intractable. For example, type IIB supergravity on $\mathrm{AdS}_3 \times S^3 \times \mathbb{T}^4$ is dual to the symmetric orbifold of a $\mathbb{T}^4$ sigma model at strong coupling and with a large number of copies, and this duality also persists in more stringy/weakly coupled regimes [55]. More pertinent to our purposes, we can describe a simple class of top-down holographic conformal interfaces in this CFT and at strong coupling through a non-supersymmetric[4] dilatonic deformation of the AdS_3 bulk. The resulting gravitational background is called Janus [57]. By using the holographic prescription initially proposed for "thin-brane"

[2]See also [51] for similar work in the context of string theory and $\mathrm{AdS}_3/\mathrm{CFT}_2$ holography.

[3]We are referring to the marginal coupling which, when turned on, takes us away from the orbifold point [54]. This coupling makes the N copies of the theory interact.

[4]There are also supersymmetric deformations of the $\mathrm{AdS}_3 \times S^3 \times \mathbb{T}^4$ vacuum [56, 9].

configurations [4] and subsequently refined by [1] and [17], one may obtain transport coefficients encoded by particular boundary states in the strongly coupled sector of the ICFT dual to type IIB on Janus.

Indeed, the holographic transmission coefficients of the Janus interface have been obtained recently [17]. In Section 3.3, we will compare these coefficients against those of the Janus interface at the orbifold point, which we obtain via applying the procedure of Section 3.2 to an appropriate boundary state of the folded $\mathbb{T}^4$ seed theory. The seed theory is four non-interacting copies of a free S^1-valued scalar field, each with a jump in mass along a defect. Under folding, each individual S^1 theory maps to two non-interacting scalar fields on half space that together are taken to satisfy a "Neumann–Dirichlet" boundary condition [8]. Transport in the folded free scalar theory with this boundary condition has long been understood [15], but the main significance of Section 3.2 is to emphasize the answer does not change in the symmetric orbifold. Our procedure ultimately yields an approximate answer for transport coefficients in the weakly coupled regime of the $\mathbb{T}^4$ symmetric orbifold theory.

Performing this type of strong-weak comparison is not a new application of the holographic nature of the Janus solution. [8] exploited the tractability of both the strongly coupled and weakly coupled regimes of the $\mathbb{T}^4$ symmetric orbifold ICFT to study how the boundary entropies S_{b} of these interfaces run with coupling.[5] They found that S_{b} is highly insensitive to coupling, running only a small amount. Going further, a similar calculation in supersymmetric Janus [9] found an exact match between the strongly coupled and weakly coupled regimes. However, in our comparison, we find that $\mathcal{T}$ changes much more nontrivially with coupling when the parameter characterizing the strength of the dilatonic deformation is not at the ends of its regime

[5]They assume the boundary entropy has no contributions from twist fields. In light of [50], a boundary state agreeing with this assumption is more consistent with a bulk geometrical interpretation (i.e. a supergravity state) but is also "atypical." We discuss this more in the Section 3.4.2.

of validity (Figure 3.6).

This makes sense. Heuristically, quantities describing transport are more sensitive to coupling than those describing thermodynamics. The classic example is $\mathcal{N} = 4$ supersymmetric Yang–Mills in which free energy [58, 59] only changes by a factor of $\frac{3}{4}$ while shear viscosity of the SYM plasma [60, 61, 62] changes infinitely. Inspired by this story, we interpret our result as additional evidence for the idea that transport is more sensitive to coupling when compared to thermodynamics.

3.2 Interface data in symmetric orbifold theories

We start by schematically discussing the physical data of conformal interfaces in the symmetric orbifold of a *known* ICFT $\mathcal{M}$. The N-fold symmetric orbifold theory $\widetilde{\mathcal{M}}_N$ consists of N copies of $\mathcal{M}$ modded out by the symmetric group S_N of permutations of the factors:

$$\widetilde{\mathcal{M}}_N = \mathcal{M}^{\otimes N}/S_N. \tag{3.1}$$

Here we focus on the "orbifold point" of the theory, in which the N copies are taken to be non-interacting. This can also be seen as the free sector of the theory.

Instead of dealing with conformal interfaces directly, it is useful to map them to conformal boundaries via folding [15]. Suppose that the seed ICFT $\mathcal{M}$ consists of two CFTs $\mathcal{C}_{\mathrm{L}}$ and $\mathcal{C}_{\mathrm{R}}$ glued along an interface. We map this to a seed BCFT $\mathcal{C}_{\mathrm{L}} \otimes \overline{\mathcal{C}}_{\mathrm{R}}$. This induces a mapping between $\widetilde{\mathcal{M}}_N$ and $\widetilde{(\mathcal{C}_{\mathrm{L}} \otimes \overline{\mathcal{C}}_{\mathrm{R}})_N}$. Thus, we can use the technology of BCFT and boundary states to study conformal interfaces (cf. [22, 23]).

Following [50], we start by assuming knowledge about interface (or boundary) data in the seed theory. Using this knowledge and the combinatorics of S_N, we then establish a recipe for interface (or boundary) data in the associated symmetric orbifold theory.

Before getting into the details, we remark that the mapping of $\widetilde{\mathcal{M}}_N$ to $\widetilde{(\mathcal{C}_{\mathrm{L}} \otimes \overline{\mathcal{C}}_{\mathrm{R}})_N}$ is subtle. Specifically, taking a symmetric orbifold of $\mathcal{M}$ then folding yields $(\widetilde{\mathcal{C}_{\mathrm{L}}})_N \otimes$

$\overline{(\widetilde{\mathcal{C}}_{\mathrm{R}})_N}$, which is not technically the same as taking the symmetric orbifold of $\mathcal{C}_{\mathrm{L}} \otimes \overline{\mathcal{C}}_{\mathrm{R}}$. However, we insist that the latter can be used as a proxy for the former when computing data associated with transport, because the relevant CFT data is encoded by overlaps of product states.

3.2.1 Twisted sectors of symmetric orbifolds

Let us first review the basic structure of symmetric orbifold theories, following [50]. There are two major differences between the spectra of the N-fold product theory $\mathcal{M}^{\otimes N}$ and of the symmetric orbifold theory $\widetilde{\mathcal{M}}_N$. The first is that only product states that are invariant under all permutations, i.e. totally symmetric product states, survive the orbifolding procedure. These particular states constitute the so-called *untwisted sector* of $\widetilde{\mathcal{M}}_N$.

The second difference is the presence of *twisted sectors* in the orbifolded theory. Recall that the permutation group acts on different seed copies of $\mathcal{M}$. We can systematically construct states of the orbifold by starting with an individual permutation $\sigma \in S_N$ and identifying ("gluing together") copies of the seed theory $\mathcal{M}$ as instructed by σ. In more mathematically precise terms, such a state (defined on the cylinder) is one where the corresponding field is periodic up to the action of the permutation [63, 64]. Concretely, for a generic field $\varphi(z)$ ($z \in S^1$) of the seed theory, we define a field $\Phi(z)$ for which a 2π rotation ($z \to e^{2\pi i} z$) maps $\Phi(z) = \varphi_{(i)}(z)$ [where $\varphi_{(i)}$ is the ith copy of φ] to $\varphi_{(\sigma(i))}(z)$. Gluing yields a Hilbert space distinct from that of $\mathcal{M}^{\otimes N}$ and consisting of "σ-twisted" states. Allowing a slight abuse of notation,[6] we write the space as $\mathcal{M}^{\otimes N}/\{\sigma\}$.

In the full symmetric orbifold, we mod out by the full group S_N, so the states that survive this procedure must be invariant under all permutations. As a result,

[6] Taking a quotient technically requires a group (which $\{\sigma\}$ is not). However, we can still use the notation of quotients to describe seed theories being glued in a particular order and by a specific permutation.

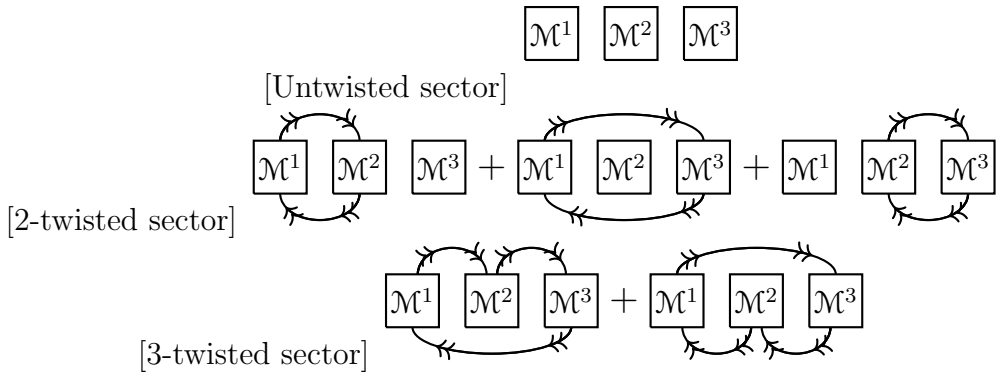

Figure 3.2: A cartoon of the sectors of the symmetric orbifold theory $\widetilde{\mathcal{M}}_3 = \mathcal{M}^{\otimes 3}/S_3$. Each box is a copy of the seed theory. Boxes connected by arrows are identified with one another (i.e. "glued"), and any remaining boxes are just factors in the symmetric product. The untwisted sector (a) is simply the symmetrized product space. The 2-twisted sector (b) is constructed by gluing together any two seed copies and symmetrizing. The 3-twisted sector (c) arises from gluing together three copies in any order and symmetrizing.

each twisted sector consists of totally symmetric sums of twisted states taken over all permutations of a particular cycle type. For example, in the $N = 3$ case, we would sum together states twisted by permutations $(1\,2), (1\,3), (2\,3) \in S_3$ (using cycle notation) to get states in one of the (symmetrized) twisted sectors, and we would similarly sum together states twisted by $(1\,2\,3), (1\,3\,2) \in S_3$ to get those of the other sector. See Figure 3.2 for a cartoon.

Note that the permutations of a particular cycle type precisely constitute a particular conjugacy class of S_N. Through this equivalence, the conjugacy classes each correspond to an integer partition of N (the cycle type). So, the number of twisted sectors in the symmetric orbifold theory matches the number of distinct integer partitions of N.

Twisted states Let us be more explicit about the properties of twisted states. First for simplicity, consider a single N-cycle $\sigma_N \in S_N$, by which we mean that σ_N is an order N ($|\sigma_N| = N$) connected permutation. In other words, σ_N has no fixed points

or subcycles. We take the N copies of the seed theory permuted by σ_N and glue them in the order dictated by σ_N. For example, taking $N = 3$, we have two 3-cycles, (1 2 3) and (1 3 2), and the corresponding gluings of seed theories are respectively visualized in Figure 3.2.1.

For some seed primary scalar $|h\rangle$ of weight h, the Hilbert space of $\mathcal{M}^{\otimes N}/\{\sigma_N\}$ has a state $|\sigma_N \cdot h^{(N)}\rangle$ of weight $\mathfrak{h}\big[h^{(N)}\big]$ (using $\mathfrak{h}$ to represents weights in the orbifold), where

$$\mathfrak{h}\big[h^{(N)}\big] \equiv \frac{c}{24}\left(N - \frac{1}{N}\right) + \frac{h}{N}. \tag{3.2}$$

The superscript (N) is meant to highlight that we are starting with N copies of the seed state $|h\rangle$ priori to gluing them by σ_N. Note that the explicit choice of σ_N does not matter.

This is still not a state of the symmetric orbifold, since it is not invariant under all permutations. Instead, we define the symmetrization of $|\sigma_N \cdot h^{(N)}\rangle$ as

$$|h^{(N)}\rangle \equiv \frac{1}{\sqrt{(N-1)!}} \sum_{\sigma \in \{N\text{-cycles}\}} |\sigma \cdot h^{(N)}\rangle. \tag{3.3}$$

Basically, we are summing over all possible N-cycles. This is mathematically equivalent to summing over all elements of S_N in the same conjugacy class as a particular σ_N. There are $(N-1)!$ such permutations, and so $\frac{1}{\sqrt{(N-1)!}}$ is a normalization factor for the symmetrized state. Furthermore, this can be rewritten as a sum over all possible conjugates of σ_N in the symmetric group, so long as we introduce a $\frac{1}{N}$ factor to prevent overcounting (cf. [65, 63]):

$$|h^{(N)}\rangle = \frac{1}{N\sqrt{(N-1)!}} \sum_{\tau \in S_N} |(\tau \sigma_N \tau^{-1}) \cdot h^{(N)}\rangle. \tag{3.4}$$

This rewriting can be found using finite group theory. We first explicitly write each distinct N-cycle in the sum as some conjugate of σ_N. We then further rewrite each term as a sum over the centralizer of σ_N [defined as $\mathcal{S}(\sigma_N) \equiv \{g \in S_N \,|\, g\sigma_N g^{-1} = \sigma_N\}$] by the replacement $\sigma_N \to \frac{1}{N}\sum_{g \in \mathcal{S}(\sigma_N)} g\sigma_N g^{-1}$ (where the factor of N is the size of the centralizer and can be found through the orbit-stabilizer theorem). We then use

the fact that the left cosets of $\mathcal{S}(\sigma_N)$ in S_N partition the symmetric group to get the right-hand side of (3.4).

The fact that $|h^{(N)}\rangle$ can be written as a sum over the full symmetric group means that it is manifestly invariant under permutations. So, it is also in the Hilbert space of the symmetric orbifold theory $\widetilde{\mathcal{M}}_N$ despite not being a product state, and it still has the same weight as its individual terms as given by (3.2). We will refer to the states of the form $|h^{(N)}\rangle$ as "maximally twisted" in that they are constructed by gluing together all N copies of the seed theory.

We can generalize the above construction to arbitrary elements of S_N to go beyond just N-cycles. Specifically, consider a permutation $\sigma = \sigma_1 \cdots \sigma_m \in S_N$, where each σ_i is a k_i-cycle (with $k_i \leq k_{i+1}$ for all i) and the different factors are disjoint. Every element of S_N can be written uniquely in this way for some $k_i \geq 1$ for which $\sum_{i=1}^m k_i = N$, and the ordered multiset $\{k_1, \ldots, k_m\}$ is the *cycle type* of σ. From m seed primaries $|h_1\rangle, \ldots, |h_m\rangle$, we construct a σ-twisted state denoted by

$$|\sigma_1 \cdot h_1^{(k_i)}\rangle \cdots |\sigma_m \cdot h_m^{(k_m)}\rangle \in \mathcal{M}^{\otimes n}/\{\sigma\}. \tag{3.5}$$

This notation unambiguously encodes both the numbering of the seed states and how identical copies of such states are twisted together, since the constituent disjoint cycles encode the initial "locations" of the seed states within the parent tensor state.[7] Additionally, the weight of the generic twisted state (3.5) is

$$\mathfrak{h}\big[h_1^{(k_i)}, \ldots, h_m^{(k_m)}\big] \equiv \sum_{i=1}^m \mathfrak{h}\big[h_i^{(k_i)}\big] = \sum_{i=1}^m \left[\frac{c}{24}\left(k_i - \frac{1}{k_i}\right) + \frac{h_i}{k_i}\right], \tag{3.6}$$

which we get by noting that (3.5) is basically an m-fold product of maximally twisted states with respect to $\mathcal{M}^{\otimes k_1}, \ldots, \mathcal{M}^{\otimes k_m}$. Indeed, if we consider a state twisted by an N-cycle ($m = 1$ and $k_1 = N$) then we recover (3.2), whereas taking the identity

[7] For example, $|(1) \cdot h_1^{(1)}\rangle|(2\,3) \cdot h_2^{(2)}\rangle$ describes a state for which we take the tensor product $|h_1\rangle \otimes |h_2\rangle \otimes |h_2\rangle$ and then glue the second and third seed factors by quotienting by $(1)(2\,3)$.

element ($m = N$ and $k_1 = \cdots = k_N = 1$) yields the weight $(h_1 + \cdots + h_N)$ of a product state in $\mathcal{M}^{\otimes N}$.

Just as in the maximally twisted case above, however, we need to symmetrize the σ-twisted state in order to get a permutation-invariant state of the full symmetric orbifold theory. Again, we define a sum over all permutations $\sigma \in S_N$ of a particular cycle type:

$$|h_1^{(k_1)}\rangle \odot \cdots \odot |h_m^{(k_m)}\rangle \equiv \frac{1}{\sqrt{\mathcal{C}(k_1,\ldots,k_m)}} \sum_{\substack{\sigma=\sigma_1\cdots\sigma_m \\ |\sigma_i|=k_i}} |\sigma_1 \cdot h_1^{(k_1)}\rangle \cdots |\sigma_m \cdot h_m^{(k_m)}\rangle,$$
$$\text{where } \ \sigma_i \cap \sigma_j\big|_{i\neq j} = \varnothing, \quad k_1 + \cdots + k_m = N, \tag{3.7}$$

where we use $\odot$ to emphasize that the factors $|h_i^{(k_i)}\rangle$ of the symmetrized state on the left-hand side *commute* by construction. As in (3.3), we introduce a normalization factor $\mathcal{C}(k_1,\ldots,k_m)$ that is equivalent to the number of terms in the sum. Note that $\mathcal{C}(k_1,\ldots,k_m)$ is just the size of the conjugacy class if $k_i = k_j \implies i = j$ (as in the maximally twisted case), but if there are multiple subcycles of the same size then this is no longer true (as in the untwisted case for which $\mathcal{C} = N!$). For simplicity, we will ignore this normalization unless working with specific cases.

Most importantly, through the same group-theoretic techniques described in the maximally twisted case, we can fix a particular $\{k_1,\ldots,k_m\}$-cycle σ and rewrite the sum as one over the full symmetric group (omitting the cycle-type-dependent normalization):

$$|h_1^{(k_1)}\rangle \odot \cdots \odot |h_m^{(k_m)}\rangle \propto \sum_{\tau\in S_N} |\sigma_1' \cdot h_1^{(k_1)}\rangle \cdots |\sigma_m' \cdot h_m^{(k_m)}\rangle,$$
$$\text{where } \tau\sigma\tau^{-1} = \sigma_1'\cdots\sigma_m', \quad |\sigma_i'| = k_i, \tag{3.8}$$

The key takeaway of (3.8) is that $|h_1^{(k_1)}\rangle \odot \cdots \odot |h_m^{(k_m)}\rangle$ is a sum over S_N and thus invariant under permutations. This construction also explicitly shows how different sectors of $\mathcal{M}^{\otimes N}/S_N$ are labeled by the cycle types, which in turn label conjugacy classes of S_N.

As a concrete example of these twisted states, consider again $N = 3$, and take two seed primaries $|h_1\rangle$ and $|h_2\rangle$ with one copy of the former and two copies of the latter. We can use these primaries to build states respectively twisted by $(1\,2)$, $(1\,3)$, or $(2\,3)$:

$$|(1)\cdot h_1\rangle|(2\,3)\cdot h_2\rangle \in \mathcal{M}^{\otimes 3}/\{(1)(2\,3)\}, \tag{3.9}$$

$$|(2)\cdot h_1\rangle|(1\,3)\cdot h_2\rangle \in \mathcal{M}^{\otimes 3}/\{(2)(1\,3)\}, \tag{3.10}$$

$$|(3)\cdot h_1\rangle|(1\,2)\cdot h_2\rangle \in \mathcal{M}^{\otimes 3}/\{(3)(1\,2)\}. \tag{3.11}$$

All three of these states have the same weight,

$$\left[\frac{c}{24}\left(1-\frac{1}{1}\right)+\frac{h_1}{1}\right]+\left[\frac{c}{24}\left(2-\frac{1}{2}\right)+\frac{h_2}{2}\right]=\frac{c}{16}+h_1+\frac{h_2}{2}. \tag{3.12}$$

The permutation-invariant state with this weight and consisting of $\mathcal{C}(1,2)=3$ terms is

$$\begin{aligned}|h_1^{(1)}\rangle\odot|h_2^{(2)}\rangle=\frac{1}{\sqrt{3}}\big[&|(1)\cdot h_1\rangle|(2\,3)\cdot h_2\rangle+|(2)\cdot h_1\rangle|(1\,3)\cdot h_2\rangle\\ &+|(3)\cdot h_1\rangle|(1\,2)\cdot h_2\rangle\big].\end{aligned} \tag{3.13}$$

This is indeed invariant under permutations and thus is a well-defined state of the symmetric orbifold, despite not being a product state.

We should mention that each twisted sector has its own ground state realized as a twist of the seed vacuum state $h = 0$. These states are called *bare twists*. In terms the notation of (3.8) above, they are written as $|0^{(k_1)}\rangle\odot\cdots\odot|0^{(k_m)}\rangle$. For instance, consider again a single N-cycle σ_N. From (3.2), the weight of the twist of the vacuum by σ_N is

$$\mathfrak{h}\big[0^{(N)}\big]=\frac{c}{24}\left(N-\frac{1}{N}\right), \tag{3.14}$$

which is below the black-hole threshold $\frac{c}{24}$ and is also the weight of the (symmetrized) bare twist $|0^{(N)}\rangle$. Weights of bare twists by more complicated cycle types can similarly be computed with (3.6), but they are all upper-bounded by $\mathfrak{h}\big[0^{(N)}\big]$.

As an example, consider the $N = 4$ case. There are five different cycle types in S_4 corresponding to the integer partitions of 4. The associated bare-twist weights are

$$\begin{aligned} &\mathfrak{h}\big[0^{(1)}, 0^{(1)}, 0^{(1)}, 0^{(1)}\big] = 0, \qquad \mathfrak{h}\big[0^{(1)}, 0^{(1)}, 0^{(2)}\big] = \frac{c}{16}, \\ &\mathfrak{h}\big[0^{(1)}, 0^{(3)}\big] = \frac{c}{9}, \qquad \mathfrak{h}\big[0^{(2)}, 0^{(2)}\big] = \frac{c}{8}, \qquad \mathfrak{h}\big[0^{(4)}\big] = \frac{5c}{32}. \end{aligned} \tag{3.15}$$

Note the untwisted sector furnishes the true vacuum of the theory $|0\rangle^{\otimes N}$ of weight $\mathfrak{h} = 0$.

Symmetry structure Take the holomorphic and antiholomorphic Virasoro symmetry of the seed theory, collectively denoted as $\mathrm{Vir}(\mathcal{M}) \oplus \overline{\mathrm{Vir}}(\mathcal{M})$ and with central charge c. The algebra of the ith copy is generated by $\big\{L_n^{(i)} \in \mathrm{Vir}(\mathcal{M})\big\}$ and $\big\{\overline{L}_n^{(i)} \in \overline{\mathrm{Vir}}(\mathcal{M})\big\}$, where

$$\begin{aligned} [L_n^{(i)}, L_{n'}^{(i)}] &= (n-n')L_{n+n'}^{(i)} + \frac{c}{12} n(n^2-1)\delta_{n+n',0}, \\ [\overline{L}_n^{(i)}, \overline{L}_{n'}^{(i)}] &= (n-n')\overline{L}_{n+n'}^{(i)} + \frac{c}{12} n(n^2-1)\delta_{n+n',0}, \\ [L_n^{(i)}, \overline{L}_{n'}^{(i)}] &= 0. \end{aligned} \tag{3.16}$$

Now consider just the chiral symmetry algebra $\mathcal{W}$ of the seed theory. $\mathcal{W}$ generically contains $\mathrm{Vir}(\mathcal{M})$. Meanwhile, the symmetric orbifold theory $\widetilde{\mathcal{M}}_N$ inherits the chiral algebra

$$\mathcal{W}^{\otimes N}/S_N \supset \mathrm{Vir}(\mathcal{M})^{\otimes N}/S_N. \tag{3.17}$$

Notably, this contains the chiral Virasoro symmetry $\mathrm{Vir}(\mathcal{M}^{\otimes N})$ of the product theory. We refer to this subalgebra as the "full" Virasoro algebra of $\widetilde{\mathcal{M}}_N$ and denote its generators by $\big\{L_n \equiv \sum_{i=1}^N L_n^{(i)}\big\}$ [resp. $\big\{\overline{L}_n \equiv \sum_{i=1}^N \overline{L}_n^{(i)}\big\}$ for the generators of the analogous antiholomorphic copy $\overline{\mathrm{Vir}}(\mathcal{M}^{\otimes N})$]. The associated stress tensor of $\mathcal{M}^{\otimes N}$ whose modes generate the full Virasoro algebra is found by summing together the stress tensors of each copy of the seed theory. Since the product theory is non-interacting (i.e. seed Virasoro generators acting on different factors commute), the

commutator of the full Virasoro generators is

$$[L_n, L_{n'}] = \sum_{i=1}^{N} [L_n^{(i)}, L_{n'}^{(i)}] = (n-n')L_{n+n'} + \frac{Nc}{12} n(n^2-1)\delta_{n+n',0}, \tag{3.18}$$

with an equivalent expression for the antiholomorphic generators. Thus, the central charge of the full Virasoro algebra is Nc.

However, note that the chiral algebra $\mathrm{Vir}(\mathcal{M})^{\otimes N}/S_N$ consists of more than just full Virasoro generators. Notably, there are also "fractional" Virasoro generators that act on twisted sectors of the theory [63, 66, 67]. To be concrete, consider the twisted sector corresponding to the cycle type $\{k_1, \ldots, k_m\}$. Restricting our attention to one of the cycles of length k_i, the associated glued copies each furnish one copy of the seed stress tensor $T^{(j)}$ $(j = 1, \ldots, k_i)$. By looking at the covering space [63], we can define fractional modes of the stress tensor $\{\ell_{n/k_i}\}$ by the equation

$$\ell_{n/k_i} \equiv \frac{1}{2\pi i} \oint dz\, z^{n/k_i+1} \sum_{j=1}^{k_i} e^{-2\pi i n(j-1)/k_i} T^{(j)}(z). \tag{3.19}$$

These and their antiholomorphic counterparts $\{\overline{\ell}_{n/k_i}\}$ together satisfy the following commutation relations:

$$\begin{aligned}
[\ell_{n/k_i}, \ell_{n'/k_i}] &= \left(\frac{n-n'}{k}\right) \ell_{(n+n')/k_i} + \frac{k_i c}{12}\left(\frac{n}{k_i}\right)\left[\left(\frac{n}{k_i}\right)^2 - 1\right]\delta_{n+n',0}, \\
[\overline{\ell}_{n/k_i}, \overline{\ell}_{n'/k_i}] &= \left(\frac{n-n'}{k_i}\right) \overline{\ell}_{(n+n')/k_i} + \frac{k_i c}{12}\left(\frac{n}{k_i}\right)\left[\left(\frac{n}{k_i}\right)^2 - 1\right]\delta_{n+n',0}, \\
[\ell_{n/k_i}, \overline{\ell}_{n'/k_i}] &= 0.
\end{aligned} \tag{3.20}$$

This looks like the usual Virasoro algebra, but with fractional modes. Indeed, (3.19) and (3.20) respectively reduce to the usual integer-moded Virasoro operators and algebra $\mathrm{Vir}(\mathcal{M}^{\otimes k_i}) \oplus \overline{\mathrm{Vir}}(\mathcal{M}^{\otimes k_i})$ with central charge $k_i c$ when taking modes $\frac{n}{k_i} \in \mathbb{Z}$. Additionally, the fractional and full Virasoro generators share a nontrivial commutation bracket [66]:

$$[L_n, \ell_{n'/k_i}] = [\ell_{nk_i/k_i}, \ell_{n'/k_i}]. \tag{3.21}$$

The generators built from the fractional modes that act on a generic state are of the form

$$L_{n_1/k_1,\ldots,n_m/k_m} \equiv \sum_{i=1}^{m} \ell_{n_i/k_i}. \tag{3.22}$$

By taking generators of the untwisted sector ($m = N$, $k_1 = \cdots = k_N = 1$) and summing over identical modes ($n_1 = \cdots = n_N \equiv n$), we recover the full Virasoro generators L_n.

The fractional Virasoro generators act on states in nontrivial twisted sectors. Hence, twisted-sector primaries and their fractional descendants may generically appear as terms in the boundary states of a symmetric orbifold theory [50], as we review in Section 3.2.2.

However, the boundary data with which we are primarily concerned do not involve these modes directly. Specifically, g-functions [20] are identified as overlaps between boundary states and the untwisted vacuum [19], while the transport coefficients of the stress tensor [15] are equated to overlaps of boundary states with full Virasoro descendents of the untwisted vacuum. Twisted-sector terms are projected out when defining either quantity. While we can extract twisted-sector data encoded by a boundary state, such as overlaps with bare twists or fractional Virasoro descendents, we will only briefly discuss such quantities in Section 3.2.4.

3.2.2 Building the boundary states

Via folding, all physical data about a conformal interface is encoded by an associated boundary state in the closed-string spectrum of the folded BCFT [12, 19]. So, a good starting point for studying transport coefficients in a symmetric orbifold theory is to explore how its boundary states might be written in terms of those of the seed theory.

Let us first clarify some fundamental statements of BCFT. A generic CFT

boundary state $|B\rangle$ must satisfy the gluing condition

$$\left(L_n - \overline{L}_{-n}\right)|B\rangle = 0, \quad \forall n \in \mathbb{Z}, \tag{3.23}$$

where we recall that $\{L_n\}$ and $\{\overline{L}_n\}$ are respectively the holomorphic and antiholomorphic generators of the full Virasoro symmetry. In addition, boundary states must satisfy the so-called Cardy condition [12, 19] obtained by equating the open-string and closed-string slicings of the 2d cylinder partition function. To classify the boundary states, one may start by finding a basis for the solution space of (3.23); the elements of such a basis are called *Ishibashi states* [68]. We may then use the Cardy conditions to compute the specific linear combinations of Ishibashi states that correspond to boundary states.

However, the full space of Ishibashi states satisfying (3.23) is not generically known when the theory is not Virasoro-diagonal, and this obstructs simple attempts to organize boundary states. A more attainable goal is to classify boundary states that also respect the chiral extension that diagonalizes the CFT [68, 69]. Mathematically, this means that we restrict our attention to a smaller space of boundary states that satisfy

$$\left[W_n - (-1)^{s(W)}\Omega(\overline{W}_{-n})\right]|B\rangle = 0, \quad \forall n \in \mathbb{Z}, \tag{3.24}$$

where $\{W_n\}$ and $\{\overline{W}_n\}$ are respectively holomorphic and antiholomorphic generators of the extended symmetry algebra corresponding to a holomorphic current W of spin $s(W)$, and Ω is an automorphism of the extended algebra. (3.24) is a generalization of the condition (3.23), since the holomorphic current T corresponding to the Virasoro modes has $s(T) = 2$. The solution space of the set of constraints (3.24) over all extended symmetry generators can be described by Ishibashi states [68].

The goal of [50] (see also related earlier work [70]) is to construct boundary states that respect the chiral algebra $\mathrm{Vir}(\mathcal{M})^{\otimes N}/S_N$ universal to symmetric orbifold theories. The main idea is to classify the solution space of (3.24), where the generators are of the form (3.22). Basically, [50] constructs "twisted" Ishibashi states from

twisted primaries and fractional descendants that, in conjunction with the expected "untwisted" Ishibashi states (i.e. symmetric products of seed Ishibashi states), act as building blocks for the boundary states. For our purposes of understanding the physical data encoded by boundary states, it is instructive to review this construction. We do so now.

As a caveat, we stress that we focus on Virasoro-diagonal seed theories for concreteness, thereby assuming that the only symmetry generators that we need to worry about are those built from the seed stress tensor. However, note that the basic construction works more generally at the cost of completeness in the classification of boundary states.

Untwisted building blocks We first suppose the seed theory $\mathcal{M}$ has boundary states $|b_\alpha\rangle$ where $\alpha = 1, \ldots, n_b$ is an index. n_b is either finite (e.g. for a rational seed theory) or formally infinite (e.g. for an irrational seed theory). These states live in the solution space of the following constraint [denoting ith seed Virasoro modes by $L_n^{(i)}$ and $\overline{L}_n^{(i)}$]:

$$\big(L_n^{(i)} - \overline{L}_{-n}^{(i)}\big)|b_\alpha\rangle = 0, \quad \forall n \in \mathbb{Z}. \tag{3.25}$$

If the seed theory is diagonal with respect to the Virasoro algebra, then we can explicitly construct the seed boundary states because the solution space of (3.25) is spanned by the Ishibashi states of $\mathcal{M}$ [68, 71]. Each of these Ishibashi states is constructed from some spinless primary of weight h as follows:

$$|h\rangle\!\rangle = \sum_{\mathfrak{m}} |h, \mathfrak{m}\rangle \otimes \overline{|h, \mathfrak{m}\rangle}, \tag{3.26}$$

where $\mathfrak{m}$ is either the empty set or an ordered multiset of positive integers ($\{m_1, \ldots, m_\kappa\}$ with $i < j \implies m_i \leq m_j$). The state $|h, \mathfrak{m}\rangle$ (resp. $\overline{|h, \mathfrak{m}\rangle}$) is a holomorphic (resp. antiholomorphic) descendent of the associated primary, with the multiset labeling

both the number and type of creation operators employed:[8]

$$\begin{aligned} |h, \{m_1, \ldots, m_\kappa\}\rangle &= \left(\prod_{i=1}^{\kappa} L^{(i)}_{-m_i} \right) |h\rangle, \\ \overline{|h, \{m_1, \ldots, m_\kappa\}\rangle} &= \left(\prod_{i=1}^{\kappa} \overline{L}^{(i)}_{-m_i} \right) |h\rangle. \end{aligned} \tag{3.27}$$

As (3.26) defines Ishibashi states of the seed theory, all seed boundary states are specific linear combinations of these states:

$$|b_\alpha\rangle = \sum_h \beta_{h,\alpha} |h\rangle\!\rangle. \tag{3.28}$$

Note that the coefficients $\beta_{h,\alpha}$ take on specific values such that $|b_\alpha\rangle$ satisfies both (3.25) and the Cardy condition [12, 19].

In the untwisted sector of the symmetric orbifold theory, a generic symmetry operator consists of sums of seed Virasoro modes that individually act on different copies. The generic gluing condition (3.24) with such symmetry operators is solved by symmetric products of seed Ishibashi states, a fact that can be seen explicitly from the seed gluing condition (3.25). We refer to such symmetric products as untwisted Ishibashi states, and we observe that they are building blocks for states of the form (neglecting the normalization)

$$|B\rangle_{\text{untw}} \equiv |b_{\alpha_1}\rangle \odot \cdots \odot |b_{\alpha_N}\rangle \propto \sum_{\sigma \in S_N} |b_{\sigma(\alpha_1)}\rangle \otimes \cdots \otimes |b_{\sigma(\alpha_N)}\rangle, \tag{3.29}$$

which are boundary states of the symmetric product theory.

If all N of the seed factors $|b_{\alpha_i}\rangle$ are distinct, then (3.29) is also the only way they can be combined in the symmetric orbifold. However, we may have degenerate factors, in which case we can also consider twists of these seed boundary states. This is an expected characteristic of orbifold theories [72].

[8] $\mathfrak{m} = \varnothing$ corresponds to the primary state itself.

Twisted building blocks We now discuss the twisted Ishibashi states of [50]. First, consider the maximally twisted sector, in which we have fractional Virasoro modes $\ell_{n/N}$ and $\overline{\ell}_{n/N}$ for all $n \in \mathbb{Z}$. Using these in the general gluing condition (3.24), we get the constraints

$$\left(\ell_{n/N} - \overline{\ell}_{-n/N}\right)|B\rangle = 0, \quad \forall n \in \mathbb{Z}. \tag{3.30}$$

We can write Ishibashi states that solve this equation in a manner similar to the usual construction. From a maximally twisted primary $|h^{(N)}\rangle$, the associated Ishibashi state is

$$|h^{(N)}\rangle\!\rangle \equiv \sum_{\mathfrak{m}} |h^{(N)}, \mathfrak{m}\rangle \otimes \overline{|h^{(N)}, \mathfrak{m}\rangle}, \tag{3.31}$$

where this time we define

$$\begin{aligned} |h^{(N)}, \{m_1, \ldots, m_\kappa\}\rangle &= \left(\prod_{i=1}^{\kappa} \ell_{-m_i/N}\right)|h^{(N)}\rangle, \\ \overline{|h^{(N)}, \{m_1, \ldots, m_\kappa\}\rangle} &= \left(\prod_{i=1}^{\kappa} \overline{\ell}_{-m_i/N}\right)|h^{(N)}\rangle. \end{aligned} \tag{3.32}$$

Now, for some seed boundary state $|b_\alpha\rangle$ whose expansion in terms of seed Ishibashi states is given by (3.28), we can write an associated maximally twisted state

$$|b_\alpha^{(N)}\rangle \equiv \sum_h \beta_{h,\alpha} |h^{(N)}\rangle\!\rangle. \tag{3.33}$$

This contributes to boundary states of the symmetric orbifold built from N identical copies of $|b_\alpha\rangle$, and so the maximally twisted Ishibashi states are also valid building blocks.

It is straightforward to generalize the above construction to arbitrary twisted sectors corresponding to cycle type $\{k_1, \ldots, k_m\}$. We can construct Ishibashi states defined with respect to states twisted along k_i copies (denoted as $|h^{(k_i)}\rangle\!\rangle$) by using the appropriate fractional Virasoro modes ℓ_{n/k_i} and $\overline{\ell}_{n/k_i}$ in (3.32). We then write symmetrized products,

$$|h_1^{(k_1)}\rangle\!\rangle \odot \cdots \odot |h_m^{(k_m)}\rangle\!\rangle. \tag{3.34}$$

Given a list of m seed boundary states $\{|b_{\alpha_1}\rangle, \ldots, |b_{\alpha_m}\rangle\}$, these twisted Ishibashi states are a basis for states of the form

$$|B\rangle_{\text{twst}} \equiv |b_{\alpha_1}^{(k_1)}\rangle \odot \cdots \odot |b_{\alpha_m}^{(k_m)}\rangle. \tag{3.35}$$

[50] discusses further how (3.29) and (3.35) can be used as building blocks for a broad class of boundary states in the symmetric orbifold theory labeled by representations of permutation subgroups in S_N, where these subgroups are those which permute identical copies of seed boundary states. The coefficients of associated Ishibashi states can be found through the Cardy condition. However, for our purposes it is sufficient to know only the general form of the boundary states—as linear combinations of (3.29) and (3.35) weighted by characters of symmetric-group representations.

We reiterate that the basic construction does not actually need a diagonal seed theory. This is only a useful assumption to make because it affords us the Ishibashi states (3.26) as a complete basis for seed boundary states [68]. For a non-diagonal seed theory, the idea of [50] to start with seed boundary states directly and sum over permutations and twists is still valid in the construction of boundary states that respect the chiral algebra $\text{Vir}(\mathcal{M})^{\otimes N}/S_N$. However, this may no longer provide a complete classification.

We also emphasize that there are other boundary states not included within this classification. In particular, we can consider just the boundary states that respect the full Virasoro algebra inherited from the symmetric product theory $\text{Vir}(\mathcal{M}^{\otimes N}) \subset \text{Vir}(\mathcal{M})^{\otimes N}/S_N$, i.e. those that only satisfy the gluing condition (3.23) but not necessarily (3.24) for all of the symmetry generators. This would be a much more unconstrained problem that would allow for many more boundary states (cf. the case of the free boson [47]).

3.2.3 Transport coefficients from seed data

Now, we discuss how the transport coefficients of [15] are encoded by the boundary states constructed from the building blocks (3.29) and (3.35). The g-

function has already been addressed by [50], and we can look to that story for inspiration. Again, for simplicity we assume that the seed theory has no extended symmetry beyond Virasoro.

The g-function of a boundary state $|B\rangle$ is defined as the overlap between the boundary state and the vacuum $|0\rangle^{\otimes N}$ [20]. Mathematically,

$$g(|B\rangle) \equiv \langle 0|^{\otimes N}|B\rangle. \tag{3.36}$$

However, the state $|0\rangle^{\otimes N}$ lives in the untwisted sector, and so it projects out any twisted-sector terms in $|B\rangle$. As a result, for $|B\rangle$ built from seed boundary states $|b_{\alpha_1}\rangle, \ldots, |b_{\alpha_N}\rangle$, the g-function is merely the vacuum overlap with (3.29) up to an overall normalization factor, so it is proportional to a product of seed g-functions:

$$g(|B\rangle) = \mathcal{F}(N, |B\rangle)\left(g_{\alpha_1} \cdots g_{\alpha_N}\right), \quad g_\alpha \equiv \langle 0|b_\alpha\rangle, \tag{3.37}$$

The normalization factor of $|B\rangle$ depends on both N and the number of twisted-sector seed terms that can be and are included. This carries over to the coefficient $\mathcal{F}$, and so the possibility of twisted-sector terms can influence g indirectly.

Now, we discuss transport. For any 2d ICFT prior to folding, we have a "left" theory whose full Virasoro generators we write as $\{L_n^{[\mathrm{L}]}, \overline{L}_n^{[\mathrm{L}]}\}$ and a "right" theory with generators $\{L_n^{[\mathrm{R}]}, \overline{L}_n^{[\mathrm{R}]}\}$ (note the square brackets). These theories also respectively have central charges c_L and c_R, respectively.[9] Upon folding, [15] defines a 2×2 "transport matrix"

$$R_{IJ}(|B\rangle) = \frac{\langle\Omega|L_2^{[I]}\overline{L}_2^{[J]}|B\rangle}{\langle\Omega|B\rangle}, \quad I, J = \mathrm{L}, \mathrm{R}, \tag{3.38}$$

where $|\Omega\rangle = |\Omega_\mathrm{L}\rangle \otimes |\Omega_\mathrm{R}\rangle$ is the vacuum of the generic folded theory. In terms of the transport matrix, [15] defines the associated "transmission" and "reflection" coeffi-

[9] We assume that the holomorphic and antiholomorphic data of the two theories are the same, e.g. $c_\mathrm{L} = \bar{c}_\mathrm{L}$ and $c_\mathrm{R} = \bar{c}_\mathrm{R}$.

cients as

$$\mathcal{T}(|B\rangle) = \frac{2}{c_{\mathrm{L}} + c_{\mathrm{R}}} \left[R_{\mathrm{LR}}(|B\rangle) + R_{\mathrm{RL}}(|B\rangle)\right], \quad \mathcal{R} = \frac{2}{c_{\mathrm{L}} + c_{\mathrm{R}}} \left[R_{\mathrm{LL}}(|B\rangle) + R_{\mathrm{RR}}(|B\rangle)\right]. \tag{3.39}$$

We can use the gluing conditions (3.23) and the Virasoro algebra to show that R_{IJ} is symmetric. Thus $\mathcal{T}$ as defined above only has one parameter (not including the central charges $c_{\mathrm{L}}, c_{\mathrm{R}}$), which we write using the notation of [14]:

$$c_{\mathrm{LR}}(|B\rangle) \equiv R_{\mathrm{LR}}(|B\rangle) + R_{\mathrm{RL}}(|B\rangle) = 2R_{\mathrm{LR}}(|B\rangle). \tag{3.40}$$

In fact, $\mathcal{T} + \mathcal{R} = 1$, and so c_{LR} is the only free parameter needed to specify the coefficients (3.39). Furthermore, the analogous matrices defined with higher-level Virasoro modes do not give additional information because by the gluing condition (3.23) (taking $n \geq 2$)

$$\begin{aligned} &\langle\Omega|L_n^{[I]}\overline{L}_{n+1}^{[J]}\big[L_1^{[\mathrm{L}]} + L_1^{[\mathrm{R}]} - \overline{L}_{-1}^{[\mathrm{L}]} - \overline{L}_{-1}^{[\mathrm{R}]}\big]|B\rangle = 0 \\ &\qquad \Longrightarrow \ \frac{\langle\Omega|L_n^{[I]}\overline{L}_n^{[J]}|B\rangle}{\langle\Omega|B\rangle} = \frac{n(n^2-1)}{6} R_{IJ}(|B\rangle). \end{aligned} \tag{3.41}$$

It is important to bear in mind that the formulas (3.39) are only one way to quantify transport probabilities, and they do so in an indirect and somewhat incomplete way because they only use Virasoro modes. Nonetheless, the boundary-state formalism had been extended by [73] to include overlaps with states created by other symmetry generators besides those of Virasoro, but each associated matrix only gives one piece of CFT data.

[14] presents another more physically motivated and complete approach. Instead of folding the ICFT and invoking the boundary-state formalism, they set up a scattering *gedankenexperiment* in the ICFT by sending a wave packet towards the interface and define transport coefficients in terms of ratios of average energy fluxes. The resulting "scattering" transmission coefficients are generically determined by the coefficients of two-point functions between spin-2 quasi-primary holomorphic currents on the left and on the right of the interface.

Notably, if the only such current on both sides is the stress tensor, then the transmission coefficient is *universal*—regardless of the in-state, transmission is a function of just one piece of CFT data c_{LR} (keeping $c_{\mathrm{L}}, c_{\mathrm{R}}$ fixed), and this quantity appears in the following two-point function of the left and right stress tensors computed in the vacuum state of the interface theory's Hilbert space:

$$\langle T_{\mathrm{L}}(z) T_{\mathrm{R}}(z') \rangle_{\text{interface}} = \frac{c_{\mathrm{LR}}/2}{(z-z')^4}. \tag{3.42}$$

If transport only cares about c_{LR}, then the coefficients (3.39) defined previously by [15] can be seen to describe *weighted averages* of the scattering coefficients, as found by [14]. So (3.39) are sometimes called "weighted-average coefficients" (e.g. by [4]).

In generic CFTs, the transport coefficients of [14] are state-dependent. Specifically, the in-state of the scattering experiment is created by some local operator, which [14] takes to be localized on the left and denotes as O_{L}, acting on the ICFT vacuum. The $O_{\mathrm{L}} \times O_{\mathrm{L}}$ OPE might contain a spin-2 holomorphic (quasi-)primary $\mathcal{O}_{\mathrm{L}} \neq T_{\mathrm{L}}$. For any such operator, there is a nontrivial two-point function $\langle \mathcal{O}_{\mathrm{L}}(z) T_{\mathrm{R}}(z') \rangle_{\text{interface}}$ with the same pole structure as (3.42). The transport coefficients for the in-state created by O_{L} thus depends not only on c_{LR} but also the coefficients of these other two-point functions. So proper characterization of energy transport across the interface requires inclusion of this additional data.

We can extract this data from the boundary state $|B\rangle$ associated to the interface. For example, consider a *primary*[10] spin-2 holomorphic current $\mathcal{O}$ whose Laurent modes are

$$\mathcal{O}_n \equiv \frac{1}{2\pi i} \oint dz\, z^{n+1} \mathcal{O}(z) \implies [L_n, \mathcal{O}_m] = (n-m)\mathcal{O}_{n+m}. \tag{3.43}$$

We then define the following quantity in analogy to (3.40):

$$\alpha^{\mathcal{O}}_{\mathrm{LR}}(|B\rangle) = 2 \frac{\langle \Omega | \mathcal{O}_2^{[\mathrm{L}]} \overline{L}_2^{[\mathrm{R}]} | B \rangle}{\langle \Omega | B \rangle}. \tag{3.44}$$

[10]Quasi-primaries would yields a nontrivial central term in the commutator with L_n, but this would not alter the qualitative discussion below.

Quantities defined with higher modes are redundant, again because of a recursion relation of the form (3.41). So $\alpha^{\mathcal{O}}_{\rm LR}$ is the specific piece of CFT data associated with $\mathcal{O}$ that describes energy transport. However, we reiterate that if the scattering state is prepared with the stress tensor (i.e. $O_{\rm L} = T_{\rm L}$), then even in a generic CFT the only datum that matters in describing transport in that state is $c_{\rm LR}$.

At this point, we focus on how the transport data of the symmetric orbifold is informed by that of the seed theory following the boundary state formalism of [15, 73, 74]. We start with $c_{\rm LR}$. We then discuss the data associated with another type of spin-2 holomorphic primary W whose existence is rooted solely in the product structure of the symmetric orbifold theory. The punchline is that $\alpha^{W}_{\rm LR} = 0$, so if transport in the seed theory only depends on $c_{\rm LR}$, then the same is true in the symmetric orbifold.

Transmission of stress tensor Our first goal is to write the datum $c_{\rm LR}$ for a symmetric orbifold theory's boundary state in terms of seed data. This will determine the $\mathcal{T}, \mathcal{R}$ coefficients (3.39).

First, recall that the nth full Virasoro generator is a sum over nth Virasoro generators of each copy of the seed theory. So, we have that

$$L_2^{[I]}\overline{L}_2^{[J]} = \left(\sum_{i=1}^{N} L_2^{(i)[I]}\right)\left(\sum_{j=1}^{N} \overline{L}_2^{(j)[J]}\right) = \sum_{i=1}^{N} L_2^{(i)[I]}\overline{L}_2^{(i)[J]} + \sum_{i\neq j} L_2^{(i)[I]}\overline{L}_2^{(j)[J]}. \tag{3.45}$$

Observe that we have decomposed the sum into two pieces, where the second sum consists of "cross terms." So to compute $R_{\rm LR}$ (which is sufficient to get $\mathcal{T}$ and $\mathcal{R}$), we write

$$\begin{aligned} R_{\rm LR}(|B\rangle) &= \frac{\langle 0|^{\otimes N} L_2^{[\rm L]}\overline{L}_2^{[\rm J]}|B\rangle}{\langle 0|^{\otimes N}|B\rangle} \\ &= \sum_{i=1}^{N} \frac{\langle 0|L_2^{(i)[\rm L]}\overline{L}_2^{(i)[\rm R]}|b_{\alpha_i}\rangle}{\langle 0|b_{\alpha_i}\rangle} + \sum_{i\neq j} \frac{\langle 0|L_2^{(i)[\rm L]}|b_{\alpha_i}\rangle}{\langle 0|b_{\alpha_i}\rangle}\frac{\langle 0|\overline{L}_2^{(j)[\rm R]}|b_{\alpha_j}\rangle}{\langle 0|b_{\alpha_j}\rangle}. \end{aligned} \tag{3.46}$$

Here we have used the facts that the twisted-sector terms are projected out of the boundary state and that the normalization factors of $|B\rangle$ cancel. However, for

$R_{\rm LR}(|B\rangle)$ to be purely a function of seed transport data $R_{\rm LR}(|b_{\alpha_i}\rangle)$, the cross terms above need to vanish. Indeed, we assert that these terms must vanish because their numerators are basically products of overlaps between seed conformal boundary states and spin-2 states. To see this explicitly, we invoke the gluing condition and the fact that global Virasoro generators annihilate $\langle 0|$:

$$\begin{aligned} 0 &= \langle 0|L_n^{(i)[I]}\left[L_{-1}^{(i)[\rm L]} + L_{-1}^{(i)[\rm R]} - \overline{L}_1^{(i)[\rm L]} - \overline{L}_1^{(i)[\rm R]}\right]|b_{\alpha_i}\rangle \\ &= \langle 0|[L_n^{(i)[I]}, L_{-1}^{(i)[I]}]|b_{\alpha_i}\rangle \\ &= (n+1)\langle 0|L_{n-1}^{(i)[I]}|b_{\alpha_i}\rangle. \end{aligned} \tag{3.47}$$

Thus, by taking $n = 3$ we have that $\langle 0|L_2^{(i)[I]}|b_{\alpha_i}\rangle = 0$, and so

$$R_{\rm LR}(|B\rangle) = \sum_{i=1}^{N} R_{\rm LR}(|b_{\alpha_i}\rangle \implies c_{\rm LR}(|B\rangle) = \sum_{i=1}^{N} c_{\rm LR}(|b_{\alpha_i}\rangle). \tag{3.48}$$

Let us also write this in terms of the weighted-average transport coefficients (3.39). First, we note that the seed transmission coefficient for a boundary state $|b_\alpha\rangle$ is

$$\mathcal{T}_{b_\alpha} \equiv \frac{2c_{\rm LR}(|b_\alpha\rangle)}{c_{\rm L}^{(\rm s)} + c_{\rm R}^{(\rm s)}}, \tag{3.49}$$

where $c_{\rm L}^{(\rm s)}$ and $c_{\rm R}^{(\rm s)}$ are respectively the central charges of the left and right seed theories. From (3.39), we have that the transmission and reflection coefficients encoded by $|B\rangle$ are

$$\mathcal{T}(|B\rangle) = \frac{2c_{\rm LR}(|B\rangle)}{Nc_{\rm L}^{(\rm s)} + Nc_{\rm R}^{(\rm s)}} = \frac{1}{N}\sum_{i=1}^{N}\mathcal{T}_{\alpha_i}, \tag{3.50}$$

$$\mathcal{R}(|B\rangle) = \frac{2}{Nc_{\rm L}^{(\rm s)} + Nc_{\rm R}^{(\rm s)}}\sum_{i=1}^{N}[R_{\rm LL}(|b_{\alpha_i}\rangle) + R_{\rm RR}(|b_{\alpha_i}\rangle)] = \frac{1}{N}\sum_{i=1}^{N}\mathcal{R}_{\alpha_i}. \tag{3.51}$$

In other words, the weighted-average coefficients encoded by some boundary state $|B\rangle$ are themselves averages the coefficients encoded by each individual seed boundary state in $|B\rangle$.

Other spin-2 primary currents We have written c_{LR} and the associated transport coefficients (3.39) in terms of seed data. However, there is in principle more data that goes into the energy transport coefficients, particularly if there are holomorphic quasi-primary currents of spin 2 apart from the stress tensor. It is indeed possible to have such currents in a symmetric orbifold, even when the seed theory does not. However, we argue that the associated transport data vanishes, and this intuitively is because the different seed copies do not interact at the orbifold point.

Let us be more specific about the construction of these spin-2 currents. It is a generic feature of symmetric orbifold theories that higher-spin (quasi-)primary currents can be written from those of the seed theory. Basically, such currents are constructed by starting with permutation-symmetric products of lower-spin (quasi-)primary currents and potentially adding derivative terms. We can check that the resulting quantity is itself primary by computing the OPE with the full stress tensor. The spin is easily seen to be the sum of the constituent factors' spins by applying a generic conformal transformation.

The existence of higher-spin currents is explored in depth by [64]. An example found for all CFTs provided therein is the following holomorphic spin-4 primary current constructed solely from the seed stress tensor:

$$\sum_{i=1}^{N}\left[T^{(i)}T^{(i)}-\frac{3}{10}\partial^2 T^{(i)}\right]-\frac{22+5c}{5c(N-1)}\sum_{i\neq j}T^{(i)}T^{(j)}. \tag{3.52}$$

Here, $T^{(i)}$ is the ith seed stress tensor, and as before c is the seed central charge.

Note that these novel currents are always higher in spin relative to the seed currents. So, if we for example only have Virasoro symmetry in the seed theory, then there will be no spin-2 currents apart from the full stress tensor in the symmetric orbifold. However, if we have a seed current of spin $s=\frac{2}{k}$ for any positive integer $k\leq N$, then the symmetric orbifold should have a spin-2 current (built from k-fold products of seed operators), even if the seed theory does not!

To make the discussion even more specific, suppose that the seed theory has a U(1) holomorphic current J corresponding to some extended symmetry.[11] [64] constructs two spin-2 holomorphic fields:

$$Y \equiv \sum_{i=1}^{N} \left[T^{(i)} - \frac{3}{2} J^{(i)} J^{(i)} \right], \quad W \equiv \sum_{i \neq j} J^{(i)} J^{(j)}. \tag{3.53}$$

Y is quasi-primary while W is primary. Of course, our goal here is to consider symmetric orbifolds for which the ith seed theory does not have a spin-2 (quasi-)primary apart from $T^{(i)}$, so we can assume that $T^{(i)}$ is given by the Sugawara construction utilizing $J^{(i)}$ (as in a WZW model). In that case, Y is actually just the full stress tensor (up to some rescaling), and so the only spin-2 holomorphic current present in the symmetric orbifold besides the full T is W. This is enough to violate the assumptions in the proof of [14] that transport only cares about c_{LR}.

At this point, we seek to compute α_{LR}^{W} using the same boundary-state approach as for c_{LR} above. To do so, first take the Laurent modes of $J^{(i)}$ and W:

$$J_n^{(i)} \equiv \frac{1}{2\pi i} \oint dz\, z^n J^{(i)}(z), \quad W_n \equiv \frac{1}{2\pi i} \oint dz\, z^{n+1} W(z). \tag{3.54}$$

Of course, each W_n can be expressed as

$$W_n = \sum_{m \in \mathbb{Z}} \sum_{i \neq j} J_m^{(i)} J_{n-m}^{(j)}. \tag{3.55}$$

We now plug into (3.44) to write

$$\alpha_{\mathrm{LR}}^{W} = 2 \sum_{i \neq j} \sum_{k=1}^{N} \frac{\langle 0|^{\otimes N} J_1^{(i)[\mathrm{L}]} J_1^{(j)[\mathrm{L}]} \overline{L}_2^{(k)[\mathrm{R}]} |B\rangle}{\langle 0|^{\otimes N} |B\rangle}. \tag{3.56}$$

When plugging in (3.55), only the $m = 1$ term will survive acting on the vacuum, which is why we only have J_1 insertions. However, each term will contain a factor of

[11] One could consider other symmetries, such as non-abelian ones. However, we do not anticipate the details of the group being relevant to the following statements.

the form $\langle 0|J_1^{(i)[I]}|b_{\alpha_i}\rangle$, which again is the overlap of a state with spin and a boundary state and will thus vanish by invoking the gluing condition (3.25).[12] So,

$$\alpha_{\mathrm{LR}}^W = 0. \tag{3.57}$$

Just to reiterate, we can consider other symmetry algebras. This would introduce nontrivial structure constants in the commutator between same-seed copies of currents. However, so long as we only have one spin-2 quasi-primary (i.e. the Sugawara stress tensor) in the seed theory, we still have that transport depends only on one parameter in the symmetric orbifold due to the non-interaction between different seed copies.

Indeed, all of the above equations and statements are only expected to hold at the orbifold point. In the strongly coupled regime far from the orbifold fixed point, mixing between the different copies would spoil (3.48) and (3.57). One known way to access this sector is through holography, as we discuss in Section 3.3.

3.2.4 Extracting twisted-sector data

Symmetric orbifold theories have a large symmetry algebra that universally includes fractional Virasoro operators. These fractional modes can be used to define twisted-sector analogs to the untwisted data covered in Section 3.2.3. We briefly elaborate on this point, but we leave much to follow-up work.

Twisted g-function and fractional entropy We start with the twisted g-function. Consider a twisted sector labeled by the integer partition $\{k_1, \ldots, k_m\}$. By analogy to the untwisted quantity (3.36), we define the twisted g-function as the overlap of a boundary state $|B\rangle$ with the appropriate bare twist $|0^{(k_1)}\rangle \odot \cdots \odot |0^{(k_m)}\rangle$:

$$g^{(k_1,\ldots,k_m)}(|B\rangle) \equiv \left(\langle 0^{(k_1)}| \odot \cdots \odot \langle 0^{(k_m)}|\right)|B\rangle. \tag{3.58}$$

[12] To show this more explicitly, we can start with $\langle 0|J_n^{(i)[I]}\left[L_{-1}^{(i)[\mathrm{L}]} + L_{-1}^{(i)[\mathrm{R}]} - \overline{L}_1^{(i)[\mathrm{L}]} - \overline{L}_1^{(i)[\mathrm{R}]}\right]|b_{\alpha_i}\rangle = 0$ and invoke the commutator $[J_n^{(i)[I]}, L_{-1}^{(i)[I]}] = nJ_{n-1}^{(i)[I]}$. Setting $n = 2$ yields $\langle 0|J_1^{(i)[I]}|b_{\alpha_i}\rangle = 0$.

How do we interpret this quantity? First, we recall that the typical g-function is related to the boundary entropy $S_{\rm b} = \log g$ that appears as a universal term in the thermodynamic limit of the entropy [12, 19]. This is often demonstrated by starting with the Euclidean cylinder partition function between two boundary states $|A\rangle$ and $|B\rangle$ in the closed-string quantization scheme. Following the normalization conventions of the review in [75], we write this partition function as

$$Z = \langle A|e^{-WH^{\rm cl}}|B\rangle, \tag{3.59}$$

where W is the width of the cylinder and $H^{\rm cl}$ is the Hamiltonian that evolves the closed-string state on the circle from $|A\rangle$ to $|B\rangle$. In terms of (full) Virasoro modes and the circumference β, this is

$$H^{\rm cl} = \frac{2\pi}{\beta}\left(L_0 + \overline{L}_0 - \frac{Nc}{12}\right), \tag{3.60}$$

where we recall that the seed central charge is c, so the symmetric orbifold's is Nc.

We can identify (3.59) with a thermal partition function (associated with the open-string quantization) and take the thermodynamic limit $W \gg \beta$. This is called the "closed-string limit" and, assuming an Ishibashi basis $\{|\mathfrak{h}\rangle\rangle\}$, yields the approximation

$$Z \approx \sum_{\mathfrak{h}} \langle A|\mathfrak{h}\rangle\langle\mathfrak{h}|B\rangle q^{\mathfrak{h}-Nc/24}, \quad q \equiv e^{-4\pi W/\beta}. \tag{3.61}$$

where we sum over primary states of weight $\mathfrak{h}$. The term that dominates in the strict limit is the one corresponding to the true vacuum $\mathfrak{h} = 0$, and so we can write the entropy as

$$S_{\rm th} \equiv -\beta^2 \frac{\partial}{\partial\beta}\left(\beta^{-1}\log Z\right) = \left(\frac{\pi Nc}{3}\right)\frac{W}{\beta} + \log g(|A\rangle) + \log g(|B\rangle) + \cdots, \tag{3.62}$$

i.e. as an extensive piece plus two constant pieces.

This limit produces an expression that is universal to all CFTs. However, in a symmetric orbifold theory, we can rearrange the partition function in the closed-string limit (3.61) into an overall sum over twisted sectors, then note that each excited state

within a particular twisted sector is suppressed by the bare twist.[13] Thus we have the approximation

$$Z \approx \sum_{\substack{k_1+\cdots+k_m=N \\ k_1\leq\cdots\leq k_m}} g^{(k_1,\ldots,k_m)}(|A\rangle)\, g^{(k_1,\ldots,k_m)}(|B\rangle)\, q^{\mathfrak{h}[0^{(k_1)},\ldots,0^{(k_m)}]-Nc/24}, \tag{3.63}$$

in which twisted g-functions appear at subleading order to the vacuum term. We deduce that twisted g-functions represent subleading terms in the thermodynamic entropy.

Twisted transport matrices We now return to transport. For brevity and concreteness, we focus on the fractional Virasoro modes associated with the maximally twisted sector, which are $\{\ell^{[\mathrm{L}]}_{n/N}, \overline{\ell}^{[\mathrm{L}]}_{n/N}\}$ for the theory left of the defect and $\{\ell^{[\mathrm{R}]}_{n/N}, \overline{\ell}^{[\mathrm{R}]}_{n/N}\}$ for the theory right of the defect. However, the discussion here can be generalized to other modes. We also emphasize that we will continue using the transport-matrix formalism of [15]. It remains to be seen how the quantities defined hereafter relate to CFT data probed through the more physical scattering processes studied by [14].

The transport matrix (3.38) specifically computes transmission and reflection coefficients associated to the full stress tensor of the theory. One could instead construct a matrix that captures the physics of other fields, as in [73, 74]. To do so, we would need to employ the generators of the extended symmetry algebra. One possible candidate is

$$\widetilde{R}_{IJ}(|B\rangle) \equiv \frac{\langle 0|^{\otimes N} \ell^{[I]}_{n/N} \overline{\ell}^{[J]}_{n/N} |B\rangle}{\langle 0|^{\otimes N}|B\rangle}, \tag{3.64}$$

where as in [73, 74] we use the true vacuum of the theory $|0\rangle^{\otimes N}$. This would measure the transmission of some "twisted" energy flux. Another possibility is to employ the maximally twisted bare twist $|0^{(N)}\rangle$, instead of the vacuum. By doing so, we define

$$R^{(N)}_{IJ}(|B\rangle) \equiv \frac{\langle 0^{(N)}| \ell^{[I]}_{2/N} \overline{\ell}^{[J]}_{2/N} |B\rangle}{\langle 0^{(N)}|B\rangle}, \tag{3.65}$$

[13] This argument should be true for any theory with superselection sectors.

in direct analogy to (3.38). Note that we must use $\ell_{2/N}$ because $\langle 0^{(N)}|\ell_{1/N} = 0$ [63], much like how $\langle 0|L_1 = 0$ for any CFT with vacuum $|0\rangle$.

If the boundary state respects the extended algebra [meaning (3.30) is satisfied], then we can derive a relation between matrices using higher fractional modes and $R^{(N)}_{IJ}$, just like (3.41) for R_{IJ}. Specifically, we use the fact that

$$\langle 0^{(N)}|\ell^{[I]}_{n/N}\overline{\ell}^{[J]}_{(n+1)/N}\big[\ell^{[\mathrm{L}]}_{1/N} + \ell^{[\mathrm{R}]}_{1/N} - \overline{\ell}^{[\mathrm{L}]}_{-1/N} - \overline{\ell}^{[\mathrm{R}]}_{-1/N}\big]|B\rangle = 0, \tag{3.66}$$

and the commutation bracket (3.20) to write the recursive relation

$$\frac{n-1}{N}\langle 0^{(N)}|\ell^{[I]}_{(n+1)/N}\overline{\ell}^{[J]}_{(n+1)/N}|B\rangle = \frac{n+2}{N}\langle 0^{(N)}|\ell^{[I]}_{n/N}\overline{\ell}^{[J]}_{n/N}|B\rangle. \tag{3.67}$$

After cancelling the $\frac{1}{N}$, we can see that the prefactors are identical to those of the recursive relation used to derive (3.41). Thus,

$$\frac{\langle 0^{(N)}|\ell^{[I]}_{n/N}\overline{\ell}^{[J]}_{n/N}|B\rangle}{\langle 0^{(N)}|B\rangle} = \frac{n(n^2-1)}{6}R^{(N)}_{IJ}(|B\rangle). \tag{3.68}$$

Yet another matrix with perhaps with the clearest physical connection to scattering [14] is

$$R^{\ell}_{IJ}(|B\rangle) \equiv \frac{\langle 0^{(N)}|\ell^{[I]}_{2/N}\overline{L}^{[J]}_{2}|B\rangle}{\langle 0|^{\otimes N}|B\rangle}, \tag{3.69}$$

This should compute energy transmission of a scattering state prepared by exciting the bare twist $|0^{(N)}\rangle$ with the stress tensor.

We refrain from pushing these alternative matrices further for now. An interesting question is how to write these quantities in terms of the seed transport matrices. One path to do so might be to employ the covering-space techniques of [65, 76] used to study fractional modes by [63, 66, 67]. Another avenue is to directly scatter excitations of bare twists (since they are essentially twisted-sector vacua) and apply the definitions of [14]. We leave these directions to future work.

3.3 The holographic symmetric orbifold of the $\mathbb{T}^4$ ICFT

As a particularly tractable example, we examine the transport datum c_{LR} in the symmetric orbifold of a $\mathbb{T}^4$ sigma model. The seed ICFT consists of four copies of a scalar field $\widetilde{\phi} : \mathbb{R} \to S^1$ which "jumps" in coupling at some interface. To approximate the weakly coupled regime, we take the seed theory to consist of free scalars described by the action

$$I_{S^1} = \frac{R_-^2}{2} \int_{\tilde{y}<0} dt\, d\tilde{y}\, (\partial \widetilde{\phi}_-)^2 + \frac{R_+^2}{2} \int_{\tilde{y}>0} dt\, d\tilde{y}\, (\partial \widetilde{\phi}_+)^2. \tag{3.70}$$

The couplings $R_\pm$ are the radii of the target space on the two sides of the interface and are generically distinct from one another.[14]

We can turn on a marginal coupling that breaks the permutation symmetry and thus deforms the symmetric orbifold theory away from the orbifold point [54]. The strongly coupled/deformed, large-N regime of the symmetric orbifold theory built from scalars with the simple jump in (3.70) is described by type IIB supergravity on 3-dimensional Janus [57] (Figure 3.3). This background is a solution to the type IIB supergravity action constructed by deforming the $\mathrm{AdS}_3 \times S^3 \times \mathbb{T}^4$ vacuum with a dilaton. 3d Janus is under a large amount of analytic control, just like the thin-brane models used in previous studies of holographic interfaces [4, 77, 78, 1].

It is possible to compute c_{LR} in the strongly coupled regime for the interface described by the Janus solution through recently developed methods [1, 17]. Additionally, working directly in pure Janus specifies a particular boundary state on the field-theory side constructed from copies of a single boundary state of the seed S^1 theory [8, 9]. With this in mind, we can also approximate the associated transport coefficients in the weakly coupled regime because the free-scalar seed theory (3.70) is rather simple (cf. [15]). Upon doing so, we compare the answer against that of [17] to bound the running of transport coefficients with the marginal coupling of the ICFT. The resulting plot is shown in Figure 3.6.

[14] Note that we are assuming the target space to be a square torus, with all of the radii equal.

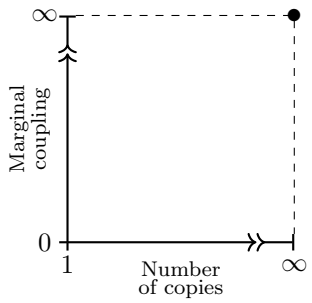

Figure 3.3: The parameter space of the symmetric orbifold of $\mathbb{T}^4$. We can dial both the number of seed copies and the marginal coupling which makes the copies interact. The bottom axis (with coupling = 0) describes the orbifold point. The black point is the holographic limit at which the description by type IIB supergravity on Janus is valid.

3.3.1 3d Janus and holography

Gravitational solution In the Einstein frame of the type IIB supergravity action, we consider solutions of the form

$$ds^2_{\text{IIB}} = e^{\phi/2}\left(ds^2_3 + d\Omega^2_3\right)^2 + e^{-\phi/2} ds^2_{\mathbb{T}^4}. \tag{3.71}$$

The dimensional reduction of the action onto the 3 noncompact dimensions is

$$S^{(3)}_{\text{GR}}[g,\phi] = \frac{1}{16\pi G^{(3)}_{\text{N}}} \int d^3x\sqrt{-g}\left(R + \frac{2}{L^2} - \partial_\alpha\phi\partial^\alpha\phi\right), \tag{3.72}$$

where $G^{(3)}_{\text{N}}$ is the 3d Newtonian constant, L is a length scale, and Greek indices run over spacetime. The classical equations of motion are

$$G_{\mu\nu} - \frac{1}{L^2} g_{\mu\nu} = \partial_\mu\phi\partial_\nu\phi - \frac{g_{\mu\nu}}{2}\partial_\alpha\phi\partial^\alpha\phi, \tag{3.73}$$

$$\nabla_\mu\nabla^\mu\phi = 0. \tag{3.74}$$

For the 3d spacetime, we assume the ansatz

$$\frac{ds^2}{L^2} = \frac{f(y)}{z^2}(-dt^2 + dz^2) + dy^2, \quad \phi = \phi(y), \tag{3.75}$$

with $t, y \in (-\infty, \infty)$ and $z > 0$. The 3d Janus solution corresponds to the metric function,

$$f(y) = \frac{1}{2}\left[1 + \sqrt{1 - 2\gamma^2}\cosh(2y)\right], \tag{3.76}$$

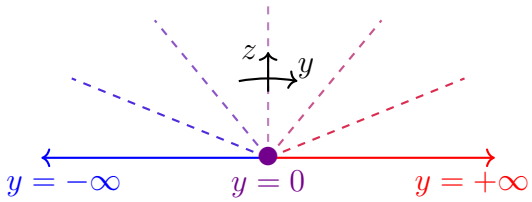

Figure 3.4: A constant-time slice of 3-dimensional Janus with radial coordinate z and hyperbolic angular coordinate y. The dashed lines are AdS_2 slices of the bulk. The $y = 0$ point is the interface between the left ($y < 0$) and right ($y > 0$) CFTs.

where $\gamma \in \left[0, \frac{1}{\sqrt{2}}\right)$ is some parameter characterizing the solution.[15] See Figure 3.4 for a visual representation of 3d Janus. In this background, the dilaton's profile is

$$\phi(y) = \phi_0 + \frac{1}{\sqrt{2}} \log\left(\frac{1 + \sqrt{1-2\gamma^2} + \sqrt{2}\gamma \tanh y}{1 + \sqrt{1-2\gamma^2} - \sqrt{2}\gamma \tanh y}\right), \tag{3.77}$$

Thus, the asymptotic values of the dilaton are

$$\phi_\pm = \lim_{y\to\pm\infty} \phi(y) = \phi_0 \pm \frac{1}{2\sqrt{2}} \log\left(\frac{1+\sqrt{2}\gamma}{1-\sqrt{2}\gamma}\right). \tag{3.78}$$

One benefit of studying the 3d Janus solution is that the dual field theory is known to be a highly deformed (i.e. strongly coupled) symmetric orbifold ICFT. The parameters of the theory can be described in terms of the number of fundamental D-branes.

Field-theory dual The starting point is to recall the holographic dual of type IIB string theory on $AdS_3 \times S^3 \times \mathbb{T}^4$. There, we take the D1/D5 system consisting of Q_1 D1-branes and Q_5 D5-branes in $\mathbb{R}^6 \times \mathbb{T}^4$ [79]. For large $Q_1, Q_5 \gg \frac{1}{g_s} \gg 1$, the AdS/CFT correspondence describes a duality between type IIB supergravity on $AdS_3 \times S^3 \times \mathbb{T}^4$ and a strongly coupled CFT on the boundary of $AdS_3 \times S^3$. The target space of the CFT is topologically $(\mathbb{T}^4)^{Q_1Q_5}/S_{Q_1Q_5}$ [5, 80, 81], and so it is a highly deformed symmetric orbifold theory consisting of $N \equiv Q_1Q_5 \gg 1$ copies of a $\mathbb{T}^4$ sigma model.

[15] $\gamma = 0$ corresponds to the non-deformed AdS_3 vacuum, and we find naked singularities if $\gamma^2 > \frac{1}{2}$ [57].

To construct the Janus solution, we are adding a (non-supersymmetric) dilatonic deformation on top of the $\mathrm{AdS}_3 \times S^3 \times \mathbb{T}^4$ vacuum. As this dilaton asymptotes to two distinct values on the AdS boundary (3.78), the bulk deformation introduces an interface in the dual symmetric orbifold theory.

We can identify the radius of each S^1 factor of the target-space torus with the asymptotic value of $e^{-\phi/2}$ [8]. However, since the dilaton profile (3.77) takes two values at infinity (3.78), the radius "jumps" between two values R_+ and R_-, where

$$R_\pm \propto e^{-\phi_\pm/2} = e^{-\phi_0/2} \left(\frac{1+\sqrt{2}\gamma}{1-\sqrt{2}\gamma} \right)^{\mp \frac{1}{4\sqrt{2}}} . \tag{3.79}$$

We interpret this nontrivial jump as describing the presence of an interface in the theory. With this in mind, observe that the ratio of the two radii,

$$\frac{R_+}{R_-} = \left(\frac{1+\sqrt{2}\gamma}{1-\sqrt{2}\gamma} \right)^{-\frac{1}{2\sqrt{2}}} , \tag{3.80}$$

goes to 1 as $\gamma \to 0$ (the interface disappears) and goes to 0 as $\gamma \to \frac{1}{\sqrt{2}}$ (there is a parametrically large separation of scales between the sides). Intuitively, we expect these limits to respectively correspond to a completely transparent or completely reflective interface.

Note that the form of the boundary state encoding the Janus interface is not obvious. However, [8] argues that it consists of N identical copies of a four-fold (one per $S^1 \subset \mathbb{T}^4$) "Neumann–Dirichlet" state in the $\mathbb{T}^4$ sigma model. While there may be twisted-sector terms, from our earlier analysis we assert that transport is not sensitive to the resulting combinatorial factors and does not probe such terms.

3.3.2 Strong-coupling transport from gravity waves

The holographic prescription for the transport datum c_{LR} [4] is to consider linearized, source-free fluctuations of the metric in Fefferman–Graham (FG) gauge

[39] (setting $L = 1$),

$$ds^2_{\rm FG} = \frac{du^2}{u^2} + \frac{1}{u^2}\left[g^{(0)}_{ij} + u^2 g^{(2)}_{ij} + \frac{u^4}{4} g^{(4)}_{ij} + \cdots\right] dw^i dw^j, \tag{3.81}$$

where $u > 0$ is the radial coordinate and the Latin indices run over the remaining $1+1$ dimensions. These fluctuations are called *surface gravity waves*, and in the boundary theory they corresponds to excitations produced by the stress tensor [39, 82]. In the thin-brane model of [4] consisting of two AdS_3 geometries glued along an AdS_2 surface, we scatter these surface gravity waves off of the brane. This corresponds to the scattering *gedankenexperiment* of [14] in the boundary theory, with the in-state being prepared by the stress tensor. The amplitudes of the reflected and transmitted waves can be translated into the transport coefficients. The bulk equations of motion and boundary conditions can then be used to constrain these transport coefficients.

Scattering on Janus We may attempt an analogous scattering experiment directly in Janus. While possible in principle, this is difficult in practice. To see why, we first write (3.75) in FG form to serve as the background of our scattering experiment. This has been done perturbatively in the Janus parameter by [83] (see also [84, 85]). Up to the first subleading term of order γ^2, we approximate the metric function f in (3.75) as

$$f(y) = \cosh^2 y - \frac{1}{2}\gamma^2 \cosh^2 y + O(\gamma^4). \tag{3.82}$$

Taking $\gamma = 0$ (pure AdS), the FG metric comes about through the coordinate transformation $z \to \sqrt{\tilde{y}^2 + u^2}$ and $y \to^{-1} \left(\frac{\tilde{y}}{u}\right)$. For Janus, we thus consider the ansatz

$$z \to \sqrt{\tilde{y}^2 + u^2} + \gamma^2 u f_z\left(\frac{\tilde{y}}{u}\right) + O(\gamma^4), \quad y \to^{-1} \left(\frac{\tilde{y}}{u}\right) + \gamma^2 f_y\left(\frac{\tilde{y}}{u}\right) + O(\gamma^4). \tag{3.83}$$

Upon plugging this in and insisting that the geometry is still asymptotically AdS (as $u \to 0$), we find the functions

$$f_z(x) = \frac{-2 + (1+2x^2)\log\left(\frac{1+x^2}{x^2}\right)}{8\sqrt{1+x^2}}, \quad f_y(x) = \frac{1 + 4x^2 + x^2 \log\left(\frac{1+x^2}{x^2}\right)}{8x\sqrt{1+x^2}}, \tag{3.84}$$

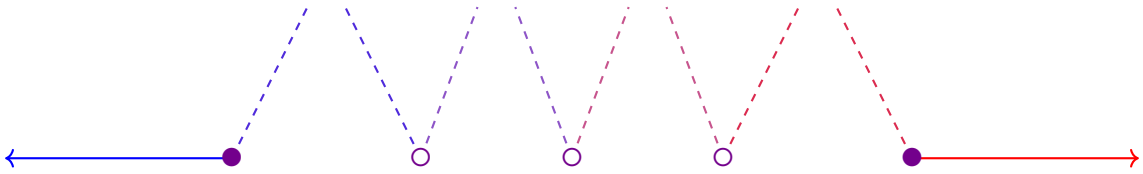

Figure 3.5: A discrete array of thin branes in AdS_3. This is the setup used by [1] to extend the prescription for transport coefficients of [4] beyond the case of a thin brane with one tension parameter. "Thick brane" configurations in which the interface is represented by a smooth geometry foliated into AdS slices can be discretized into an array of thin branes.

for which the transformed metric truncated at order γ^2 is[16]

$$\begin{aligned} ds^2 \sim \frac{du^2}{u^2} &- \left[\frac{1}{u^2} + \frac{\gamma^2}{4}\left(\frac{1}{u^2+\tilde{y}^2} - \frac{1}{u^2}\log\left(1+\frac{u^2}{\tilde{y}^2}\right)\right)\right] dt^2 \\ &+ \left[\frac{1}{u^2} - \frac{\gamma^2}{4}\left(\frac{1}{\tilde{y}^2} - \frac{1}{u^2}\log\left(1+\frac{u^2}{\tilde{y}^2}\right)\right)\right] d\tilde{y}^2 \\ &= \frac{du^2}{u^2} + \frac{1}{u^2}\left[\left(-dt^2+d\tilde{y}^2\right) - \frac{u^4}{4}\frac{\gamma^2}{2\tilde{y}^4}\left(-dt^2+d\tilde{y}^2\right) + \cdots\right]. \end{aligned} \tag{3.85}$$

Unlike the thin-brane solution on AdS_3 of [4], the metric does not truncate at the $g^{(4)}_{ij}$ term and breaks down near the interface. These features make it difficult to compute constraints from fluctuations on Janus even up to order-γ^2 terms. Additionally, the fluctuations may themselves need γ-dependence in order for the constraints to be nontrivial.

Most importantly, our goal is to perform a strong-weak comparison over the full range of the Janus parameter γ. As such, while a perturbative calculation might be a useful proof of principle, it is not particularly helpful in accomplishing our ultimate purpose.

Stacking branes Fortunately, a different γ-exact calculation of the transport coefficients in 3d Janus has been performed by [17]. The first step had been taken by

[16]The transformation (3.83) induces terms which are $O(\gamma^4)$, but we omit these terms.

[1], which extended the earlier thin-brane method to "arrays" of thin branes (Figure 3.5). This provides more parametric freedom in the bulk and allows for holographic computations of transport coefficients encoded by a broader class of interfaces.

[17] considers interfaces which are holographically described by continuous $(d+1)$-dimensional bulk geometries that can be foliated into AdS_d slices, such as the Janus solution. They observe that these "thick-brane" geometries can be treated as a limit of a discrete array of thin branes. For 3d Janus[17] in particular, they find a tension "density" for the branes in this array and integrate to compute an "effective" tension. Plugging this into the original thin-brane formula [4] yields a γ-exact holographic transmission coefficient:

$$\mathcal{T}^{\mathrm{GR}} \equiv c_{\mathrm{LR}}^{\mathrm{Janus}} = \frac{\gamma}{\sqrt{2}} \left(\mathrm{Tanh}^{-1} \sqrt{\frac{1-\sqrt{1-2\gamma^2}}{1+\sqrt{1-2\gamma^2}}} \right)^{-1} \tag{3.86}$$

$$= \frac{\sqrt{2}\gamma}{\mathrm{Tanh}^{-1}(\sqrt{2}\gamma)} = 1 - \frac{2}{3}\gamma^2 - \frac{16}{45}\gamma^4 + O(\gamma^6). \tag{3.87}$$

This is expected to be equivalent to the answer obtained by scattering surface gravity waves directly on Janus. Nonetheless, the stacking approach is much less tedious and more powerful.

It is worth comparing the Janus result against that of the thin-brane models [4]. In the latter, the underlying action is Einstein plus a Randall–Sundrum term [16, 24]. The tension is thus an effective coupling constant, and tuning the transport coefficients requires fixing the tensions by hand—a fine-tuning problem. However, 3d Janus is a genuine top-down solution, and so we should not require fine-tuning to achieve a particular $\mathcal{T}$ and $\mathcal{R}$. Indeed, the Janus parameter γ is an integration constant labeling the solutions rather than a coupling, and the full physical range of γ furnishes the full unitary range $\mathcal{T} \in [0, 1]$.

[17] [17] uses a slightly different Janus parameter. We present their result in terms of γ.

3.3.3 Weak-coupling transport from seed theory

We now calculate the transport coefficients in the free sector of the $\mathbb{T}^4$ symmetric orbifold ICFT. As we are at the orbifold point, we only need the transport coefficients of the individual seed boundary states used to construct the Janus interface. Then, just as in [8], we take $4N = 4Q_1Q_5$ copies of the Neumann–Dirichlet state in the free scalar theory. With the seed coefficients in hand, we then employ the prescription of Section 3.2—namely (3.50)–(3.51)—to write the "full" transport coefficients.

The seed theory consists of four copies of a free scalar field on 2d Minkowski spacetime $-dt^2 + d\tilde{y}^2$ whose target space is S^1 and with an interface at $\tilde{y} = 0$:

$$S_{\text{FT}}[\widetilde{\phi}] = \frac{R_-^2}{2} \int_{\tilde{y}<0} dt\, d\tilde{y}\, \partial_i \widetilde{\phi}_- \partial^i \widetilde{\phi}_- + \frac{R_+^2}{2} \int_{\tilde{y}>0} dt\, d\tilde{y}\, \partial_i \widetilde{\phi}_+ \partial^i \widetilde{\phi}_+, \tag{3.88}$$

where i here is a spacetime index running over $(t, \tilde{y})$.

The transmission and reflection coefficients in this S^1 theory have been computed by [15] (based on [10]) in a different parameterization. For now, we simply need to recast their results in terms of $R_\pm$. To complete this exercise, we require the behavior of the fields at the interface. Reintroducing coordinate dependence as $\widetilde{\phi} \to \widetilde{\phi}(t, \tilde{y})$, we demand $\delta\widetilde{\phi}_+(t, 0) = \delta\widetilde{\phi}_-(t, 0)$ [8]. By varying the action and integrating by parts, we then get the boundary condition at $\tilde{y} = 0$:

$$R_+^2 \partial_{\tilde{y}} \widetilde{\phi}_+ = R_-^2 \partial_{\tilde{y}} \widetilde{\phi}_-. \tag{3.89}$$

This can be rewritten as a matrix equation in the form presented by [15]. Upon making the substitution $\pm\partial_{\tilde{y}} \to \partial_\pm$, we write

$$\begin{pmatrix} \partial_- \widetilde{\phi}_- \\ \partial_+ \widetilde{\phi}_+ \end{pmatrix} = S \begin{pmatrix} \partial_+ \widetilde{\phi}_- \\ \partial_- \widetilde{\phi}_+ \end{pmatrix}, \quad S = \begin{pmatrix} -\cos(2\theta) & \sin(2\theta) \\ \sin(2\theta) & \cos(2\theta) \end{pmatrix}, \tag{3.90}$$

where we have identified the θ parameter of [15] with $R_\pm$ as follows:

$$\cos(2\theta) = 1 - \frac{2R_-^4}{R_+^4 + R_-^4}, \quad \sin(2\theta) = \frac{2R_+^2 R_-^2}{R_+^4 + R_-^4}. \tag{3.91}$$

The transmission and reflection coefficients in the free theory on S^1 are then

$$\mathcal{T}^{\mathrm{FT}}_{S^1} = \sin^2(2\theta) = \frac{4}{\left[\left(\frac{R_+}{R_-}\right)^2 + \left(\frac{R_-}{R_+}\right)^2\right]^2}, \tag{3.92}$$

$$\mathcal{R}^{\mathrm{FT}}_{S_1} = \cos^2(2\theta) = \left[\frac{\left(\frac{R_+}{R_-}\right)^2 - \left(\frac{R_-}{R_+}\right)^2}{\left(\frac{R_+}{R_-}\right)^2 + \left(\frac{R_-}{R_+}\right)^2}\right]^2. \tag{3.93}$$

The seed $\mathbb{T}^4$ sigma model consists of four non-interacting S^1 factors. For boundary states in the product theory, a similar argument to that of a symmetric orbifold theory at the orbifold point (Section 3.2.3) applies; the transport coefficients of a product state are averages of the transport coefficients of the individual factors (3.50)–(3.51). As the S^1 factors have the same boundary condition, we deduce that the transmission and reflection coefficients in the $\mathbb{T}^4$ theory are still given by (3.92)–(3.93). Furthermore, as all of the seed boundary states are also identical, the total transmission and reflection coefficients (respectively $\mathcal{T}^{\mathrm{FT}}$ and $\mathcal{R}^{\mathrm{FT}}$) are simply the seed values, because they too are computed as averages.

Now, we may recast the transport coefficients in terms of the Janus parameter γ using (3.80). Doing so for the transmission coefficient $\mathcal{T}^{\mathrm{FT}}$, we have that

$$\mathcal{T}^{\mathrm{FT}} \equiv c_{\mathrm{LR}}^{\mathrm{Sym}(\mathbb{T}^4)} = \frac{4\left(1+\sqrt{2}\gamma\right)^{\sqrt{2}}\left(1-\sqrt{2}\gamma\right)^{\sqrt{2}}}{\left[\left(1+\sqrt{2}\gamma\right)^{\sqrt{2}} + \left(1-\sqrt{2}\gamma\right)^{\sqrt{2}}\right]^2} = 1 - 4\gamma^2 + \frac{16}{3}\gamma^4 + O(\gamma^6). \tag{3.94}$$

3.3.4 Comparing across regimes

Equipped with the transport coefficients of the Janus interface both at strong and weak coupling, we now compare the results. To reiterate, the strong-coupling transmission coefficient is approximately the answer obtained from the Janus solution,

$$\mathcal{T}_{\mathrm{strong}} \sim \frac{\sqrt{2}\gamma}{^{-1}(\sqrt{2}\gamma)} = 1 - \frac{2}{3}\gamma^2 - \frac{16}{45}\gamma^4 + O(\gamma^6), \tag{3.95}$$

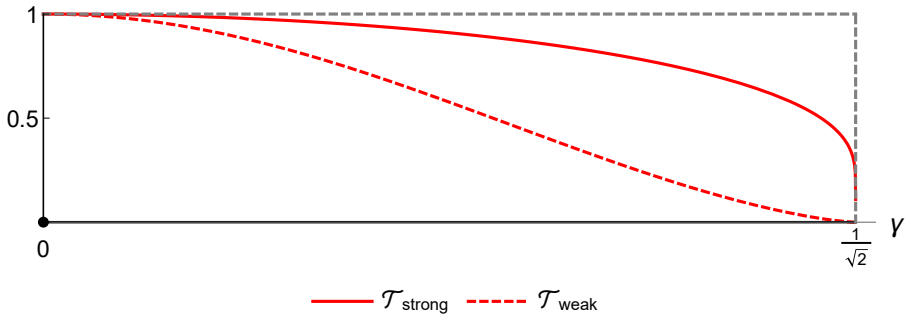

Figure 3.6: The transmission coefficients as functions of the Janus parameter $\gamma \in \left[0, \frac{1}{\sqrt{2}}\right)$ both at strong coupling (solid) and at weak coupling (dashed). While they match at the extremal values of γ, the values at strong coupling are consistently larger than those at weak coupling. Furthermore, the weak-coupling coefficient has an inflection point at $\gamma \approx 0.406$, whereas the strong-coupling coefficient has a strictly negative derivative.

while the weak-coupling transmission coefficient is approximately the one computed directly from the $\mathbb{T}^4$ symmetric orbifold theory at the orbifold point,

$$\mathcal{T}_{\text{weak}} \sim \frac{4\left(1+\sqrt{2}\gamma\right)^{\sqrt{2}}\left(1-\sqrt{2}\gamma\right)^{\sqrt{2}}}{\left[\left(1+\sqrt{2}\gamma\right)^{\sqrt{2}}+\left(1-\sqrt{2}\gamma\right)^{\sqrt{2}}\right]^2} = 1 - 4\gamma^2 + \frac{16}{3}\gamma^4 + O(\gamma^6). \tag{3.96}$$

These are both plotted in Figure 3.6.

We immediately observe that $\mathcal{T}_{\text{strong}} > \mathcal{T}_{\text{weak}}$ away from the extremal values of γ. In other words, turning on the marginal coupling which deforms the symmetric orbifold theory also increases the proportion of energy transmitted through the interface at fixed γ. This makes intuitive sense—energy is able to be exchanged between different copies of the seed left and right CFTs, whereas at the orbifold point these copies do not interact at all.

We also observe that the two functions are structurally different. While $\mathcal{T}_{\text{strong}}(\gamma)$ has a strictly negative derivative and approaches 0 rapidly, $\mathcal{T}_{\text{weak}}(\gamma)$ has an inflection point at $\gamma \approx 0.406$ and approaches 0 more slowly. This indicates that the functional form of the coefficient $\mathcal{T}$ changes as the coupling runs.

We conclude by emphasizing that this result is very different from the situation for boundary entropy $S_{\rm b}$ [8], in which the analogous strong-weak comparison using the Janus solution involves two numerically similar functions of γ. The answer at strong coupling was approximated by employing the Ryu–Takayanagi formula:

$$\frac{S_{\rm b}^{\rm strong}}{N} \sim \log\left(\frac{1}{\sqrt{1-2\gamma^2}}\right) = \gamma^2 + \gamma^4 + O(\gamma^6), \tag{3.97}$$

while the answer at weak coupling was found in field theory to be

$$\frac{S_{\rm b}^{\rm weak}}{N} \sim \log\left[\frac{\left((1+\sqrt{2}\gamma)^{1/\sqrt{2}} + (1-\sqrt{2}\gamma)^{1/\sqrt{2}}\right)^2}{4(1-2\gamma^2)^{1/\sqrt{2}}}\right] = \gamma^2 + \frac{7}{6}\gamma^4 + O(\gamma^6). \tag{3.98}$$

Unlike the strong and weak values of $\mathcal{T}$ (3.95)–(4.3), the strong and weak values of boundary entropy are the same at order-γ^2, and the difference at order-γ^4 is much smaller [an $O(1)$ fraction]. In other words, the boundary entropy appears to be more protected from the running of the coupling than transmission.

3.4 Discussion

To summarize, we have first explored transport coefficients of interfaces in generic symmetric orbifold theories (taken at their orbifold points). In particular, we have used BCFT techniques to write them in terms of "seed" transport coefficients, using the boundary-state construction of [50] and applying the transport-matrix approach of [15]. We have found that, regardless of the number of copies N, the transport coefficients of the boundary states in a symmetric orbifold theory are averages of transport coefficients encoded by seed-theory boundary states, as per the formulas (3.50)–(3.51).

The second part of this paper is a study of the $\mathbb{T}^4$ symmetric orbifold theory. This theory can be understood at strong marginal coupling (away from the orbifold point) through the AdS/CFT correspondence. A simple class of interfaces in this theory are described by the 3d Janus solution to type IIB supergravity [57].

From the tools of gravity, one can extract transport coefficients for this class of interfaces at strong coupling [17]. Furthermore, we compute the transport coefficients at weak coupling (at the orbifold point) by combining our earlier methods and with our knowledge of the seed $\mathbb{T}^4$ sigma model.

This sets the stage for a comparison between the transport coefficients at strong coupling and at weak coupling for Janus interfaces in the symmetric orbifold of $\mathbb{T}^4$. We ultimately find a marked difference. The coefficients are structurally different functions of γ, but transmission through the interface is larger at strong coupling than at weak coupling.

3.4.1 Transport versus thermodynamics

We reiterate that our final result in the symmetric orbifold of $\mathbb{T}^4$ is notably different from previous analogous computations of the boundary entropy [8, 9]. In those cases, boundary entropy of the Janus interface had been found to be relatively protected from the running of the coupling, with supersymmetry *completely* protecting it [9]. Meanwhile, the transport coefficients develop different functional features entirely—most notably the loss of the inflection point at strong coupling in Figure 3.6.

This is reasonable in light of other strong-weak comparisons in holography. One can look to the case of $\mathcal{N} = 4$ 4d supersymmetric Yang–Mills (SYM) theory, which at strong 't Hooft coupling is dual to type IIB supergravity on $\mathrm{AdS}_5 \times S^5$. There, the free energy, which like boundary entropy is a thermodynamic quantity, has been computed both in the free theory and at strong coupling through holography [58, 59]. While the coupling runs over an infinite range, the free energy only changes by a finite factor of $\frac{3}{4}$.

Another quantity which has been compared at both regimes is the shear viscosity of the SYM plasma [60, 61, 62]. This quantity is associated with transport, and its story is very different from that of the free energy. In units of entropy density, it

is well-known that the shear viscocity reaches a finite value of $\frac{1}{4\pi}$ at strong coupling. However, it blows up at weak coupling. Thus, the functional dependence on coupling is not described by a finite interpolating function, unlike for free energy.

Of course, we are comparing different quantities—the boundary entropy versus the transmission coefficient—from those of the $\mathcal{N} = 4$ SYM story. However, they are still respectively facets of thermodynamics and transport, and we again see that the thermodynamic quantity (boundary entropy) is much more strongly [8] (or even completely [9]) protected from the running of the coupling than the transport quantity (transmission coefficient). If would thus be interesting to further scrutinize the validity of this idea that "transport rushes as thermodynamics dawdles" in coupling, with Janus setups (including the higher-dimensional version [86, 87]) being a realm for doing so.

3.4.2 The Janus boundary state

We emphasize that the specific form of the boundary state encoding a Janus interface is not obvious. To glean some insight, we look to the holographic calculation of the boundary entropy in [8] and assume that this should be (reasonably) protected from the running of the marginal coupling. Employing the Ryu–Takayanagi formula [21] yields

$$S_{\mathrm{b}}^{\mathrm{GR}} = N \log\left(\frac{1}{\sqrt{1-2\gamma^2}}\right), \quad N = Q_1 Q_5 \gg 1. \tag{3.99}$$

From this, we see that boundary entropy is an order-N quantity at large N. Furthermore, in performing their comparison with the value at the orbifold point, [8] argues and uses the fact that all copies of the seed boundary state are identical—they are 4-fold products of a "Neumann-Dirichlet" boundary state in the S^1 theory $|b_{\mathrm{ND}}\rangle$.

However, this is not enough to specify the form of the boundary state $|B_{\mathrm{J}}\rangle$.

For example, we can imagine that it takes the form[18]

$$|B_{\rm J}\rangle = \left(|b_{\rm ND}\rangle^{\otimes 4}\right)^{\otimes N}. \tag{3.100}$$

This is assumed by [8, 9] in computing boundary entropy at the orbifold point. In support of this, a lack of twisted-sector terms is not unreasonable. Janus is a type IIB supergravity vacuum. The density of states (in scaling dimension) of the ICFT dual to supergravity on Janus should obey supergravity-like (slow) growth (cf. [88, 89, 64]). Twisted sectors in the symmetric orbifold theory, however, obey Hagedorn (fast) growth at large N [90]. As such, we might only expect to get an interface consistent with the Janus solution if we omit twisted-sector terms even in the free symmetric orbifold. Furthermore, that the two calculations in [8] match to a reasonable degree can be taken as additional evidence for the veracity of (3.100) if one assumes that boundary entropy should not change with coupling.

Another option is to posit the presence of twisted-sector terms, i.e. that the boundary state encoding the Janus interface is built from building blocks (3.29) and (3.35) obtained from a $\mathbb{T}^4$ seed theory [50]. Note however that this state should not describe a "typical" interface in the symmetric orbifold. A more typical state would be built from all distinct seed states (rather than N copies of $|b_{\rm ND}\rangle^{\otimes 4}$), since the seed theory is irrational and thus itself has an infinite number of boundary states. Furthermore, the boundary entropy of a typical state would (at the orbifold point) have a divergence proportional to $N \log N$ as $N \to \infty$ stemming from both the overall $\frac{1}{\sqrt{N!}}$ normalization and the combinatorics. Thus, such boundary states would not describe an interface with a good geometric description.

From the discussion of [50], the boundary state encoding the Janus interface would be "atypical." The coefficients of the twisted-sector terms would be given by characters of some representation of S_N because all N seed states are identical. For

[18] This would not be the sort of a boundary state constructed by [50].

the large-N boundary entropy at the orbifold point to be consistent with the gravitational calculation (3.99) (or more specifically, its order-N scaling as $N \to \infty$), the representation of S_N from which the coefficients are determined would need to have a dimension

$$d_{\text{rep}} \sim N^{N/2}, \quad N \to \infty, \tag{3.101}$$

thereby eliminating any imprint of the twisted-sector terms.

It would be interesting to understand more precisely the form of the boundary state describing the Janus interface. We do not anticipate the simple transport coefficients here being helpful towards this goal due to their expected sensitivity to coupling and insensitivty to combinatorics. However, we expect that calculations of boundary entropy for more stringy states (i.e. with a weak marginal coupling turned on [91]) could probe more of the parameter space in Figure 3.3, thereby revealing more information about the twisted-sector coefficients in the boundary state. Along these lines, it would be interesting to consider the feasibility of applying the tensionless string program (e.g. [51]) in a Janus background.

3.4.3 Other future directions

We also briefly describe some other directions for follow-up work.

Other boundary data One could study other types of data besides entropy or transport. For example, there is "defect complexity" [92]. This has been studied in the Janus solution through different prescriptions by [93, 94]. It would be interesting to see if similar quantities could be realized directly in the symmetric orbifold theory at the orbifold point.

Another approach along these lines would be to study scattering processes involving states created by extended symmetry generators (i.e. fractional Virasoro generators), which are known to probe CFT data distinct from the transport coefficients discussed here [14].

Entanglement in ICFT Transport is only facet of physics made manifest by the presence of an interface. We can study other facets of ICFT, such as entanglement entropy [28, 95]. We can ask whether entanglement entropy generically encodes more information about the conformal interface beyond the boundary entropy of the boundary state.

Acknowledgements

We thank Alexandre Belin, Shovon Biswas, Elena Cáceres, Andreas Karch, and Jani Kastikainen for useful discussions. We are also grateful to Constantin Bachas, Stefano Baiguera, Shira Chapman, Andreas Karch, and Giuseppe Policastro for feedback on the draft. We deeply appreciate the extensive and useful critiques of an anonymous referee.

The work of SB was supported in part by the U.S. Department of Energy under Grant DE-SC0022021 and by a grant from the Simons Foundation (Grant 651440, AK). SS is supported by National Science Foundation (NSF) Grant No. PHY-2112725. SB and SS are also both supported by NSF Grant No. PHY-1914679.

Chapter 4: Transmission Coefficient of Super-Janus Solution[1]

Abstract

We calculate the transmission coefficient of the super-Janus interface conformal field theory, both at weak and at strong coupling, where latter is described holographically as a domain-wall solution on $\mathrm{AdS}_2 \times S^2 \times M_4 \times \Sigma$. Surprisingly we find perfect agreement between the free and strong coupling answer, mirroring a similar unexpected equivalence previously found for the entanglement entropy.

4.1 Introduction

Interface conformal field theories (ICFTs) [23, 96, 10] share the same symmetry as the much more widely studied boundary conformal field theories (BCFTs), but display several novel features, which only recently have found wide appreciation both in the high energy and condensed matter communities.

While ICFTs can always be mapped to BCFTs via the folding trick, they give rise to novel physical quantities that, while they of course also exist in the folded picture, only make natural sense in the ICFT: the entanglement entropy (EE) of generic regions including the interface [30, 97, 98, 99] and the energy transmission across the interface [10, 14, 15]. In particular, in this paper the focus is on the transmission coefficient of a codimensional-1 interface dividing CFT_1 and CFT_2 with central charges c_1 and c_2, which is given by the correlation function of the stress tensor across the interface:

[1] Published in JHEP with Mianqi Wang and Andreas Karch

$$\mathcal{T} = \frac{2c_{LR}}{c_1 + c_2} = \frac{\langle T^1 T^2 + \overline{T}^1 \overline{T}^2 \rangle_{1|2}}{\langle (T^1 + \overline{T}^1)(T^2 + \overline{T}^2) \rangle_{1|2}} \tag{4.1}$$

Together, c_{eff} and c_{LR} define two novel "central charges" governing the properties of the interface: c_{LR} appearing in the transmission, and c_{eff} as the coefficient of log divergent terms in the EE for regions ending on the interface. Some universal bounds on these two quantities have recently been derived in [98, 99]. Another interesting quantity related to the EE is the usual boundary entropy or g-factor $g = \langle 0|B\rangle$ associated with symmetric intervals, which fold to the standard BCFT EE which is uniquely determined by g. For generic asymmetric intervals, g actually becomes a function of l_L/l_R where $l_{L/R}$ stands for the length of the part of the interval on either side of the interface. Little is known about this function $g(l_L/l_R)$. For the particular example of the bosonic Janus ICFT it has for example been worked out in [28] in the strong coupling limit.

An interesting class of examples of ICFTs is provided by holographic ICFTs, that is ICFTs which in a suitable large N and strong coupling limit have an equivalent description in terms of classical gravity in a higher dimensional spacetime. Simple solutions to Einstein equations that have the right symmetries to correspond to the dual of an ICFT can be constructed in terms of branes [24, 6]. Generically the field theory dual to these "bottom-up" constructions is not known and may not even exist. To realize a concrete dual pair, we rely on "top-down" constructions as they actually arise in string theory. The simplest such top-down ICFTs are the Janus solution and its supersymmetric generalization.

The original Janus solution [86] describes a 4d ICFT. The CFT on both sides of the interface is given by $\mathcal{N} = 4$ SYM, but with different values of the coupling constant. The 2d Janus ICFT has been constructed in [57] and its supersymmetric generalization in [56].

The 2d Janus ICFT is based on a famous holographic CFT, the D1-D5 system. In the free limit, the D1-D5 CFT is described by a symmetric orbifold. We start with

a theory of $4N$ free compact scalars together with their free fermion superpartners. This gives a sigma model with a $(T^4)^N/S_N$ target space, which we consider in the large N limit. For simplicity we are working at a special point in moduli space where T^4 is just a product of 4 circles with identical radii. This orbifold CFT is what we call the free limit. All properties of the orbifolded theory can be deduced from the free seed theory of free compact bosons and fermions. In order to have a holographic description, we need to drive the theory to strong coupling. Here the coupling corresponds to a marginal deformation that in terms of the sigma model is a blow up mode of the orbifold singularity. In the infinite coupling limit holography applies and the D1-D5 CFT is dual to type IIB supergravity on $AdS_3 \times S^3 \times T^4$ [5].

The (bosonic) Janus ICFT now corresponds to a deformation of the D1-D5 system where the radius of the T^4 jumps across the interface taking the values $r_{1,2}$ on the right and left of the interface respectively. While this jump breaks all supersymmetries, some supersymmetries can be restored by imposing non-trivial boundary conditions across the interface for the fermions as well. This latter is the super-Janus ICFT of interest to us.

The g-factor for a symmetric interval in the bosonic Janus ICFT has been calculated at both weak and strong coupling in [8]. One should note that this is not a single number, but a function of r_1/r_2, the ratios of the T^4 radii on the two sides of the interface. While the two functions obtained in the two limits are definitely not identical, the difference is numerically remarkably small.

In contrast, in the supersymmetric case it was shown that both g [9] as well as c_{eff} [100] as a function of r_1/r_2 are identical in the free theory and in the strong coupling limit, that is the CFT calculation of $S = \log g$ on the orbifold target space T^{4N}/S_N matches with the holographic calculation of the RT surface [21] in the bulk. While supersymmetry often gives rise to non-renormalization theorems, the remarkable insensitivity of these two entropic quantities to the coupling constant is, as of now, not understood.

In [2] a similar comparison was performed for the energy transmission coefficient, or equivalently c_{LR}, for the bosonic Janus ICFT. Once again, they studied the free orbifold CFTs and its holographically dual (non-susy) Janus solution of type IIB supergravity, which is valid at strong coupling. Similar to the EE calculation, they found that without supersymmetry for a generic ratio of r_1/r_2, the strongly coupled transmission coefficient $\mathcal{T}$ by the holographic calculation is different, in fact strictly bigger, than that in the weakly coupling regime given by the free CFT calculation at the orbifold point.

Given that for both entropic quantities, c_{eff} and g, perfect agreement between weak and strong coupling answers had been found in the supersymmetric case, it is natural to ask whether this miracle repeats itself for the transmission coefficient. We set out to answer this question in this work by once again calculating this quantity in the free orbifold CFT, this time with a supersymmetric boundary condition, and its holographic dual valid at strong coupling. Amazingly enough we once again find perfect agreement between the weak and strong coupling answer for all values of r_1/r_2. All key quantities in this supersymmetric ICFT seem to be remarkably insensitive to the coupling constant of the bulk CFT, a fact which begs for a deeper understanding.

This paper is organized as follows: in Section 4.2 we calculate the transmission coefficient in the 2d $\mathcal{N} = (4, 4)$ orbifold CFT, in presence of jumping radii and $\mathbb{Z}_2$ orbifold twist operators for the free boson sector. In Section 4.3 we calculate it in the bulk type IIB Janus model on $\text{AdS}_2 \times S^2 \times \Sigma$ by KK reducing the 6D supergravity to a 3D toy model, and find a perfect match with the CFT result. In Section 4.4 an alternative way of deriving the transmission coefficient of the super-Janus model is presented by solving the spin-2 fluctuations in $\text{AdS}_2/\text{CFT}_1$. Finally in Section 4.5 we discuss a surprising conjecture on the relation between c_{eff} and c_{LR} for supersymmetric theories, and other future directions on the subject.

4.2 CFT calculation

To determine the transmission coefficient in the free orbifold CFT one simply calculates the transmission coefficient for $4N$ real scalars. As shown in [2], the fact that we are orbifolding does not affect the transport of the conserved total energy. So in the bosonic theory the task is to calculate the transmission coefficient for a free boson with compactification radius r_1 and r_2 on the two sides of the interface respectively. In fact, this system allows many different conformal interface, after folding we are looking for a BCFT of two compact scalars, or equivalently all D-branes on a torus with side lengths r_1 and r_2. As argued already in [8], following similar arguments for the original 4d Janus ICFT in [101], the particular interface boundary conditions corresponding to Janus are uniquely obtained by varying the action of the compact free bosons *without* adding any extra terms on the interface.

As shown in [2] these particular boundary conditions fit into the general framework of bosons whose components to the left and right of the interface are related to each other by a matrix S that was analyzed already in the early work of [10]. To calculate the transmission coefficient in the free Janus CFT all that needed to be done is to extract the correct form of the matrix S from the boundary conditions in [8]. Here we want to redo this calculation for the supersymmetric case. Specifically, the CFT here is a 2d $\mathcal{N} = (4, 4)$ NLSM with an interface. The free-field limit again corresponds to a (supersymmetric) sigma model where the target space is an orbifold $(T^4)^N/S_N$.

One subtlety in the free theory is that the theory has more than one conserved stress tensor, so the analysis of [14] does not directly apply. In principle we could get a different transmission coefficient whether the energy comes in as fermions or as bosons: the stress tensor of free fermion and boson is separately conserved. Of course this ambiguity would disappear the moment we move away from the orbifold point which couples bosons and fermions. But we really want to calculate the transmission coefficient at the orbifold point itself. Fortunately we will see that both fermions and

bosons have the same transmission coefficient in the free super-Janus ICFT, so this subtlety is immaterial. To see this note that the boundary condition for super-Janus worked out in (6.8) of [9] once again has exactly the form of a generic free fermion interface also worked out in [10], see eq. (3.12).[2]

In the comparison one finds that the angle ϑ characterizing the interface in [10] is related to the radii of T^4 on the two sides by

$$\sin(2\vartheta) = 2\frac{r_1 r_2}{(r_1^2 + r_2^2)}. \tag{4.2}$$

This is exactly what one finds in the bosonic case: fermion and boson in the free super-Janus ICFT have the same transmission coefficient, which hence is equal to the transmission coefficient of total energy. That is, in free super-Janus we again get the same state-independent transmission coefficient as in the in free bosonic case:

$$\mathcal{T}_{\text{weak}} = \frac{4}{\left(\frac{r_1}{r_2} + \frac{r_2}{r_1}\right)^2} \tag{4.3}$$

More generally, one can obtain a class of ICFTs by adding in an exactly marginal deformation, which in turn gives the gluing condition at the boundary/interface [9]. In addition to the radii deformation above, let us consider a $\mathbb{Z}_2$ orbifold twist deformation [102]. It is obtained by perturbing the theory with a dimension $(h, \bar{h}) = (1, 1)$ twist operator T_0, with an OPE of $T_0(z, \bar{z})T_0(w, \bar{w}) \sim 1/|z - w|^4$. Under this twist, the orbifold CFTs on the two sides live on different points in their moduli space. Following [9] it was further argued that the orbifold twist deformation is one of the many possible Kähler moduli deformations. By counting distinct two forms on the orbifold point of a Kähler manifold (e.g. a $T^4/\mathbb{Z}_2$ orbifold point in K_3), one can naturally extrapolate the presence of orbifold twist-fields to jumping world-sheet B fields across the interface.

[2] To see this one has to identify in the region to the left of the interface Ψ from the first reference with ψ_- in the second, and $\tilde{\Psi}$ in the first with ψ_+ in the second, whereas in the region to the right of the interface the roles of $\psi_\pm$ are reversed. This flip can be attributed to the fact that the former reference works in the folded picture.

Concretely, let us follow Appendix C of [9] and consider two free compact bosons on each side of the interface $\sigma = 0$ coupling to anti-symmetric B field, with both jumping radii r_1, r_2 and B field b_1, b_2 on the left and right side of the interface. The action before folding is

$$\int_{\sigma>0} \left(r_1^2 \eta^{\mu\nu} \partial_\mu X^i \partial_\nu X^i + 2\epsilon^{\mu\nu} b_1 \partial_\mu X^1 \partial_\nu X^2\right) + \int_{\sigma<0} \left(r_2^2 \eta^{\mu\nu} \partial_\mu \tilde{X}^i \partial_\nu \tilde{X}^i + 2\epsilon^{\mu\nu} b_2 \partial_\mu \tilde{X}^1 \partial_\nu \tilde{X}^2\right) \tag{4.4}$$

Let us do a change of variables from r_1, r_2 and the jump in B fields $\Delta b = b_1 - b_2$ to parameters k, ψ and θ:

$$\Delta b = 4k \sinh\theta, \quad r_1 = \sqrt{\frac{2ke^{\psi}}{\cosh\psi}}, \quad r_2 = \sqrt{\frac{2ke^{-\psi}}{\cosh\psi}} \tag{4.5}$$

and hence in particular

$$\frac{r_1}{r_2} = e^{\psi}. \tag{4.6}$$

The new parameters give a simpler expression for the transmission coefficient $\mathfrak{T}$, and as we will see in Section 4.3 they arise naturally in the bulk supergravity solution. An overall shift on the B fields will be a total derivative and leave all quantities of interest invariant.

Let us do a transformation $X^i \to r_1 X^i, \tilde{X}^i \to r_2 \tilde{X}^i$ as in [10] to normalize the energy-momentum tensor. The boundary conditions are

$$\begin{aligned} r_1 \partial_\sigma X^i - r_2 \partial_\sigma \tilde{X}^i + \epsilon_{ij} \left(\frac{b_1}{r_1} \partial_\tau X^j - \frac{b_2}{r_2} \partial_\tau \tilde{X}^j\right) = 0, \quad i = 1, 2 \\ r_2 \partial_\tau X^i = r_1 \partial_\tau \tilde{X}^i, \quad i = 1, 2 \end{aligned} \tag{4.7}$$

One can then write down the scattering matrix of this 2-boson system under this boundary condition at the interface,

$$\begin{pmatrix} \partial_- X^1 \\ \partial_- X^2 \\ \partial_+ \tilde{X}^1 \\ \partial_+ \tilde{X}^2 \end{pmatrix} = S \begin{pmatrix} \partial_+ X^1 \\ \partial_+ X^2 \\ \partial_- \tilde{X}^1 \\ \partial_- \tilde{X}^2 \end{pmatrix} \tag{4.8}$$

where we only write out the 2×2 transmission submatrix S_{21} for $\partial_- X^i$ and $\partial_- \tilde{X}^i$

$$\begin{pmatrix} \partial_- X^1 \\ \partial_- X^2 \end{pmatrix} = \begin{pmatrix} \frac{2r_1 r_2 (r_1^2+r_2^2)}{(r_1^2+r_2^2)^2+\Delta b^2} & \frac{2r_1 r_2 \Delta b}{(r_1^2+r_2^2)^2+\Delta b^2} \\ \frac{2r_1 r_2 \Delta b}{(r_1^2+r_2^2)^2+\Delta b^2} & -\frac{2r_1 r_2 (r_1^2+r_2^2)}{(r_1^2+r_2^2)^2+\Delta b^2} \end{pmatrix} \begin{pmatrix} \partial_- \tilde{X}^1 \\ \partial_- \tilde{X}^2 \end{pmatrix} \tag{4.9}$$

Following [15], we can fold the theory via $\sigma \to -\sigma$ (and adding a minus sign in front of the B field), and calculate the energy transmission coefficient using the above S matrix on the conformal boundary state $|b\rangle$. Explicitly, we can write down the 2×2 R-matrix

$$R_{ij} = \frac{\langle 0 | L_2^i \bar{L}_2^j | b \rangle}{\langle 0 | b \rangle}, \tag{4.10}$$

where $L_2^{1,2}$ are the virasoro generators for the left and right hand side. The energy transmission coefficient is then

$$\mathcal{T}_{\text{weak}} = \frac{2}{c_1 + c_2} \left(\frac{\langle 0 | L_2^1 \bar{L}_2^2 | b \rangle}{\langle 0 | b \rangle} + \frac{\langle 0 | L_2^2 \bar{L}_2^1 | b \rangle}{\langle 0 | b \rangle} \right) = \frac{1}{2} \sum_{I,J=1,2} \left| (S_{21})_{IJ} \right|^2 \tag{4.11}$$

Plugging in (4.9) leads to the result

$$\mathcal{T}_{\text{weak}} = \frac{4}{\left(\frac{r_1}{r_2} + \frac{r_2}{r_1} \right)^2 + \frac{\Delta b^2}{r_1^2 r_2^2}} = \frac{1}{\cosh^2 \psi \cosh^2 \theta} \tag{4.12}$$

4.3 Holography calculation with KK reduction

In this section we consider the holographic dual of the 2D supersymmetric Janus ICFT. As mentioned above, the dual spacetime is a solution of type IIB supergravity of the form $\text{AdS}_2 \times S^2 \times M_4 \times \Sigma$ dictated by symmetry [9]. The solution is supported by R-R and/or NS-NS charges. The manifold M_4 can be T^4 or K_3, corresponding to the target space of the sigma model on the CFT side. While in the CFT calculation we focused on the special case of a T^4 made from 4 identical S^1 factors, the gravity side calculation is completely insensitive to the details of M_4. For calculational simplicity, we will only consider the case with a simple self-dual R-R three-form flux where the harmonic functions in [9] only have two singularities, and

leave the cases of arbitrary charge deformations to future work (these would correspond to the case of F1-NS5 solutions or more general branes preserving the same amount of supersymmetry).

To calculate the transmission coefficient $\mathcal{T}$, we need to study a linearized gravity wave propagating on this background, corresponding to a boundary wave incoming from (say) the left, leading to a transmitted and reflected wave due to the presence of the interface. In [4] this was done for the holographic ICFT dual to a thin-brane model. $\mathcal{T}$ was related to the tension of the thin brane dividing the two parts of the spacetime. Soon after [1] showed that the generalization to two thin branes is almost trivial: the tensions simply add. This was generalized to the 'thick-brane' model in [17] where $\mathcal{T}$ of the non-supersymmetric Janus solution was presented. Anytime the geometry only depends non-trivially on a single coordinate, as is in the case of an AdS_2 slicing of AdS_3, one can approximate the smooth stress tensor corresponding to the fields supporting the geometry by an array of delta functions, effectively treating the spacetime as one with multiple thin branes. In the limit that the comb of delta functions goes back to a smooth configuration one obtains the transmission coefficient of the original geometry[3]

However a caveat with this method is that if there is non-trivial dependence on some extra compact dimensions (like in our super-Janus solution where the metric and matter fields depend non-trivial on both coordinates on Σ), the method needs to be modified. To resolve this issue, in this section we will use Kaluza-Klein compactification to reduce the 10D supergravity above to a 6D supergravity in Einstein frame, and then further to an effective 3D model, where we can compute the transmission coefficient via the thick-brane model. An alternative way of matching the higher dimensional model with the effective 3D model in the spirit of the above discussion is

[3]It would be reassuring to reproduce the formula for $\mathcal{T}$ directly from studying fluctuation around the continuous geometry. This was left for future work in [17]. Here we assume that the answer presented there as one obtains it from taking the continuum limit of the discretized geometry is, in fact, correct.

in Section 4.4 by considering the spin-2 fluctuation wavefunction.

4.3.1 6D supergravity with R-R charge

We consider a type IIB solution on $\mathrm{AdS}_2 \times S^2 \times M_4$ over a strip Σ. We will use the most general metric with two asymptotic $\mathrm{AdS}_3 \times S^3$ regions, which contains five parameters θ, ψ, L, k, b. Following [9], the relevant functions for our solution are two independent holomorphic functions A and B, and two independent harmonic functions H and $\hat{h}$. The complex coordinate on the strip Σ will be written as $w = x+iy$ below, where x is non-compact and $y \in [0, \pi]$.

The metric reads

$$ds^2 = f_1^2 ds^2_{AdS_2} + f_2^2 ds^2_{S^2} + f_3^2 ds^2_{M_4} + \rho^2 ds^2_{\Sigma}, \tag{4.13}$$

where the dilaton and the various functions appearing in the metric are given by

$$\begin{aligned}
e^{-2\phi} &= \frac{1}{4}\left(A + \bar{A} - \frac{(B+\bar{B})^2}{\hat{h}}\right)\left(A + \bar{A} - \frac{(B-\bar{B})^2}{\hat{h}}\right) \\
f_3^4 &= 4\frac{e^{-\phi}\hat{h}}{A+\bar{A}} \\
f_1^2 &= \frac{e^{\phi}}{2f_3^2}\frac{|H|}{\hat{h}}\left((A+\bar{A})\hat{h} - (B-\bar{B})^2\right) \\
f_2^2 &= \frac{e^{\phi}}{2f_3^2}\frac{|H|}{\hat{h}}\left((A+\bar{A})\hat{h} - (B+\bar{B})^2\right) \\
\rho^4 &= e^{-\phi}\hat{h}\frac{|\partial_w H|^4}{H^2}\frac{A+\bar{A}}{|B|^4}
\end{aligned} \tag{4.14}$$

Let us consider the case with nonzero R-R charge and zero NS-NS charge. The generic solutions to the harmonic and holomorphic functions are

$$\begin{aligned}
H &= -iL\sinh(w+\psi) + c.c. \\
A &= ik^2\frac{\cosh\theta + \sinh\theta\cosh w}{\sinh w} + ib \\
B &= ik\frac{\cosh(w+\psi)}{\cosh\psi\sinh w} \\
\hat{h} &= i\frac{\cosh\theta - \sinh\theta\cosh w}{\sinh w} + c.c.
\end{aligned} \tag{4.15}$$

Under (4.14), the dilaton is

$$e^{-2\phi} = k^4 \frac{\cosh^2(x+\psi)\ \mathrm{sech}^2\psi + (\cosh^2\theta - \mathrm{sech}^2\psi)\sin^2 y}{(\cosh x - \cos y \tanh\theta)^2}, \tag{4.16}$$

and metric factors are

$$\begin{aligned}
\rho^4 &= e^{-\phi}\frac{L^2}{k^2}\frac{\cosh^2 x\cosh^2\theta - \cos^2 y\sinh^2\theta}{\cosh^2(x+\psi)}\cosh^4\psi, \\
f_3^4 &= e^{-\phi}\frac{4}{k^2}\frac{\cosh x\cosh\theta - \cos y\sinh\theta}{\cosh x\cosh\theta + \cos y\sinh\theta}, \\
f_1^2 &= \rho^2\frac{\cosh^2(x+\psi)}{\cosh^2\theta\cosh^2\psi}, \\
f_2^2 &= \rho^2\left(\frac{1}{\sin^2 y} + \frac{\cosh^2\theta\cosh^2\psi - 1}{\cosh^2(x+\psi)}\right)^{-1}.
\end{aligned} \tag{4.17}$$

The pure $\mathrm{AdS}_3 \times S^3$ solution corresponds to $\theta = \psi = 0$. At the asymptotic regions of the strip $x \to \pm\infty$ near the ICFT boundary the six dimensional dilaton dual to the volume of T^4 is

$$\lim_{x\to\pm\infty} e^{-\phi} f_3^4 = 4k^2\mathrm{sech}^2\psi\ e^{\mp 2\psi} \tag{4.18}$$

Similarly, the asymptotic values for the combination of the axion χ and the RR four form C_4 near the boundary are

$$\lim_{x\to\pm\infty} e^{\phi/2} f_3^2\chi - 4\frac{e^{-\phi/2}}{f_3^2}C_4 = \pm 4k\sinh\theta \tag{4.19}$$

and is dual to the $\mathbb{Z}_2$ orbifold twist operator T_0 mentioned above. From the above two equations it is clear that the parameters k, ψ, θ are the same ones inside the variable change (4.5).

4.3.2 KK compactify to 3D

Our goal is to reduce the system to an effective 3D geometry, so we can use the expression in [17] to derive the transmission coefficient for the system on the strip.

We can consider compactifying the above 10D metric down to 6D, keeping it in the Einstein frame. The 6D metric is $\mathrm{AdS}_2 \times S^2$ fibred over Σ, which simplifies to [9]

$$ds^2_{6D} = R^2\ K(x,y)\left(\frac{\cosh^2(x+\psi)}{\cosh^2\psi\cosh^2\theta}ds^2_{AdS_2} + dx^2 + dy^2\right) + \frac{R^2\sin^2 y}{K(x,y)}ds^2_{S^2} \qquad (4.20)$$

where $R^2 = 2L\cosh\psi\cosh\theta$ is the AdS_3 radius and

$$K(x,y) = \sqrt{1 + \frac{(\cosh^2\theta\cosh^2\psi - 1)\sin^2 y}{\cosh^2(x+\psi)}}. \qquad (4.21)$$

For the AdS_2 metric, we will use the Poincare patch $ds^2_{AdS_2} = (dz^2 - dt^2)/z^2$.

The reduction so far was fairly standard as the metric was completely independent of the coordinates on T^4. The non-trivial dependence of the overall size of the T^4 on Σ as encoded in f_3 simply got absorbed into the 6D dilaton. To further reduce to 3D, we have to be very careful as, in addition to the S^2, we need to reduce on the compact part of Σ, on which all functions depend.

We start with the 6D Einstein-Hilbert action $S = 1/(16\pi G_6)\int\sqrt{-g_6}R_6$, and integrate out the sphere S^2 trivially. This gives us an effective 4D Einstein-Hilbert action with x,y-dependent Newton constant $S = 1/16\pi\int G_4(x,y)^{-1}\sqrt{-g_4}R_4$.

Now we further compactify along the compact y direction by integrating the above action over $y\in[0,\pi]$. Effectively, we now have a 3D action $S = 1/16\pi\int G_3(x)^{-1}\sqrt{-g_3}R_3$ with a x-dependent Newton constant $G_3(x)$, and a certain 3D metric that obeys the Einstein equation.

After changing the frame for the 3D metric $g_3 \to g_3\ G_3(x)^{1/2}$, we got the standard Einstein-Hilbert action $S = 1/16\pi G_3\int\sqrt{-g_3}R_3^{EH}$. Explicitly, after integrating out S^2 and y and gauging away $G_3(x)$, the action becomes

$$S = -\frac{R^4}{48\pi G_6}\int_{AdS_2\times\mathbb{R}_x}\frac{3\cosh 2(x+\psi) + \cosh 2\psi + 2}{z^2\cosh^2\psi\cosh^2\theta}. \qquad (4.22)$$

The ansatz for such a 3D solution is an AdS_2-slicing 3D effective model with warpfactor $e^{2A(x)}$:

$$ds^2_{3\mathrm{D}} = R^2\left(e^{2A(x)}ds^2_{AdS_2} + dx^2\right). \qquad (4.23)$$

It has an Einstein-Hilbert action of

$$S_{3\mathrm{D}} = -\frac{R}{16\pi G_3}\int \frac{e^{2A}(2e^{-2A}+6A'^2+4A'')}{z^2}. \tag{4.24}$$

Matching the above ansatz with the integrated 6D action from (4.22) and using the KK relation of Newton constants $G_6 = R^3 G_3/3$, the solution is

$$A(x) = \log\left(\frac{\cosh(x+\psi)}{\cosh\psi\cosh\theta}\right), \tag{4.25}$$

and that gives us the effective 3D metric

$$ds^2_{3\mathrm{D}} = R^2\left(\frac{\cosh^2(x+\psi)}{\cosh^2\psi\cosh^2\theta}ds^2_{AdS_2} + dx^2\right) \tag{4.26}$$

4.3.3 $\mathcal{T}$ from the 3D effective model

In order to calculate the transmission coefficient from the thick brane method as in [17], we do a change in coordinate x to a compact $\tilde{x}$, lining up with the ones used in the cited paper. Consider $\tilde{x} \in (-\pi\cosh\psi\cosh\theta/2, \pi\cosh\psi\cosh\theta/2)$ where

$$\cos\frac{\tilde{x}}{\cosh\psi\cosh\theta} = \frac{1}{\cosh(x+\psi)} \tag{4.27}$$

The effective 3D model above then becomes

$$ds^2_{\mathrm{toy}} = R^2 e^{2A(\tilde{x})}\left(ds^2_{AdS_2} + d\tilde{x}^2\right) \tag{4.28}$$

where

$$e^{2A(\tilde{x})} = \left(\cosh^2\psi\cosh^2\theta\ \cos^2\frac{\tilde{x}}{\cosh\psi\cosh\theta}\right)^{-1}. \tag{4.29}$$

From Eq. (2) and Eq. (17) in [17], we finally obtain the strong coupling transmission coefficient of the super-Janus solution

$$\mathcal{T}_{\mathrm{strong}} = \frac{2c_{LR}}{c_L + c_R} = \frac{1}{\cosh^2\psi\cosh^2\theta} \tag{4.30}$$

which, as advertised, is identical to the free field theory answer of (4.12) with jumping radii and B field deformation.

4.4 Alternative Derivation: Graviton reduction for AdS_2/CFT_1

Another way to derive the transmission coefficient is via graviton fluctuation as illustrated in Section 5 of [17]. Previously, the reduction of the AdS graviton from a higher-dimensional solution has been done in various dimensions [103, 104, 105]. Below, we will derive the fluctuation wavefunction Ψ for the AdS_2 graviton from the 10D solution, and will indirectly read off $\mathcal{T}$ from the asymptotic behavior of Ψ at the ends of the strip.

4.4.1 Fluctuation wavefunction in AdS_2/CFT_1

We wish to obtain the spin-2 spectrum reduced from a top-down supergravity solution to AdS_2. Following [106], we rewrite the perturbations of the 10D metric (4.13) as

$$ds^2 = e^{2A(w)}(\bar{g}_{\mu\nu} + h_{\mu\nu})dX^\mu dX^\nu + \hat{g}_{ab}dw^a dw^b, \tag{4.31}$$

where X^μ are the AdS_2 coordinates, w^a are for the internal manifold, and e^{2A} is the warpfactor. We want to find the AdS_2 graviton fluctuation of the form

$$h_{\mu\nu}(X,u) = h^{[tt]}_{\mu\nu}(X|\lambda)\Psi(w|\lambda) \tag{4.32}$$

where $h^{[tt]}_{\mu\nu}(X|\lambda)$ is the Pauli-Fierz transverse-traceless solution for a spin-2 particle in AdS with mass $m^2 = \lambda + 2$. For our 10D supergravity, the internal wavefunction $\Psi(w|\lambda)$ is solved by [103, 106]

$$-\frac{1}{\sqrt{[\hat{g}]}}(\partial_a\sqrt{[\hat{g}]}\hat{g}^{ab}e^{2A}\partial_b)\Psi = m^2\Psi, \tag{4.33}$$

where $[\hat{g}]$ is the determinant of $\hat{g}_{ab}$.

We can see that the lowest mass solution has $l = 0$ and the lowest energy $\Delta_4 = 0$ for M_4.

In our metric the above $\hat{g}$ is

$$\hat{g}_{ab}dy^a dy^b = f_2^2 ds_{S^2}^2 + f_3^2 ds_{M_4}^2 + \rho^2 dz d\bar{z}, \tag{4.34}$$

and we will use the spherical harmonic function for Ψ as

$$\Psi = Y_{lm}\Psi_l(x, y). \tag{4.35}$$

Plugging this ansatz into (4.33), we have

$$-f_1^2\left(\frac{\delta^{ij}}{\rho^2}\partial_i\partial_j + \frac{2\delta^{ij}}{\rho^2}(\partial_i \log\big(f_1 f_2 f_3^2\big))\partial_j - \frac{l(l+1)}{f_2^2} - \frac{\Delta_4}{f_3^2}\right)\Psi_l(y^1, y^2) = m^2\Psi_l(y^1, y^2). \tag{4.36}$$

Since we will only consider $\Delta_4 = l = 0$, below we abuse the notation and use Ψ for the 0th component Ψ_0. We can substitute Ψ with a more convenient $\tilde{\Psi}$:

$$\tilde{\Psi} = \frac{\cosh(x+\psi)\sin y}{2\cosh\psi\cosh\theta}\Psi, \tag{4.37}$$

and write the equation for the $l = 0$, $\Delta_4 = 0$ component as

$$-\cosh^2(x+\psi)(\partial_x^2 + \partial_y^2)\tilde{\Psi} = m^2\cosh^2\psi\cosh^2\theta\ \tilde{\Psi}. \tag{4.38}$$

The variables are separable in this case, and imposing the Neumann boundary condition on y for Ψ, we have the general solution $\tilde{\Psi}_0 = \sum_n \tilde{\xi}_n(x)\sin((2n+1)y)$, where $\tilde{\xi}_n$ satisfies the Legendre equation, and has solution

$$\tilde{\xi}_n = c_1\ P_\kappa^{2n+1}(\tanh(x+\psi)) + c_2\ Q_\kappa^{2n+1}(\tanh(x+\psi)), \quad \kappa(\kappa+1) = m^2\cosh^2\psi\cosh^2\theta. \tag{4.39}$$

For a nonzero and convergent $\tilde{\xi}_n$, κ has to be an integer greater than 0, and $c_2 = 0$. At first glance, the lowest massive excitation of AdS_2 is $m^2 = 2/(\cosh^2\psi\cosh^2\theta)$.

However, the $m^2 = 0$ excitation corresponds to the wavefunction satisfying

$$(\partial_x^2 + \partial_y^2)\tilde{\Psi} = 0, \tag{4.40}$$

which after seperating variables gives a nontrivial equation

$$\tilde{\Psi} = \sum_n (A_n \cosh(2n+1)(x+\psi) + B_n \sinh(2n+1)(x+\psi)) \sin(2n+1)y. \quad (4.41)$$

The non-divergent terms for Ψ are then only the $n = 0$ components:

$$\Psi = A_0 + B_0 \tanh(x+\psi). \quad (4.42)$$

In principle we should be able to extract $\mathcal{T}$ from this fluctuation.

4.4.2 From Ψ to $\mathcal{T}$

The fluctuation wavefunction (4.42) in principle encodes all the information about the fluctuation and one should be able to directly read off $\mathcal{T}$ from it. A general recipe of how one would go about doing this has been outlined in [17], even though the calculation hasn't been carried out explicitly as one has to deal with matching the various asymptotic forms of the metric which proves to be surprisingly cumbersome.

As a workaround, we are going to pursue the following alternate strategy. As the transmission coefficient is encoded in the graviton fluctuation wavefunction (4.42), we can simply construct a toy model in 3D that has the same fluctuation function. Explicitly, the PDE (4.36) on x, y for the wavefunction $\Psi(x, y)$ with mass zero is

$$\frac{\cosh^2(x+\psi)}{\cosh^2\psi \cosh^2\theta} \left(2\tanh(x+\psi)\ \partial_x + \partial_x^2 + 2\cot y\ \partial_y + \partial_y^2\right) \Psi(x,y) = 0. \quad (4.43)$$

Its solution (4.42) is actually the solution to an ODE eigenvalue equation on x. Namely, let us reduce the y direction of the above equation and consider the fluctuation of a 3d gravity

$$\left(\partial_x^2 + 2\tanh(x+\psi)\ \partial_x + M^2\right) \Psi(x) = 0. \quad (4.44)$$

Recall the ansatz for 3D Einstein gravity with isometry $SO(2,1)$ in the form of (4.23). Analogous to the modeling in [107] for AdS_4-slicing of a 5d model, the

fluctuation wavefunction of the transverse-traceless mode $\Psi(x)$ of 3D gravity obeys the ODE

$$\left(\partial_x^2 + 2A'(x)\partial_x - e^{-2A}\Box\right)\Psi(x) = 0 \tag{4.45}$$

Comparing (4.42) with (4.44), the warpfactor $A(x)$ satisfies

$$A'(x) = \tanh(x + \psi). \tag{4.46}$$

Integrating the above equation we get the warpfactor $e^{2A} = k\cosh^2(x + \psi)$. To determine the constant k we demand that the toy model has the same asymptotic behavior in the $x \to \pm\infty$ region as the original metric (4.20). Low and behold we reach a 3D toy model with a metric that is identical to what we found by explicitly doing the KK reduction in (4.26).

Strictly speaking, this alternate method can be viewed as a check of the KK-reduction procedure in the previous chapter: we explicitly verified that the fluctuation equation in the full 6D metric is identical to the one of the effective 3D metric.

As before, we now can simply plug in the 3D toy model metric into the formulas of [17] and, of course, once more obtain (4.12).

More generally, this procedure allows us to derive the transmission coefficient $\mathcal{T}$ from the graviton fluctuation wavefunction, in particular for top-down models with internal dimensions dependence where the spin-2 wavefunction happens to be separable.

4.5 Discussion and future directions

In this work we demonstrated that the remarkable agreement between strongly coupled super-Janus that was previously seen in c_{eff} and g continues to hold for the transmission coefficient. The obvious next future direction is understanding why. Clearly novel non-renormalization theorems are at work in these supersymmetric ICFTs.

Another interesting finding involves the two important quantities in an (1+1)D ICFT: entanglement entropy c_{eff} and transmission coefficient c_{LR}. They are interestingly bounded by each other [99]. According to the calculations in [100], the entanglement entropy across the interface in the super Janus solution in Section 4.3 is

$$c_{\text{eff}} = \frac{c}{\cosh\psi \cosh\theta} \tag{4.47}$$

in the strong-coupling gravity calculation, and agrees with the weak-coupling limit of the dual 2d $\mathcal{N} = (4,4)$ orbifold ICFT[4], just like the transmission coefficient. Morever, we observe that in presence of supersymmetry, the relation between c_{eff} and c_{LR} becomes more stringent: in the case of super Janus solution where c_{LR} is given by (4.30) and $c_L = c_R = c$, we observe a simple relation

$$\mathcal{T} = \frac{c_{LR}}{c} = \left(\frac{c_{\text{eff}}}{c}\right)^2 . \tag{4.48}$$

One can ask whether this relation holds true for most general type IIB supergravity BPS solutions in the form of (4.13) with two poles in the harmonic functions corresponding to two asymptotic AdS_3 regions. Concretely, from the BPS equations for the metric factors $f_1^2 f_2^2 f_3^4 = H^2$ we can write the general 6D metric in terms of

[4]The weak-coupling CFT calculation for the entanglement entropy was given under no jumping RR modulus, i.e. $\theta = 0$, and was not yet performed in presence of the orbifold twist θ.

the harmonic functions $H, \hat{h}$ and holomorphic functions A, B as

$$\begin{aligned} ds^2 = \rho^2 f_3^2 \left(\frac{H^2|B|^2}{|\partial_w H|^2((A+\bar{A})\hat{h} - (B+\bar{B})^2)} ds^2_{AdS_2} + dx^2 + dy^2 \right) \\ + \frac{|\partial_w H|^2((A+\bar{A})\hat{h} - (B+\bar{B})^2)}{|B|^2 \rho^2 f_3^2} ds^2_{S^2} \end{aligned} \tag{4.49}$$

and the KK reduced 3D action after integrating the y direction is expected to have the 3D effective model in the form of

$$ds^2_{\text{3D}} = R^2(k^2 \cosh^2(x+s)\ d^2_{AdS_2} + dx^2) \tag{4.50}$$

which leads to the above relation between c_{eff} and c_{LR}. In fact, this relation has already been pointed out for supersymmetric free theories with $c = 3/2$ across a conformal interface [30]. It is curious to see whether it is a general rule for supersymmetric ICFT with a conformal interface.

Another interesting question is to further explore the role of the internal manifold. Our supergravity answer did not at all depend on the shape of the internal torus, or even whether we replace T^4 with K3 altogether. On the field theory side we limited ourselves to a very symmetric torus. The supergravity answer makes one suspect that in the field theory $\mathfrak{T}$ should also be independent of the shape of the internal manifold. It would be interesting to verify this explicitly.

Acknowledgements

We'd like to thank Costas Bachas for collaboration at initial stages of this work, and him as well as Stefano Baiguerra, Shira Chapman, Giuseppe Policastro, and Tal Schwartzman for discussions of their work in [17]. Thanks to Ilka Brunner, Michael Gutperle, Yuya Kusuki, and Hiroshi Ooguri for comments on a draft of our manuscript. This work was supported in part by the U.S. Department of Energy under Grant No. DE-SC0022021 and a grant from the Simons Foundation (Grant 651678, AK).

Appendix A: Linear order differential equations and their solutions

This appendix contains the details of the linearized differential equations and their solutions and applied constraints for order 1 of ϵ.

Matching the metric gives the first 3 equations and the 4th one is from the non-diagonal element of the extrinsic curvature tensor's junction condition (2.7). The exact form of the 4th equation is arrived at after substituting one of the three equations to simplify the expression.

$$\begin{aligned}
\Delta_1(z_1) + iwz_1\lambda_1(z_1) &= z_1^3\left(\frac{\cos\theta_L}{2}(I+R_1) - \frac{\cos\theta_{CL}}{2}(T_{1l}+R_{2l})\right)\\
\Delta_1(z_1) + z_1\partial_{z_1}\zeta_1(z_1) &= z_1^3\left(\frac{\sin^2\theta_{CL}\cos\theta_{CL}}{2}(T_{1l}+R_{2l}) - \frac{\sin^2\theta_L\cos\theta_L}{2}(I+R_1)\right)\\
iwz_1\zeta_1(z_1) - z_1\partial_{z_1}\lambda_1(z_1) &= z_1^3\left(\cos\theta_L\sin\theta_L(I-R_1) - \cos\theta_{CL}\sin\theta_{CL}(T_{1l}-R_{2l})\right)\\
z_1\partial_{z_1}D_1(z_1) &= z_1^3\Bigg(\frac{I-R_1-T_{1l}+R_{2l}}{iwz_1} + \frac{\cos^2\theta_{CL}\sin\theta_{CL}}{2}(T_{1l}+R_{2l})\\
&\quad - \frac{\cos^2\theta_L\sin\theta_L}{2}(I+R_1)\Bigg)
\end{aligned} \tag{A.1}$$

where I and R_1 are the exponentials printed on the left brane and T_{1l} and R_{2l} the exponentials printed on the centre-left brane, given by:

$$\begin{aligned}
I &= e^{-iw\sin\theta_L z_1}, & R_1 &= \mathcal{R}_{L1}e^{iw\sin\theta_L z_1},\\
T_{1l} &= \mathcal{T}_{L1}e^{-iw\sin\theta_{CL} z_1}, & R_{2l} &= \mathcal{R}_{L2}e^{iw\sin\theta_{CL} z_1}.
\end{aligned} \tag{A.2}$$

$$
\begin{aligned}
\Delta_2(z_2) + iwz_2\lambda_2(z_2) &= z_2^3\left(\frac{\cos\theta_{CR}}{2}(T_{1r}+R_{2r}) - \frac{\cos\theta_R}{2}T_2\right)\\
\Delta_2(z_2) + z_2\partial_{z_2}\zeta_2(z_2) &= z_2^3\left(\frac{\sin^2\theta_R\cos\theta_R}{2}T_2 - \frac{\sin^2\theta_{CR}\cos\theta_{CR}}{2}(T_{1r}+R_{2r})\right)\\
iwz_2\zeta_2(z_2) - z_2\partial_{z_2}\lambda_2(z_2) &= z_2^3\left(\cos\theta_{CR}\sin\theta_{CR}(T_{1r}-R_{2r}) - \cos\theta_R\sin\theta_R T_2\right)\\
z_2\partial_{z_2}D_2(z_2) &= z_2^3\Bigg(\frac{T_{1r}-R_{2r}-T_2}{iwz_2} - \frac{\cos\theta_{CR}{}^2\sin\theta_{CR}}{2}(T_{1r}+R_{2r})\\
&\qquad + \frac{\cos^2\theta_R\sin\theta_R}{2}T_2\Bigg)
\end{aligned}
\tag{A.3}
$$

where T_{1r} and R_{2r} are the exponentials printed on the center-right brane and T_2 the exponential printed on the right brane, given by:

$$
\begin{aligned}
T_{1r} &= \mathfrak{T}_{L1}e^{-iw\sin\theta_{CR}z_2}, \qquad R_{2r} = \mathfrak{R}_{L2}e^{iw\sin\theta_{CR}z_2},\\
T_2 &= \mathfrak{T}_{L1}e^{-iw\sin\theta_R z_2}.
\end{aligned}
\tag{A.4}
$$

The $z_1 = 0$ and $z_2 = 0$ limits of these functions correspond to sources in the dual ICFT - displacing the interface or reparametrizing it. Since we are considering a non-fluctuating interface, we want to set the functions to 0 at the boundary (so for example $D_1(0) = 0 \to \delta_L(0) = \delta_{CL}(0)$ so there is no relative change in the interface). If you only look at the homogeneous equations where there are no gravitational waves scattered at the boundary, the solution looks like:

$$
\begin{aligned}
\lambda_1(z_1) &= \frac{i}{w}\left(a_{1+}e^{iwz_1} + a_{1-}e^{-iwz_1}\right) & \lambda_2(z_2) &= \frac{i}{w}\left(a_{2+}e^{iwz_2} + a_{2-}e^{-iwz_2}\right)\\
\zeta_1(z_1) &= \frac{i}{w}\left(a_{1+}e^{iwz_1} - a_{1-}e^{-iwz_1}\right) & \zeta_2(z_2) &= \frac{i}{w}\left(a_{2+}e^{iwz_2} - a_{2-}e^{-iwz_2}\right)\\
\Delta_1(z_1) &= z_1\left(a_{1+}e^{iwz_1} + a_{1-}e^{-iwz_1}\right) & \Delta_2(z_2) &= z_2\left(a_{2+}e^{iwz_2} + a_{2-}e^{-iwz_2}\right)\\
D_1(z_1) &= c_1 & D_2(z_2) &= c_2
\end{aligned}
\tag{A.5}
$$

Setting (A.5) to 0 at the boundary, we get a constraint on the constants. Furthermore, it shows there are no solutions in the vacuum background supported purely by the interface:

$$
\begin{gathered}
c_1 = 0 \qquad c_2 = 0\\
a_{1+} = 0 \qquad a_{1-} = 0 \qquad a_{2+} = 0 \qquad a_{2-} = 0
\end{gathered}
\tag{A.6}
$$

Using (A.5), the full solution to the full differential equations is:

$$\begin{aligned}
\lambda_1(z_1) &= \frac{i}{w}\left(a_{1+}e^{iwz_1} + a_{1-}e^{-iwz_1}\right) + \frac{i}{w^3\cos\theta_L}\left(1 - \frac{\cos^2\theta_L w^2 z_1^2}{2}\right)(I + R_1) \\
&\quad - \frac{i}{w^3\cos\theta_{CL}}\left(1 - \frac{\cos^2\theta_{CL} w^2 z_1^2}{2}\right)(T_{1l} + R_{2l}) \\
\zeta_1(z_1) &= \frac{i}{w}\left(a_{1+}e^{iwz_1} - a_{1-}e^{-iwz_1}\right) + \frac{i\tan\theta_{CL}}{w^3}\left(1 + \frac{\cos^2\theta_{CL} w^2 z_1^2}{2}\right)(T_{1l} - R_{2l}) \\
&\quad - \frac{i\tan\theta_L}{w^3}\left(1 + \frac{\cos^2\theta_L w^2 z_1^2}{2}\right)(I - R_1) - \frac{z_1\cos\theta_L}{w^2}(I + R_1) + \frac{z_1\cos\theta_{CL}}{w^2}(T_{1l} + R_{2l}) \\
\Delta_1(z_1) &= z_1\left(a_{1+}e^{iwz_1} + a_{1-}e^{-iwz_1} + \frac{1}{w^2\cos\theta_L}(I + R_1) - \frac{1}{w^2\cos\theta_{CL}}(T_{1l} + R_{2l})\right) \\
D_1(z_1) &= c_1 - \frac{i}{w^3}\left(1 + \frac{w^2 z_1^2\cos^2\theta_L}{2}\right)(I - R_1) + \frac{i}{w^3}\left(1 + \frac{w^2 z_1^2\cos^2\theta_{CL}}{2}\right)(T_{1l} - R_{2l}) \\
&\quad + \frac{z_1}{w^2}\left(\sin\theta_L(I + R_1) - \sin\theta_{CL}(T_{1l} + R_{2l})\right)
\end{aligned} \tag{A.7}$$

$$\begin{aligned}
\lambda_2(z_2) &= \frac{i}{w}\left(a_{2+}e^{iwz_2} + a_{2-}e^{-iwz_2}\right) + \frac{i}{w^3\cos\theta_{CR}}\left(1 - \frac{\cos^2\theta_{CR} w^2 z_2^2}{2}\right)(T_{1r} + R_{2r}) \\
&\quad - \frac{i}{w^3\cos\theta_R}\left(1 - \frac{\cos^2\theta_R w^2 z_2^2}{2}\right)T_2 \\
\zeta_2(z_2) &= \frac{i}{w}\left(a_{2+}e^{iwz_2} - a_{2-}e^{-iwz_2}\right) - \frac{i\tan\theta_{CR}}{w^3}\left(1 + \frac{\cos^2\theta_{CR} w^2 z_2^2}{2}\right)(T_{1r} - R_{2r}) \\
&\quad + \frac{i\tan\theta_R}{w^3}\left(1 + \frac{\cos^2\theta_R w^2 z_2^2}{2}\right)T_2 - \frac{z_2\cos\theta_{CR}}{w^2}(T_{1r} + R_{2r}) + \frac{z_2\cos\theta_R}{w^2}T_2 \\
\Delta_2(z_2) &= z_2\left(a_{2+}e^{iwz_2} + a_{2-}e^{-iwz_2} + \frac{1}{w^2\cos\theta_{CR}}(T_{1r} + R_{2r}) - \frac{1}{w^2\cos\theta_R}T_2\right) \\
D_2(z_2) &= c_2 - \frac{i}{w^3}\left(1 + \frac{w^2 z_2^2\cos^2\theta_{CR}}{2}\right)(T_{1r} - R_{2r}) + \frac{i}{w^3}\left(1 + \frac{w^2 z_2^2\cos^2\theta_R}{2}\right)T_2 \\
&\quad + \frac{z_2}{w^2}\left(\sin\theta_{CR}(T_{1r} + R_{2r}) - \sin\theta_R T_2\right)
\end{aligned} \tag{A.8}$$

For our non-fluctuating interface, we can again impose the sources go to 0 at the boundary.

$\lambda_1(0) = 0$ and $\zeta_1(0) = 0$ give:

$$\begin{aligned} a_{1+} &= \frac{\sec\theta_{CL}(\mathcal{R}_{L2} + \mathcal{T}_{L1}) + \tan\theta_{CL}(\mathcal{R}_{L2} - \mathcal{T}_{L1}) - \sec\theta_L(1 + \mathcal{R}_{L1}) + \tan\theta_L(1 - \mathcal{R}_{L1})}{2w^2} \\ a_{1-} &= \frac{\sec\theta_{CL}(\mathcal{R}_{L2} + \mathcal{T}_{L1}) - \tan\theta_{CL}(\mathcal{R}_{L2} - \mathcal{T}_{L1}) - \sec\theta_L(1 + \mathcal{R}_{L1}) - \tan\theta_L(1 - \mathcal{R}_{L1})}{2w^2} \end{aligned} \tag{A.9}$$

$\lambda_2(0) = 0$ and $\zeta_2(0) = 0$ give:

$$\begin{aligned} a_{2+} &= \frac{-\sec\theta_{CR}(\mathcal{R}_{L2} + \mathcal{T}_{L1}) - \tan\theta_{CR}(\mathcal{R}_{L2} - \mathcal{T}_{L1}) + (\sec\theta_R - \tan\theta_R)\mathcal{T}_{L2})}{2w^2} \\ a_{2-} &= \frac{-\sec\theta_{CR}(\mathcal{R}_{L2} + \mathcal{T}_{L1}) + \tan\theta_{CR}(\mathcal{R}_{L2} - \mathcal{T}_{L1}) + (\sec\theta_R + \tan\theta_R)\mathcal{T}_{L2})}{2w^2} \end{aligned} \tag{A.10}$$

a_{1+} and a_{2+} correspond to the modes coming out of the horizon. These are unphysical and should be set to 0. Then, imposing $D_1(0) = 0$, $D_2(0) = 0$, $a_{1+} = 0$ and $a_{2+} = 0$ gives:

$$\begin{aligned} 1 &= \mathcal{R}_{L1} + \mathcal{T}_{L2} \\ \mathcal{T}_{L2} &= \frac{2\sec\theta_{CR}\sec\theta_L}{\sec\theta_{CR}(\sec\theta_L - \tan\theta_{CL} + \tan\theta_L) + \sec\theta_{CL}(\sec\theta_R + \tan\theta_{CR} - \tan\theta_R)} \\ \mathcal{R}_{L2} &= \frac{\sec\theta_L\cos\theta_{CL}(\sec\theta_R - \sec\theta_{CR} + \tan\theta_{CR} - \tan\theta_R)}{\sec\theta_R + \tan\theta_{CR} - \tan\theta_R - \sec\theta_{CR}\sin\theta_{CL} + \sec\theta_{CR}\cos\theta_{CL}(\sec\theta_L + \tan\theta_L)} \\ \mathcal{T}_{L1} &= \frac{\sec\theta_L\cos\theta_{CL}(\sec\theta_R + \sec\theta_{CR} + \tan\theta_{CR} - \tan\theta_R)}{\sec\theta_R + \tan\theta_{CR} - \tan\theta_R - \sec\theta_{CR}\sin\theta_{CL} + \sec\theta_{CR}\cos\theta_{CL}(\sec\theta_L + \tan\theta_L)} \end{aligned} \tag{A.11}$$

Appendix B: Expressions for the minimal area lengths and log g

We obtain expressions for the minimal area lengths and correspondingly $\log g$ by imposing (2.27) for the case where the M_C wedge is finite and found extending on both sides interface line. Based on the signs of the lengths of R_L and R_R, we have constraints on $l_{L,R,C}$ and the tension bounds.

For positive R_L, negative R_R (all possible $l_{L,R,C}$):

$$\begin{aligned}
R_L &= \frac{1}{2} l_L \log\left(\frac{l_L^2 - (\tau_1 l_C l_L + l_C)^2}{l_C^2 (\tau_1 l_L - 1)^2 - l_L^2}\right) \\
R_{CL} &= -l_C \log\left(\frac{(\tau_1 l_C l_L + l_C + l_L)(l_C(\tau_1 l_L - 1) + l_L)}{\sqrt{l_C^4(-(\tau_1^2 l_L^2 - 1)^2) + 2l_C^2(\tau_1^2 l_L^4 + l_L^2) - l_L^4}}\right) \\
R_{CR} &= \frac{1}{2} l_C \log\left(\frac{(\tau_2 l_C l_R + l_C + l_R)(l_C(\tau_2 l_R - 1) + l_R)}{(\tau_2 l_C(-l_R) + l_C + l_R)(\tau_2 l_C l_R + l_C - l_R)}\right) \\
R_R &= -l_R \log\left(\frac{(\tau_2 l_C l_R + l_C)^2 - l_R^2}{\sqrt{l_C^4(-(\tau_2^2 l_R^2 - 1)^2) + 2l_C^2(\tau_2^2 l_R^4 + l_R^2) - l_R^4}}\right)
\end{aligned} \tag{B.1}$$

where

$$\sqrt{\left|\frac{1}{l_L^2} - \frac{1}{l_C^2}\right|} < \tau_1 < \frac{1}{l_L} + \frac{1}{l_C}, \qquad \sqrt{\left|\frac{1}{l_R^2} - \frac{1}{l_C^2}\right|} < \tau_2 < \frac{1}{l_C} + \frac{1}{l_R} \tag{B.2}$$

$$\begin{aligned}
\log g = \frac{1}{8G}\Bigg(& 2l_C \log\left(\frac{(\tau_1 l_C l_L - l_C + l_L)(\tau_1 l_C l_L + l_C + l_L)}{\sqrt{l_C^4(-(\tau_1^2 l_L^2 - 1)^2) + 2l_C^2(\tau_1^2 l_L^4 + l_L^2) - l_L^4}}\right) \\
&+ l_L \log\left(\frac{l_L^2 - (\tau_1 l_C l_L + l_C)^2}{l_C^2(\tau_1 l_L - 1)^2 - l_L^2}\right) + l_C \log\left(\frac{(\tau_2 l_C l_R - l_C + l_R)(\tau_2 l_C l_R + l_C + l_R)}{(\tau_2 l_C(-l_R) + l_C + l_R)(\tau_2 l_C l_R + l_C - l_R)}\right) \\
&+ 2l_R \log\left(\frac{(\tau_2 l_C l_R + l_C)^2 - l_R^2}{\sqrt{l_C^4(-(\tau_2^2 l_R^2 - 1)^2) + 2l_C^2(\tau_2^2 l_R^4 + l_R^2) - l_R^4}}\right)\Bigg)
\end{aligned} \tag{B.3}$$

For $l_L = l_R$, it turns out that this $\log g$ expression is equivalent to the ones we express below (the different tension bounds and $l_{L,R,C}$ constraints still hold).

For negative R_L, positive R_R, ($l_{L,R,} > l_C$):

$$\begin{aligned}
R_L &= -\frac{1}{2} l_L \log\left(\frac{l_L^2 - l_C^2\left(\tau_1 l_L - 1\right)^2}{\left(\tau_1 l_C l_L + l_C\right)^2 - l_L^2}\right) \\
R_{CL} &= -l_C \log\left(\frac{\left(\tau_1 l_C l_L + l_C + l_L\right)\left(l_C\left(\tau_1 l_L - 1\right) + l_L\right)}{\sqrt{l_C^4\left(-\left(\tau_1^2 l_L^2 - 1\right)^2\right) + 2 l_C^2\left(\tau_1^2 l_L^4 + l_L^2\right) - l_L^4}}\right) \\
R_{CR} &= \frac{1}{2} l_C \log\left(\frac{\left(\tau_2 l_C l_R + l_C + l_R\right)\left(l_C\left(\tau_2 l_R - 1\right) + l_R\right)}{\left(\tau_2 l_C\left(-l_R\right) + l_C + l_R\right)\left(\tau_2 l_C l_R + l_C - l_R\right)}\right) \\
R_R &= l_R \log\left(\frac{\left|l_R^2 - l_C^2\left(l_R^2 \tau_2^2 + 1\right)\right| + 2\tau_2 l_C^2 l_R}{\sqrt{-\left(l_C^4\left(\tau_2^2 l_R^2 - 1\right)^2 - 2 l_C^2\left(\tau_2^2 l_R^4 + l_R^2\right) + l_R^4\right)}}\right)
\end{aligned} \tag{B.4}$$

where

$$\frac{1}{l_C} - \frac{1}{l_L} < \tau_1 < \sqrt{\frac{1}{l_C^2} - \frac{1}{l_L^2}}, \qquad \frac{1}{l_C} - \frac{1}{l_R} < \tau_2 < \sqrt{\frac{1}{l_C^2} - \frac{1}{l_R^2}} \tag{B.5}$$

$$\begin{aligned}
\log g = \frac{1}{8G}\Bigg(&-2 l_R \log\left(\frac{\left|l_R^2 - l_C^2\left(l_R^2 \tau_2^2 + 1\right)\right| + 2\tau_2 l_C^2 l_R}{\sqrt{-\left(l_C^4\left(\tau_2^2 l_R^2 - 1\right)^2 - 2 l_C^2\left(\tau_2^2 l_R^4 + l_R^2\right) + l_R^4\right)}}\right) \\
&+ l_C \log\left(\frac{\left(\tau_2 l_C l_R - l_C + l_R\right)\left(\tau_2 l_C l_R + l_C + l_R\right)}{\left(\tau_2 l_C\left(-l_R\right) + l_C + l_R\right)\left(\tau_2 l_C l_R + l_C - l_R\right)}\right) - l_L \log\left(\frac{l_L^2 - l_C^2\left(\tau_1 l_L - 1\right)^2}{\left(\tau_1 l_C l_L + l_C\right)^2 - l_L^2}\right) \\
&+ 2 l_C \log\left(\frac{\left(\tau_1 l_C l_L - l_C + l_L\right)\left(\tau_1 l_C l_L + l_C + l_L\right)}{\sqrt{l_C^4\left(-\left(\tau_1^2 l_L^2 - 1\right)^2\right) + 2 l_C^2\left(\tau_1^2 l_L^4 + l_L^2\right) - l_L^4}}\right)\Bigg)
\end{aligned} \tag{B.6}$$

For negative R_L, negative R_R ($l_L > l_C$), we can obtain similar expressions for R_L, R_{CL}, R_{CR}, R_R and Log g but, perhaps more interestingly, the tension bounds are given by:

$$\frac{1}{l_C} - \frac{1}{l_L} < \tau_1 < \sqrt{\frac{1}{l_C^2} - \frac{1}{l_L^2}}, \qquad \sqrt{\left|\frac{1}{l_R^2} - \frac{1}{l_C^2}\right|} < \tau_2 < \frac{1}{l_C} + \frac{1}{l_R} \tag{B.7}$$

Likewise, for positive R_L, positive R_R ($l_R > l_C$), we can obtain similar expressions for R_L, R_{CL}, R_{CR}, R_R and Log g but now the tension bounds are:

$$\sqrt{\left|\frac{1}{l_L^2} - \frac{1}{l_C^2}\right|} < \tau_1 < \frac{1}{l_C} + \frac{1}{l_L}, \qquad \frac{1}{l_C} - \frac{1}{l_R} < \tau_2 < \sqrt{\frac{1}{l_C^2} - \frac{1}{l_R^2}} \tag{B.8}$$

Works Cited

[1] Saba Asif Baig and Andreas Karch. Double brane holographic model dual to 2d ICFTs. *JHEP*, 10:022, 2022. doi: 10.1007/JHEP10(2022)022.

[2] Saba Asif Baig and Sanjit Shashi. Transport across interfaces in symmetric orbifolds. *JHEP*, 10:168, 2023. doi: 10.1007/JHEP10(2023)168.

[3] Saba Asif Baig, Andreas Karch, and Mianqi Wang. Transmission coefficient of super-Janus solution. *JHEP*, 10:235, 2024. doi: 10.1007/JHEP10(2024)235.

[4] Constantin Bachas, Shira Chapman, Dongsheng Ge, and Giuseppe Policastro. Energy Reflection and Transmission at 2D Holographic Interfaces. *Phys. Rev. Lett.*, 125(23):231602, 2020. doi: 10.1103/PhysRevLett.125.231602.

[5] Juan Martin Maldacena. The Large N limit of superconformal field theories and supergravity. *Adv. Theor. Math. Phys.*, 2:231–252, 1998. doi: 10.1023/A:1026654312961.

[6] Andreas Karch and Lisa Randall. Open and closed string interpretation of SUSY CFT's on branes with boundaries. *JHEP*, 06:063, 2001. doi: 10.1088/1126-6708/2001/06/063.

[7] Tadashi Takayanagi. Holographic Dual of BCFT. *Phys. Rev. Lett.*, 107:101602, 2011. doi: 10.1103/PhysRevLett.107.101602.

[8] Tatsuo Azeyanagi, Andreas Karch, Tadashi Takayanagi, and Ethan G. Thompson. Holographic calculation of boundary entropy. *JHEP*, 03:054, 2008. doi: 10.1088/1126-6708/2008/03/054.

[9] Marco Chiodaroli, Michael Gutperle, and Ling-Yan Hung. Boundary entropy of supersymmetric Janus solutions. *JHEP*, 09:082, 2010. doi: 10.1007/JHEP09(2010)082.

[10] C. Bachas, J. de Boer, R. Dijkgraaf, and H. Ooguri. Permeable conformal walls and holography. *JHEP*, 06:027, 2002. doi: 10.1088/1126-6708/2002/06/027.

[11] Joseph Polchinski. *String Theory. Vol. 2: Superstring Theory and Beyond*. Cambridge University Press, 1998. ISBN 9780521633045.

[12] John L. Cardy. Conformal Invariance and Surface Critical Behavior. *Nucl. Phys. B*, 240:514–532, 1984. doi: 10.1016/0550-3213(84)90241-4.

[13] Marco Meineri, Joao Penedones, and Antonin Rousset. Colliders and conformal interfaces. *JHEP*, 02:138, 2020. doi: 10.1007/JHEP02(2020)138.

[14] Marco Meineri, Joao Penedones, and Antonin Rousset. Colliders and conformal interfaces. *JHEP*, 02:138, 2020. doi: 10.1007/JHEP02(2020)138.

[15] Thomas Quella, Ingo Runkel, and Gerard M. T. Watts. Reflection and transmission for conformal defects. *JHEP*, 04:095, 2007. doi: 10.1088/1126-6708/2007/04/095.

[16] Lisa Randall and Raman Sundrum. An Alternative to compactification. *Phys. Rev. Lett.*, 83:4690–4693, 1999. doi: 10.1103/PhysRevLett.83.4690.

[17] Constantin Bachas, Stefano Baiguera, Shira Chapman, Giuseppe Policastro, and Tal Schwartzman. Energy Transport for Thick Holographic Branes. *Phys. Rev. Lett.*, 131(2):021601, 2023. doi: 10.1103/PhysRevLett.131.021601.

[18] Sebastian de Haro, Kostas Skenderis, and Sergey N. Solodukhin. Holographic reconstruction of spacetime¶and renormalization in the ads/cft correspondence. *Communications in Mathematical Physics*, 217(3):595–622, March 2001. ISSN 1432-0916. doi: 10.1007/s002200100381. URL `http://dx.doi.org/10.1007/s002200100381`.

[19] John L. Cardy. Boundary conformal field theory. 11 2004.

[20] Ian Affleck and Andreas W. W. Ludwig. Universal noninteger 'ground state degeneracy' in critical quantum systems. *Phys. Rev. Lett.*, 67:161–164, 1991. doi: 10.1103/PhysRevLett.67.161.

[21] Shinsei Ryu and Tadashi Takayanagi. Holographic derivation of entanglement entropy from AdS/CFT. *Phys. Rev. Lett.*, 96:181602, 2006. doi: 10.1103/PhysRevLett.96.181602.

[22] E. Wong and I. Affleck. Tunneling in quantum wires: A Boundary conformal field theory approach. *Nucl. Phys. B*, 417:403–438, 1994. doi: 10.1016/0550-3213(94)90479-0.

[23] Masaki Oshikawa and Ian Affleck. Boundary conformal field theory approach to the critical two-dimensional Ising model with a defect line. *Nucl. Phys. B*, 495:533–582, 1997. doi: 10.1016/S0550-3213(97)00219-8.

[24] Andreas Karch and Lisa Randall. Locally localized gravity. *JHEP*, 05:008, 2001. doi: 10.1088/1126-6708/2001/05/008.

[25] Oliver DeWolfe, Daniel Z. Freedman, and Hirosi Ooguri. Holography and defect conformal field theories. *Phys. Rev. D*, 66:025009, 2002. doi: 10.1103/PhysRevD.66.025009.

[26] Tadashi Takayanagi. Holographic Dual of BCFT. *Phys. Rev. Lett.*, 107:101602, 2011. doi: 10.1103/PhysRevLett.107.101602.

[27] J. David Brown and M. Henneaux. Central Charges in the Canonical Realization of Asymptotic Symmetries: An Example from Three-Dimensional Gravity. *Commun. Math. Phys.*, 104:207–226, 1986. doi: 10.1007/BF01211590.

[28] Andreas Karch, Zhu-Xi Luo, and Hao-Yu Sun. Universal relations for holographic interfaces. *JHEP*, 09:172, 2021. doi: 10.1007/JHEP09(2021)172.

[29] C. Bachas, I. Brunner, and D. Roggenkamp. Fusion of Critical Defect Lines in the 2D Ising Model. *J. Stat. Mech.*, 1308:P08008, 2013. doi: 10.1088/1742-5468/2013/08/P08008.

[30] Enrico M. Brehm and Ilka Brunner. Entanglement entropy through conformal interfaces in the 2D Ising model. *JHEP*, 09:080, 2015. doi: 10.1007/JHEP09(2015)080.

[31] John L. Cardy. Boundary Conditions, Fusion Rules and the Verlinde Formula. *Nucl. Phys. B*, 324:581–596, 1989. doi: 10.1016/0550-3213(89)90521-X.

[32] Hirosi Ooguri and Tadashi Takayanagi. Cobordism Conjecture in AdS. 6 2020.

[33] Jacob McNamara and Cumrun Vafa. Cobordism Classes and the Swampland. 9 2019.

[34] Sidney R. Coleman and Frank De Luccia. Gravitational Effects on and of Vacuum Decay. *Phys. Rev. D*, 21:3305, 1980. doi: 10.1103/PhysRevD.21.3305.

[35] Juan Maldacena. Vacuum decay into Anti de Sitter space. 12 2010.

[36] Pasquale Calabrese and John L. Cardy. Entanglement entropy and quantum field theory. *J. Stat. Mech.*, 0406:P06002, 2004. doi: 10.1088/1742-5468/2004/06/P06002.

[37] Constantin Bachas and Vassilis Papadopoulos. Phases of Holographic Interfaces. *JHEP*, 04:262, 2021. doi: 10.1007/JHEP04(2021)262.

[38] W. Israel. Singular hypersurfaces and thin shells in general relativity. *Nuovo Cim. B*, 44S10:1, 1966. doi: 10.1007/BF02710419. [Erratum: Nuovo Cim.B 48, 463 (1967)].

[39] Kostas Skenderis and Sergey N. Solodukhin. Quantum effective action from the AdS / CFT correspondence. *Phys. Lett. B*, 472:316–322, 2000. doi: 10.1016/S0370-2693(99)01467-7.

[40] Dam T. Son and Andrei O. Starinets. Minkowski space correlators in AdS / CFT correspondence: Recipe and applications. *JHEP*, 09:042, 2002. doi: 10.1088/1126-6708/2002/09/042.

[41] C. P. Herzog and D. T. Son. Schwinger-Keldysh propagators from AdS/CFT correspondence. *JHEP*, 03:046, 2003. doi: 10.1088/1126-6708/2003/03/046.

[42] Shinsei Ryu and Tadashi Takayanagi. Aspects of Holographic Entanglement Entropy. *JHEP*, 08:045, 2006. doi: 10.1088/1126-6708/2006/08/045.

[43] Ian Affleck. Conformal field theory approach to the Kondo effect. *Acta Phys. Polon. B*, 26:1869–1932, 1995.

[44] Ian Affleck. Conformal field theory approach to quantum impurity problems. In *Field Theories for Low-Dimensional Condensed Matter Systems: Spin Systems and Strongly Correlated Electrons*, pages 117–141, Berlin, Heidelberg, 2000. Springer Berlin Heidelberg. ISBN 978-3-662-04273-1. doi: 10.1007/978-3-662-04273-1. URL `https://doi.org/10.1007/978-3-662-04273-1`.

[45] Augusto Sagnotti. Open Strings and their Symmetry Groups. In *NATO Advanced Summer Institute on Nonperturbative Quantum Field Theory (Cargese Summer Institute)*. 9 1987.

[46] Joseph Polchinski. Dirichlet Branes and Ramond-Ramond charges. *Phys. Rev. Lett.*, 75:4724–4727, 1995. doi: 10.1103/PhysRevLett.75.4724.

[47] Matthias R Gaberdiel. D-branes from conformal field theory. *Fortsch. Phys.*, 50:783–801, 2002. doi: 10.1002/1521-3978(200209)50:8/9⟨783::AID-PROP783⟩3.0.CO;2-J.

[48] Andreas Recknagel and Volker Schomerus. *Boundary Conformal Field Theory and the Worldsheet Approach to D-Branes*. Cambridge Monographs on Mathematical Physics. Cambridge University Press, 2013. ISBN 978-0-521-83223-6, 978-0-521-83223-6, 978-1-107-49612-5. doi: 10.1017/CBO9780511806476.

[49] Marco Billò, Vasco Gonçalves, Edoardo Lauria, and Marco Meineri. Defects in conformal field theory. *JHEP*, 04:091, 2016. doi: 10.1007/JHEP04(2016)091.

[50] Alexandre Belin, Shovon Biswas, and James Sully. The spectrum of boundary states in symmetric orbifolds. *JHEP*, 01:123, 2022. doi: 10.1007/JHEP01(2022)123.

[51] Matthias R. Gaberdiel, Bob Knighton, and Jakub Vošmera. D-branes in $AdS_3 \times S^3 \times \mathbb{T}^4$ at k = 1 and their holographic duals. *JHEP*, 12:149, 2021. doi: 10.1007/JHEP12(2021)149.

[52] Felix M. Haehl and Mukund Rangamani. Permutation orbifolds and holography. *JHEP*, 03:163, 2015. doi: 10.1007/JHEP03(2015)163.

[53] Alexandre Belin, Christoph A. Keller, and Alexander Maloney. String Universality for Permutation Orbifolds. *Phys. Rev. D*, 91(10):106005, 2015. doi: 10.1103/PhysRevD.91.106005.

[54] Steven G. Avery, Borun D. Chowdhury, and Samir D. Mathur. Deforming the D1D5 CFT away from the orbifold point. *JHEP*, 06:031, 2010. doi: 10.1007/JHEP06(2010)031.

[55] Lorenz Eberhardt, Matthias R. Gaberdiel, and Rajesh Gopakumar. Deriving the AdS_3/CFT_2 correspondence. *JHEP*, 02:136, 2020. doi: 10.1007/JHEP02(2020)136.

[56] Marco Chiodaroli, Michael Gutperle, and Darya Krym. Half-BPS Solutions locally asymptotic to AdS(3) x S**3 and interface conformal field theories. *JHEP*, 02:066, 2010. doi: 10.1007/JHEP02(2010)066.

[57] Dongsu Bak, Michael Gutperle, and Shinji Hirano. Three dimensional Janus and time-dependent black holes. *JHEP*, 02:068, 2007. doi: 10.1088/1126-6708/2007/02/068.

[58] Steven S. Gubser, Igor R. Klebanov, and Arkady A. Tseytlin. Coupling constant dependence in the thermodynamics of N=4 supersymmetric Yang-Mills theory. *Nucl. Phys. B*, 534:202–222, 1998. doi: 10.1016/S0550-3213(98)00514-8.

[59] A. Fotopoulos and T. R. Taylor. Comment on two loop free energy in N=4 supersymmetric Yang-Mills theory at finite temperature. *Phys. Rev. D*, 59:061701, 1999. doi: 10.1103/PhysRevD.59.061701.

[60] G. Policastro, Dan T. Son, and Andrei O. Starinets. The Shear viscosity of strongly coupled N=4 supersymmetric Yang-Mills plasma. *Phys. Rev. Lett.*, 87:081601, 2001. doi: 10.1103/PhysRevLett.87.081601.

[61] Alex Buchel, James T. Liu, and Andrei O. Starinets. Coupling constant dependence of the shear viscosity in N=4 supersymmetric Yang-Mills theory. *Nucl. Phys. B*, 707:56–68, 2005. doi: 10.1016/j.nuclphysb.2004.11.055.

[62] Simon C. Huot, Sangyong Jeon, and Guy D. Moore. Shear viscosity in weakly coupled N = 4 super Yang-Mills theory compared to QCD. *Phys. Rev. Lett.*, 98:172303, 2007. doi: 10.1103/PhysRevLett.98.172303.

[63] Benjamin A. Burrington, Ian T. Jardine, and Amanda W. Peet. The OPE of bare twist operators in bosonic S_N orbifold CFTs at large N. *JHEP*, 08:202, 2018. doi: 10.1007/JHEP08(2018)202.

[64] Luis Apolo, Alexandre Belin, Suzanne Bintanja, Alejandra Castro, and Christoph A. Keller. Deforming symmetric product orbifolds: a tale of moduli and higher spin currents. *JHEP*, 08:159, 2022. doi: 10.1007/JHEP08(2022)159.

[65] Oleg Lunin and Samir D. Mathur. Correlation functions for M**N / S(N) orbifolds. *Commun. Math. Phys.*, 219:399–442, 2001. doi: 10.1007/s002200100431.

[66] Benjamin A. Burrington and A. W. Peet. Fractional conformal descendants and correlators in general 2D S_N orbifold CFTs at large N. *JHEP*, 02:091, 2023. doi: 10.1007/JHEP02(2023)091.

[67] Benjamin A. Burrington and A. W. Peet. Larger twists and higher n-point functions with fractional conformal descendants in S_N orbifold CFTs at large N. *JHEP*, 02:229, 2023. doi: 10.1007/JHEP02(2023)229.

[68] Nobuyuki Ishibashi. The Boundary and Crosscap States in Conformal Field Theories. *Mod. Phys. Lett. A*, 4:251, 1989. doi: 10.1142/S0217732389000320.

[69] Ralph Blumenhagen and Erik Plauschinn. Boundary conformal field theory. In *Introduction to Conformal Field Theory*, pages 205–256, Berlin, Heidelberg, 2009. Springer Berlin Heidelberg. ISBN 978-3-642-00450-6. doi: 10.1007/978-3-642-00450-6. URL `https://doi.org/10.1007/978-3-642-00450-6`.

[70] Andreas Recknagel. Permutation branes. *JHEP*, 04:041, 2003. doi: 10.1088/1126-6708/2003/04/041.

[71] Tetsuya Onogi and Nobuyuki Ishibashi. Conformal Field Theories on Surfaces With Boundaries and Crosscaps. *Mod. Phys. Lett. A*, 4:161, 1989. doi: 10.1142/S0217732389000228. [Erratum: Mod.Phys.Lett.A 4, 885 (1989)].

[72] Marco Billo, Ben Craps, and Frederik Roose. Orbifold boundary states from Cardy's condition. *JHEP*, 01:038, 2001. doi: 10.1088/1126-6708/2001/01/038.

[73] Taro Kimura and Masaki Murata. Current Reflection and Transmission at Conformal Defects: Applying BCFT to Transport Process. *Nucl. Phys. B*, 885:266–279, 2014. doi: 10.1016/j.nuclphysb.2014.05.026.

[74] Taro Kimura and Masaki Murata. Transport Process in Multi-Junctions of Quantum Systems. *JHEP*, 07:072, 2015. doi: 10.1007/JHEP07(2015)072.

[75] Shovon Biswas, Jani Kastikainen, Sanjit Shashi, and James Sully. Holographic BCFT spectra from brane mergers. *JHEP*, 11:158, 2022. doi: 10.1007/JHEP11(2022)158.

[76] Oleg Lunin and Samir D. Mathur. Three point functions for M(N) / S(N) orbifolds with N=4 supersymmetry. *Commun. Math. Phys.*, 227:385–419, 2002. doi: 10.1007/s002200200638.

[77] Constantin Bachas, Zhongwu Chen, and Vassilis Papadopoulos. Steady states of holographic interfaces. *JHEP*, 11:095, 2021. doi: 10.1007/JHEP11(2021)095.

[78] Tarek Anous, Marco Meineri, Pietro Pelliconi, and Julian Sonner. Sailing past the End of the World and discovering the Island. *SciPost Phys.*, 13(3):075, 2022. doi: 10.21468/SciPostPhys.13.3.075.

[79] Gary T. Horowitz, Juan Martin Maldacena, and Andrew Strominger. Nonextremal black hole microstates and U duality. *Phys. Lett. B*, 383:151–159, 1996. doi: 10.1016/0370-2693(96)00738-1.

[80] Nathan Seiberg and Edward Witten. The D1 / D5 system and singular CFT. *JHEP*, 04:017, 1999. doi: 10.1088/1126-6708/1999/04/017.

[81] Justin R. David, Gautam Mandal, and Spenta R. Wadia. Microscopic formulation of black holes in string theory. *Phys. Rept.*, 369:549–686, 2002. doi: 10.1016/S0370-1573(02)00271-5.

[82] Kostas Skenderis. Asymptotically Anti-de Sitter space-times and their stress energy tensor. *Int. J. Mod. Phys. A*, 16:740–749, 2001. doi: 10.1142/S0217751X0100386X.

[83] Ioannis Papadimitriou and Kostas Skenderis. Correlation functions in holographic RG flows. *JHEP*, 10:075, 2004. doi: 10.1088/1126-6708/2004/10/075.

[84] John Estes, Kristan Jensen, Andy O'Bannon, Efstratios Tsatis, and Timm Wrase. On Holographic Defect Entropy. *JHEP*, 05:084, 2014. doi: 10.1007/JHEP05(2014)084.

[85] Michael Gutperle and Andrea Trivella. Note on entanglement entropy and regularization in holographic interface theories. *Phys. Rev. D*, 95(6):066009, 2017. doi: 10.1103/PhysRevD.95.066009.

[86] Dongsu Bak, Michael Gutperle, and Shinji Hirano. A Dilatonic deformation of AdS(5) and its field theory dual. *JHEP*, 05:072, 2003. doi: 10.1088/1126-6708/2003/05/072.

[87] A. Clark and A. Karch. Super Janus. *JHEP*, 10:094, 2005. doi: 10.1088/1126-6708/2005/10/094.

[88] Alexandre Belin, Nathan Benjamin, Alejandra Castro, Sarah M. Harrison, and Christoph A. Keller. $\mathcal{N} = 2$ Minimal Models: A Holographic Needle in a Symmetric Orbifold Haystack. *SciPost Phys.*, 8(6):084, 2020. doi: 10.21468/SciPostPhys.8.6.084.

[89] Nathan Benjamin, Suzanne Bintanja, Alejandra Castro, and Jildou Hollander. The stranger things of symmetric product orbifold CFTs. *JHEP*, 11:054, 2022. doi: 10.1007/JHEP11(2022)054.

[90] Alexandre Belin, Alejandra Castro, Christoph A. Keller, and Beatrix Mühlmann. The Holographic Landscape of Symmetric Product Orbifolds. *JHEP*, 01:111, 2020. doi: 10.1007/JHEP01(2020)111.

[91] Matthias R. Gaberdiel, Cheng Peng, and Ida G. Zadeh. Higgsing the stringy higher spin symmetry. *JHEP*, 10:101, 2015. doi: 10.1007/JHEP10(2015)101.

[92] Shira Chapman, Dongsheng Ge, and Giuseppe Policastro. Holographic Complexity for Defects Distinguishes Action from Volume. *JHEP*, 05:049, 2019. doi: 10.1007/JHEP05(2019)049.

[93] Roberto Auzzi, Stefano Baiguera, Sara Bonansea, Giuseppe Nardelli, and Kristian Toccacelo. Volume complexity for Janus AdS_3 geometries. *JHEP*, 08:045, 2021. doi: 10.1007/JHEP08(2021)045.

[94] Roberto Auzzi, Stefano Baiguera, Sara Bonansea, and Giuseppe Nardelli. Action complexity in the presence of defects and boundaries. *JHEP*, 02:118, 2022. doi: 10.1007/JHEP02(2022)118.

[95] Andreas Karch and Mianqi Wang. Universal behavior of entanglement entropies in interface CFTs from general holographic spacetimes. *JHEP*, 06:145, 2023. doi: 10.1007/JHEP06(2023)145.

[96] Masaki Oshikawa and Ian Affleck. Defect lines in the Ising model and boundary states on orbifolds. *Phys. Rev. Lett.*, 77:2604–2607, 1996. doi: 10.1103/PhysRevLett.77.2604.

[97] Kazuhiro Sakai and Yuji Satoh. Entanglement through conformal interfaces. *JHEP*, 12:001, 2008. doi: 10.1088/1126-6708/2008/12/001.

[98] Andreas Karch, Yuya Kusuki, Hirosi Ooguri, Hao-Yu Sun, and Mianqi Wang. Universality of effective central charge in interface CFTs. *JHEP*, 11:126, 2023. doi: 10.1007/JHEP11(2023)126.

[99] Andreas Karch, Yuya Kusuki, Hirosi Ooguri, Hao-Yu Sun, and Mianqi Wang. Universal Bound on Effective Central Charge and Its Saturation. 4 2024.

[100] Michael Gutperle and John D. Miller. Entanglement entropy at holographic interfaces. *Phys. Rev. D*, 93(2):026006, 2016. doi: 10.1103/PhysRevD.93.026006.

[101] A. B. Clark, D. Z. Freedman, A. Karch, and M. Schnabl. Dual of the Janus solution: An interface conformal field theory. *Phys. Rev. D*, 71:066003, 2005. doi: 10.1103/PhysRevD.71.066003.

[102] Finn Larsen and Emil Martinec. U(1) charges and moduli in the d1-d5 system. *Journal of High Energy Physics*, 1999(06):019–019, June 1999. ISSN 1029-8479. doi: 10.1088/1126-6708/1999/06/019. URL `http://dx.doi.org/10.1088/1126-6708/1999/06/019`.

[103] Constantin Bachas and John Estes. Spin-2 spectrum of defect theories. *JHEP*, 06:005, 2011. doi: 10.1007/JHEP06(2011)005.

[104] Stefano Speziali. Spin 2 fluctuations in 1/4 BPS AdS_3/CFT_2. *JHEP*, 03:079, 2020. doi: 10.1007/JHEP03(2020)079.

[105] Kevin Chen, Michael Gutperle, and Christoph F. Uhlemann. Spin 2 operators in holographic 4d $\mathcal{N} = 2$ SCFTs. *JHEP*, 06:139, 2019. doi: 10.1007/JHEP06(2019)139.

[106] Konstantinos C. Rigatos. Spin-2 operators in AdS_2/CFT_1. *JHEP*, 06:026, 2023. doi: 10.1007/JHEP06(2023)026.

[107] O. DeWolfe, D. Z. Freedman, S. S. Gubser, and A. Karch. Modeling the fifth-dimension with scalars and gravity. *Phys. Rev. D*, 62:046008, 2000. doi: 10.1103/PhysRevD.62.046008.